A SPHERICAL SLOT ARRAY ANTENNA

CHUWONG PHONGCHAROENPANICH

A THESIS SUBMITTED IN PARTIAL FULFILLMENT OF
THE REQUIREMENT FOR THE DEGREE
DOCTOR OF ENGINEERING IN ELECTRICAL ENGINEERING
SCHOOL OF GRADUATE STUDIES
KING MONGKUT'S INSTITUTE OF TECHNOLOGY LADKRABANG
2001

ISBN 974-648-375-7

หัวข้อวิทยานิพนธ์	สายอากาศแถวลำดับแบบร่องบนผิวทรงกลม
นักศึกษา	นายชูวงค์ พงศ์เจริญพาณิชย์
รหัสประจำตัว	41060001
ปริญญา	วิศวกรรมศาสตรดุษฎีบัณฑิต
สาขา	วิชาวิศวกรรมไฟฟ้า
พ.ศ.	2544
อาจารย์ผู้ควบคุมวิทยานิพนธ์	รศ.ดร.โมไนย ไกรฤกษ์

บทคัดย่อ

วิทยานิพนธ์ฉบับนี้นำเสนอสายอากาศชนิดแถวลำดับแบบร่องบนผิวทรงกลม โดยโครงสร้างของสายอากาศประกอบด้วยร่องจำนวนหลายร่องที่มาจัดเรียงกันเป็นแถวลำดับบนผิวของคาวิตี้ตัวนำทรงกลมสองชั้นซ้อนกันและด้านข้างของคาวิตี้ถูกปิดล้อมด้วยส่วนของผิวกรวยตัวนำ ระบบการป้อนสัญญาณเป็นโพรบไฟฟ้าเชิงเส้นที่วางบนผิวตัวนำอันในของคาวิตี้ ข้อดีของสายอากาศชนิดนี้คือ เป็นสายอากาศที่มีโครงสร้างไม่ซับซ้อนเพราะตัวแบ่งกำลังงานและตัวป้อนสัญญาณได้ถูกรวมเป็นโครงสร้างเดียวกัน สำหรับในวิทยานิพนธ์นี้ได้เลือกออกแบบสายอากาศให้มีแบบรูปการแพร่กระจายคลื่นรูปกรวยและมีการโพลาไรซ์แบบวงกลมสำหรับการประยุกต์ใช้งานกับการสื่อสารเคลื่อนที่ผ่านดาวเทียมและระบบโครงข่ายท้องถิ่นไร้สาย ในขั้นแรกได้คำนวณแบบรูปการแพร่กระจายคลื่นของสายอากาศเมื่อเปลี่ยนค่าพารามิเตอร์ต่างๆ เพื่อหาเงื่อนไขเบื้องต้นสำหรับการประยุกต์ใช้งานจริง จากนั้นจึงได้คำนวณละเอียดโดยรวมผลของโครงสร้างทั้งหมดไว้โดยการตั้งสมการเชิงอินทิกรัล โดยอาศัยฟังก์ชันของกรีนและใช้วิธีโมเมนต์แก้สมการเชิงอินทิกรัลดังกล่าว จะทำให้สามารถหาคุณลักษณะการแพร่กระจายคลื่นของสายอากาศอันได้แก่ แบบรูปการแพร่กระจายคลื่น ค่ามุมเงยและสภาพเจาะจงทิศทาง พารามิเตอร์ที่ให้คุณลักษณะการแพร่กระจายคลื่นที่เหมาะสมกับการประยุกต์ใช้งานจะถูกใช้ในการวิเคราะห์หาค่าอิมพีแดนซ์ขาเข้าและอัตราส่วนแกนของการโพลาไรซ์วงกลมที่ดีที่สุด และค่าพารามิเตอร์ที่ดีที่สุดทั้งหมดนี้ได้ถูกใช้นำมาสร้างสายอากาศต้นแบบ และได้ทำการทดสอบคุณลักษณะของสายอากาศเพื่อยืนยันหลักการที่นำเสนอ จากผลทางทฤษฎีและทางปฏิบัติแสดงให้เห็นว่าสายอากาศนี้เหมาะสำหรับที่จะใช้เป็นสายอากาศสำหรับลูกข่ายของระบบสื่อสารดาวเทียมเคลื่อนที่ที่อยู่ไกลจากเส้นศูนย์สูตร และใช้เป็นสายอากาศสำหรับสถานีฐานในระบบโครงข่ายท้องถิ่นไร้สาย

Thesis Title	A Spherical Slot Array Antenna
Student	Mr. Chuwong Phóngchàroenpanich
Student ID.	41060001
Degree	Doctor of Engineering
Programme	Electrical Engineering
Year	2001
Thesis Advisor	Assoc. Prof. Dr. Monai Krairiksh

ABSTRACT

A spherical slot array antenna is proposed in this thesis. The structure of the antenna is made up of a number of slots cut on an outer surface of the concentric conducting spherical cavity enclosed by the conducting conical surface. The feeding structure is a linear electric probe excited on the inner surface of the cavity. The advantage of this antenna is that it belongs to the simple structure because the power divider and the feeder are integrated into a single structure. This thesis is focused on the design of this antenna to radiate the circularly polarized conical beam for the applications of the land mobile satellite communications and wireless Local Area Network systems. The radiation pattern of this antenna is preliminarily calculated to find the initial parameters that meet the requirements of the practical applications. Then, the Method of Moments is conducted with the aids of the dyadic Green's functions to solve the integral equations that rigorously include all phenomenal antenna structure. The antenna radiation characteristics such as radiation pattern, elevational angle and directivity are subsequently investigated. The optimum antenna parameters that fulfill the requirements of the radiation characteristics for particular applications are consequently used for clarifying the matching condition and polarization circularity. With the optimum parameters, the prototype of the antenna is fabricated. The antenna measurement is set up to verify the proposed principle. From the results of the theoretical and experimental investigations, it is obvious that this antenna is useful for applying to the land mobile subscriber units located far from equator and the base-station antenna for the wireless LAN system.

Acknowledgements

There are numerous individual contributions whose assistances were crucial to the successful completion of this thesis.

First of all, I would like to express my invaluable profound gratitude to my advisor Associate Professor Monai Krairiksh, for his valuable continuous guidance, helpful suggestion and constant encouragement since the first day I was his advisee (15/6/1994) when I was undergraduate student. His hard work of supervising me for more than 7 years of my Bachelor, Master and Doctor studies is forever recognized. I would also like to express my gratitude to Associate Professor Jun-ichi Takada of Tokyo Institute of Technology for his generous suggestion and for keeping me on the right track in calculation.

I am particularly grateful to some lecturers in my department, Assistant Professor Sompol Kosulvit for his hospitality and fruitful discussions, and Professor Wiwat Kiranon for his substantial lectures throughout my study. I am also grateful to Associate Professor Charray Surawatpunya for his valuable comments and suggestions for many years and Assistant Professor Kraisin Songwattana for his kind giving me the references.

The support from my bosses, Associate Professor Tawil Paungma, Dean of Faculty of Engineering, Associate Professor Kobchai Dejhan and Dr. Tongtod Vanisri, present and past Head of Telecommunication Department, must be acknowledged.

I would like to extend my sincere appreciation to Professor Toshio Wakabayashi of Tokai University for his strong effort for seminar in our

lab. Special thanks to all of my Master Thesis committee members for their valuable comments.

Again, the encouragement of the fellow members of the Wireless Communication Laboratory, Mr.Komsak Meksamoot, Mr.Rangsan Wongsan and Mr.Chanchai Thongsopa, who gave me kind discussions. The assistance of Mr.Titipong Lertwiriyaprapa, Mr.Phaisan Ngamjanyaporn, Mr.Chaiwat Leekpai, Mr.Duang-arthit Srimoon, Mr.Anat Mearnchu, Miss Suthasinee Lamultree, Mr.Phairote Wounchoum, Miss Wanlika Buasomboon, Mr.Sanya Amnartpluk, Mr.Thanarat Sroysuwan, Miss Nitikarn Pasri and Miss Annapa Mahamongkol have much appreciated. Cordial thank is also to Miss Titiporn Tuesikares for her encouragements and precious stimulations.

I also would like to acknowledge to the Japan International Cooperation Agency (JICA) for providing the supports for me to present this work. The Visiting Research Scholar from the International Cooperation Center for Sciences and Technology of Tokyo Institute of Technology for me to find many references should be sincerely acknowledged.

Finally, I am greatly indebted to my parents for their unlimited patience, perpetual support and unceasing help.

Chuwong Phongcharoenpanich

Table of Contents

Table of Contents (continued)

List of Tables

List of Figures

List of Figures (continued)

Fig. page

List of Figures (continued)

Chapter 1

Introduction

Enclosed within this chapter introduces the background of the spherical slot array antenna. The cited literatures of the slot array antenna on the spherical surface, the feasible applications of this antenna, the purpose and the scope of this thesis and the outline of remaining chapters that summarizes information of the succeeding chapters are addressed.

1.1 Background of the Spherical Slot Array Antenna

1.1.1 Historical Notes of the Slot Array Antenna on Spherical Surface

Nowadays, wireless communications can be considered as a part of daily-life essence. A key device for transmitting and receiving signal between communication sides is antenna. There have been various kinds of antennas extensively and continuously invented to accomplish the requirements for different features of the communications. Generally, each antenna has its own advantages and disadvantages. Therefore, it has been individually applied for specific applications. Its electrical and mechanical properties have to meet the specification of the actual usage.

The slot cut on the conducting surface is one of many antenna types that is very useful for the application that the radiator is desirable to be flush-mounted with the conducting surface. The merit of the slot antenna is the flush-mounted structure conforming to the conducting surface. This property makes it low profile. Traditionally, there are many configurations of slots cut on the conductor; both flat and curved surfaces. The slot on the plane is essential in case of the geometry of location to be installed is restricted to be flat in order to reduce the wind resistance.

There are many researches and developments on the slots on the conducting plane in literature [1-1]. Mostly, they are backed by the parallel plates [1-2], rectangular waveguide [1-3] and rectangular cavity [1-4]. However, for some particular applications of the curved surfaces [1-5] such as a portion of the vehicle, ship, aircraft and missile, the slot on the planar structure is inappropriately applied.

The conformal slot antenna is the most promising candidate for those requirements. Additionally, in case of the slot radiators located on the planar structure to form the planar slot antenna, the deterioration of gain or pattern occurs while the main beam is scanning especially when the beam points toward the low elevational angle. The conformal slot antennas such as slot antennas located on the cylindrical [1-6], conical [1-7] and spherical [1-8] surfaces are the attractive candidates to overcome the drawback of the planar slot antennas for the particular applications of the curved surface.

In historical literatures, most of substantial works relating to the conformal slot antennas have been paid to the analysis of the slots imposed on the cylindrical and conical surfaces because the antenna can be steered in azimuthal plane without the degradation of radiation characteristics. This can be realized due to its rotationally symmetrical structure in a circular cross section. Furthermore, in order to yield the entirely symmetrical structure, the spherical slot antenna is the most appropriate. The similar pattern, while the beam is scanned in both elevational and azimuthal directions, is obtainable. As far as we know in literatures, only a few of research works have been studying on the spherical slot antenna. The important reason is due to the difficulties to analyze its mathematical model since it must be involved with the higher transcendental functions such as spherical Bessel function and Associated Legendre functions. Noticeably, the use of the spherical slot antennas is of particular importance in stationary structures and mobile vehicles, particularly

those have portions of their bodies with the spherical shape. In addition, for radar applications which require the constant radiation pattern in any direction, the spherical array antenna has still been employed.

Furthermore, mobile satellite communication is popular lately. The antenna on the mobile unit must have the capability of satellite tracking in a similar fashion to that of the radar system, the spherical array is also appropriate since its beam can be tilted without the gain degradation. In the mobile system the alternative way is to apply the conical beam antenna instead of using the sophisticated tracking system. In this manner, the antenna pattern can cover any position in azimuthal plane since the field strength is identical for all directions. There have been many research works about the conical beam antenna such as helical [1-9] and microstrip [1-10] antennas. The disadvantage of those antennas is the difficulty in fabrication because the power divider and the feeding structure are separated.

Recently, the radial line slot antenna (RLSA) [1-11], the circular array of slot pairs cut on the top plate of the radial line waveguide, was developed to radiate circularly polarized conical beam pattern. The merit of that antenna belongs to its simple structure since the power divider and the feeding circuit are integrated into a single structure. However, it was found that the elevational beam direction is relatively high (about 30° from boresight direction). In some applications such as the land mobile subscriber unit located far from the equator, the elevational angle must be lowered. Takada, *et al.*, proposed to feed the radial line slot array antenna by the rotating mode generator [1-12], but this effort was achieved at some expenses of gain degradation and more complicated feeding structure. A spherical slot array antenna radiating circularly polarized conical beam [1-13] has proposed and it provides the pattern in elevational plane direct toward a low angle direction. This antenna is

simple and it is expected to be suitable for mass production i.e., a ring of perpendicular slot pairs cut on an outer surface of the concentric conducting spherical cavity enclosed by the conducting conical surface. The feeding structure is simple that it is a linear electric probe excited at the inner surface of the cavity and integrated with the power divider. This fact has motivated the presentation of this thesis.

1.1.2 Applications of the Spherical Slot Array Antenna

A spherical slot array antenna, which is designed to radiate the circularly polarized conical beam, is proposed to serve as the antenna for installing on the land subscriber unit of the mobile satellite communication system and the base-station antenna of the wireless Local Area Network system.

1.1.2.1 Mobile Satellite Communication

Recently, the mobile communication using satellite becomes very popular [1-14]. If the antenna used for this application radiates the conical beam pattern, the sophisticated tracking system is not necessary anymore. The conical beam pattern has the following characteristics:

(1) The theoretical null occurs in boresight axis.

(2) The elevational beam peak directs toward the satellite. The elevational angle is generally between *10* to *80* degrees. It is pointed that the lower the elevational beam peak the further the location of the mobile terminal from the equator.

(3) The azimuthal pattern at an angle of the elevational beam peak is non-direction.

For the land mobile satellite communication subscriber, the antenna is required to radiate right-hand circular polarization with the gain of 6.6 ± 0.9 dBi and the axial ratio less than *2.5* dB. A circularly polarized spherical slot array antenna

is proposed [1-15] for applying to this system as the antenna for various mobile terminals such as cars, buses and others. This antenna can be installed at any part of those vehicles especially at their rooftops as shown in Fig.1.1. The advantage of the spherical slot array antenna is that the elevational beam peak can be lower without the gain deterioration. Therefore, it is suitable for installing at the mobile subscriber unit located far from equator.

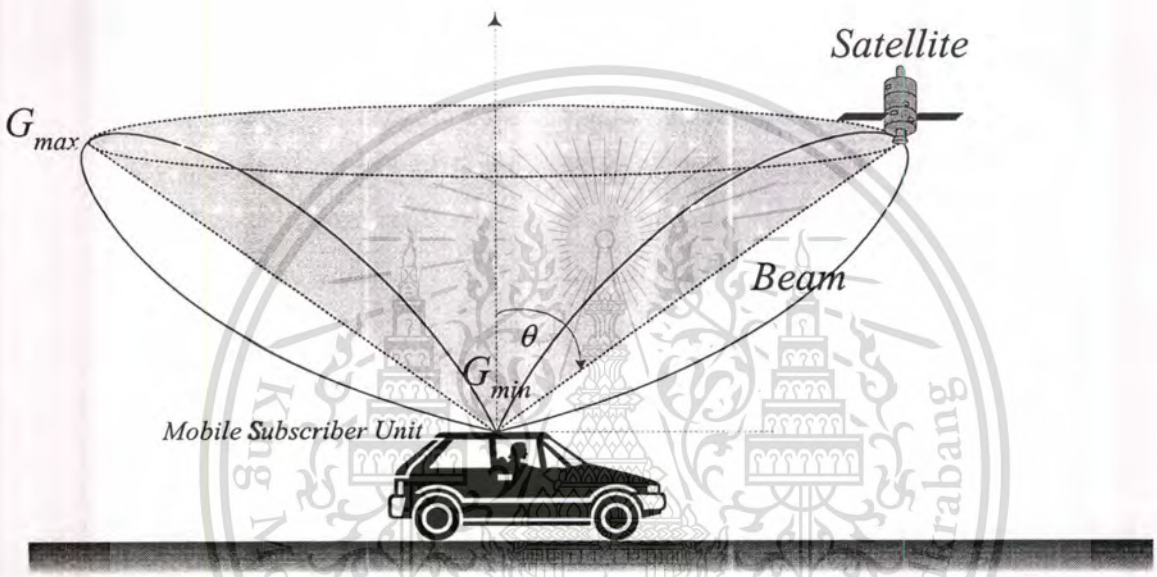

Fig 1.1 Application of a circularly polarized conical beam spherical slot array antenna for land mobile satellite communication

1.1.2.2 Wireless Local Area Network

The wireless Local Area Network [1-16] is another application of interest for the circularly polarized conical beam spherical slot array antenna. The antenna used in this system can be divided into two categories according to the location of the applications. The first one acts as the antenna for the base station. It may be installed at the ceiling of the room. The other one is the antenna for remote or mobile terminal. This might be installed at the body of the computers or laptop as shown in Fig.1.2.

A circularly polarized conical beam spherical slot array antenna is proposed for applying as the antenna for base station. This antenna is designed to radiate the conical beam pattern. It can be conveniently installed on the ceiling as figured in Fig.1.2. The gain of *4.2* dBi is desired for this system. Since this antenna type can be designed to radiate the lower elevational beam peak, the coverage of the service area may be expanded. Moreover, the gain as well as beamwidth shall be designed considering propagation scenario.

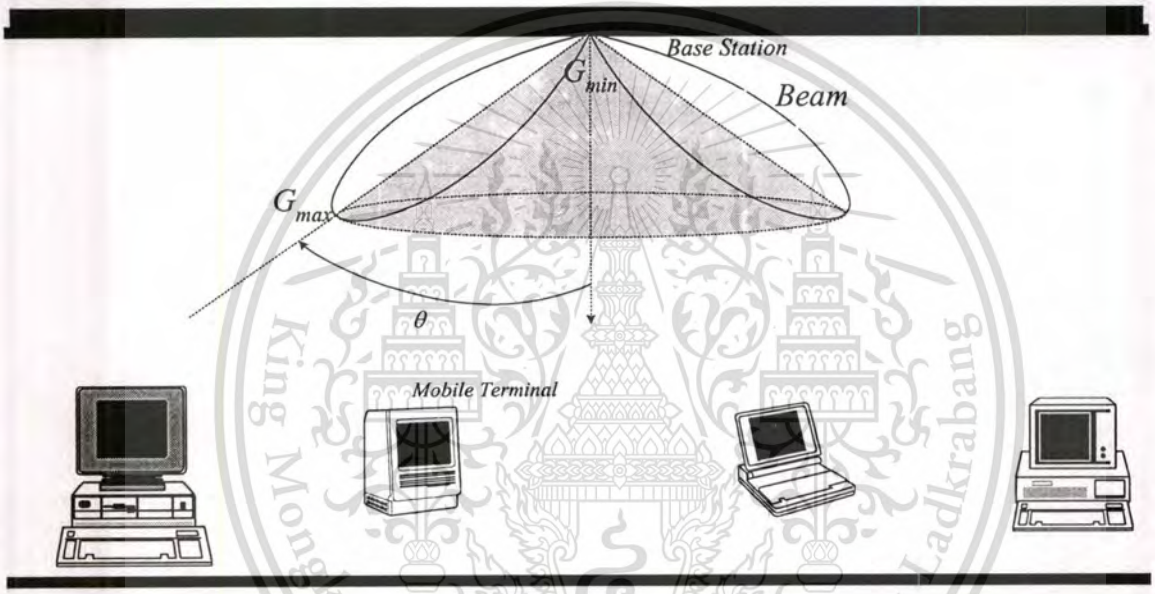

Fig.1.2 Application of a circularly polarized conical beam spherical slot array antenna for wireless Local Area Network system

1.2 Purpose and Scope of the Thesis

This thesis has proposed a so-called spherical slot array antenna. The structure of the antenna is simple and suitable for mass production. This thesis is focused on the design of the spherical slot array antenna to radiate the circularly polarized conical beam to meet the requirement of the land mobile satellite communication and broadcasting service in addition to wireless Local Area Network systems. The antenna characteristics such as radiation pattern,

directivity, elevational angle and azimuthal pattern are consequently investigated by using Method of Moments with the aids of the dyadic Green's functions. Also, the design criteria of the further applications are provided. The antenna measurement is set up to confirm the proposed principle.

1.3 Outline of Remaining Chapters

As an introductory chapter, this chapter has mentioned about the overview of this thesis. The usefulness, objective, scope and organization of this thesis are summarized. As referred above that this thesis aims to propose a so-called spherical slot array antenna, the electromagnetic field radiated from a spherical slot array antenna will be preliminarily studied in the next chapter, Chapter 2. The field radiated from all the slots is derived by solving the boundary value problem. To simplify in calculation, the sinusoidal current distribution is reasonably assumed. The radiation patterns for various parameters are substantially investigated. The antenna design parameters that meet the optimum radiation characteristics are primarily selected as the guideline of the antenna design. However, the rigorous analysis of the antenna characteristics is still to be essentially conducted.

Chapter 3 expresses the rigorous theoretical formulations of the antenna characteristics using the Method of Moments. The integral equations are significantly formulated based on the Field Equivalent Principle and the boundary conditions. They can be written in the form of the integration of the product between dyadic Green's functions and unknown currents to be determined. The dyadic Green's functions are derived to complete the integral equations.

Chapter 4 investigates characteristics of the spherical slot array antenna. The basis function and weighting function are expanded to solve the integral equation by means of Method of Moments. The unknown currents are

determined by solving the integral equations and the antenna characteristics are subsequently examined.

Chapter 5 characterizes the other significant antenna properties i.e., impedance and polarization. The matching condition between the antenna and the transmission line is clarified and the axial ratio is significantly revealed. Ultimately, the optimum design parameters of the antenna are determined.

Chapter 6 verifies the proposed principle and theory that has presented in the preceding chapters by the measurements. The prototypes of the antenna were fabricated corresponding to the design parameters suggested in the previous chapters. The experimental results of radiation pattern, input impedance and axial ratio are reported.

Chapter 7 summarizes the consequence of the material presented in the preceding chapters together with the discussions for the further study.

Eventually, the expression of the special functions in spherical coordinates that is very useful for the study of the spherical slot array antenna as well as the derivation of the dyadic Green's functions are reported in the appendices.

References

[1-1]S.R.Rengarajarn and L.G.Josefsson, "Slotted waveguide array antenna technology," *IEEE AP-S and URSI National Radio Science Meeting*, California, June 1995.

[1-2]J.Hirokawa, M.Ando, and N.Goto, "Waveguide-fed parallel plate slot array antenna," *IEEE Trans. Antennas Propagat.*, vol.40, no.2, pp.218-223, Feb.1992.

[1-3]A.F.Stevenson, "Theory of slots in rectangular wave-guides," *J. Appl. Phys.*, vol. 19, no.1, pp.24-38, Jan.1948.

[1-4]J.Galejs, "Admittance of rectangular slot which is backed by a rectangular cavity," *IEEE Trans. Antennas Propagat.*, vol.11, no.3, pp.119-126, Mar.1963.

[1-5]A.Kumar and H.D.Hristov, *Microwave Cavity Antennas*, Artech House, Inc., Norwood, 1989.

[1-6]A.F.Peterson and R.Mittra, "Mutual Admittance between Slot in Cylinders of Arbitrary Shape," *IEEE Trans. Antennas Propagat.*, vol. 37, no.7, pp.858-864, July 1989.

[1-7]R.F.Goodrich, R.F.Kleinman, A.L.Maffett, C.E.Schensted, K.M. Siegel, M.G.Chernin, H.E.Shanks and R.E.Plummers, "Radiation from Slot Arrays on Cones," *IRE Trans. Antennas Propagat.*, pp. 213-222, July 1959.

[1-8]Y.Mushiake and R.E.Webster, "Radiation characteristics with power gain for slots on sphere," *IRE Trans. Antennas Propagat.*, vol.5, no.1, pp.47-55, Jan.1957.

[1-9]N.Terada and K.Kagoshima, "Conical beam bifilar helical antenna for mobile satellite communications," *IEICE Technical Report*, AP91-38, June 1991.

[1-10]T.Hori, N.Terada and K.Kagoshima, "Broadband circularly polarized microstrip antenna with a conical beam," *IEICE Nat. Conv. Rec.,637*, March 1986.

[1-11]J.Takada, A.Tanisho, K.Ito and M.Ando, "Circularly polarised conical beam radial line slot antenna," *Electronic Letters*, vol.30, no.21, pp.1729-1730, Oct.1994.

[1-12]J.Takada, T.Yamamoto, M.Ando and N.Goto, "Circularly polarized multibeam radial line slot antennas for mobile satellite communication," *Proc. IEEE Antennas Propagat. Society Int. Symp.*, pp.1430-1433, June 1995.

[1-13]C.Phongcharoenpanich, M.Krairiksh and J.Takada, "Investigations of radiation characteristics of a circularly polarized conical beam spherical slot array antenna," *IEICE Trans. Electronics*, vol.E82-C, no.7, pp.1242-1247, July 1999.

[1-14]R.Cochetti, *Mobile Satellite Communications Handbook*, Quantumn Publishing, Inc., California, 1995.

[1-15]C.Phongcharoenpanich, M.Maruekin, M.Krairiksh and J.Takada, "A circularly polarized conical beam spherical slot array antenna for land mobile satellite communication," *Proceedings of the 39th Kasetsart University Annual Conference*, Bangkok, pp.217-226, April 2001.

[1-16]J.D.Gibson, *The Mobile Communications Handbook*, CRC Press, Florida, 1996.

Chapter 2

Preliminary Investigations of a Spherical Slot Array Antenna

2.1 Introduction

A spherical slot array antenna is proposed in this chapter. The structure of the antenna is revealed. In order to meet the applications of the mobile satellite communications and wireless LAN systems, the spherical slot array antenna is designed to generate circularly polarized conical beam pattern. The preliminary principle of the antenna design is consequently described and the radiated field from the antenna is expressed. Then, the radiation patterns of the antenna for various parameters are investigated. In the last place, the parameters that yield the conical beam pattern will be selected as the initial parameters for further investigations of the antenna in the succeeding chapters.

2.2 Configuration of a Spherical Slot Array Antenna

As previously mentioned that this thesis is focused on the design of the circularly polarized conical beam spherical slot array antenna. In this circumstance, the antenna is composed of a number of two perpendicular slots, to form a slot pair, cut on an outer surface of the concentric conducting spherical cavity enclosed by the conducting conical surface. Fig.2.1 shows two slots that are perpendicularly arranged to form a unit of circularly polarized radiator. The slot length and width are l_s and w_s, respectively. A number of slot pairs are arranged as a ring along an azimuthal circumference of the outer surface of the concentric conducting spherical cavity. Each slot is separated, along an elevational plane, at a certain distance so that the phase quadrature is obtained to provide the circularly polarized radiation. Fig.2.2(a) and Fig.2.2(b) show the top and bottom views of a circularly polarized conical beam spherical

slot array antenna. One of the slots in a pair is oriented counterclockwise at an angle γ_1 with respect to the horizontal line of the concentric conducting spherical cavity whereas the perpendicular counterpart is oriented at an angle of γ_2 as illustrated in Fig.2.2(c). These slots are backed by the concentric conducting spherical cavity of which the inner and outer spherical radii are R_a and R_b, respectively. These spherical conductors are shorted by the conducting conical surface at an angle θ_c. The cross-sectional view of the antenna is figured in Fig.2.2(d). This cavity-backed slot array antenna is excited by a linear electric probe of the length l_p in the radial direction. It is protruded through the inner surface of the cavity. The location of the excitation is at the position $R_a \leq R_f \leq R_a+l_p$, $\theta_f=\theta_p$, $\phi_f=0°$ as shown in Fig.2.3. The center of each slot pair is denoted by an angle θ_s. Each slot in a pair is offset from this position at the distance d_θ in opposite direction so that phase quadrature between these two of a slot pair is obtained. The azimuthal spacing between slot pairs is s_ϕ. The number of slot pairs is N_s.

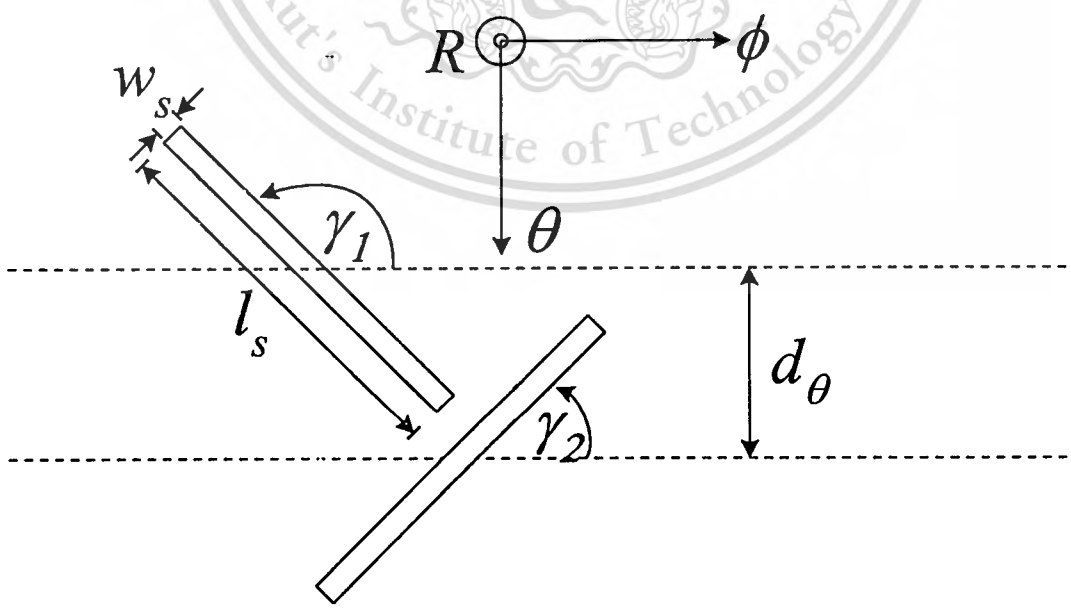

Fig.2.1 Two perpendicular slots form a slot pair of circularly polarized radiator

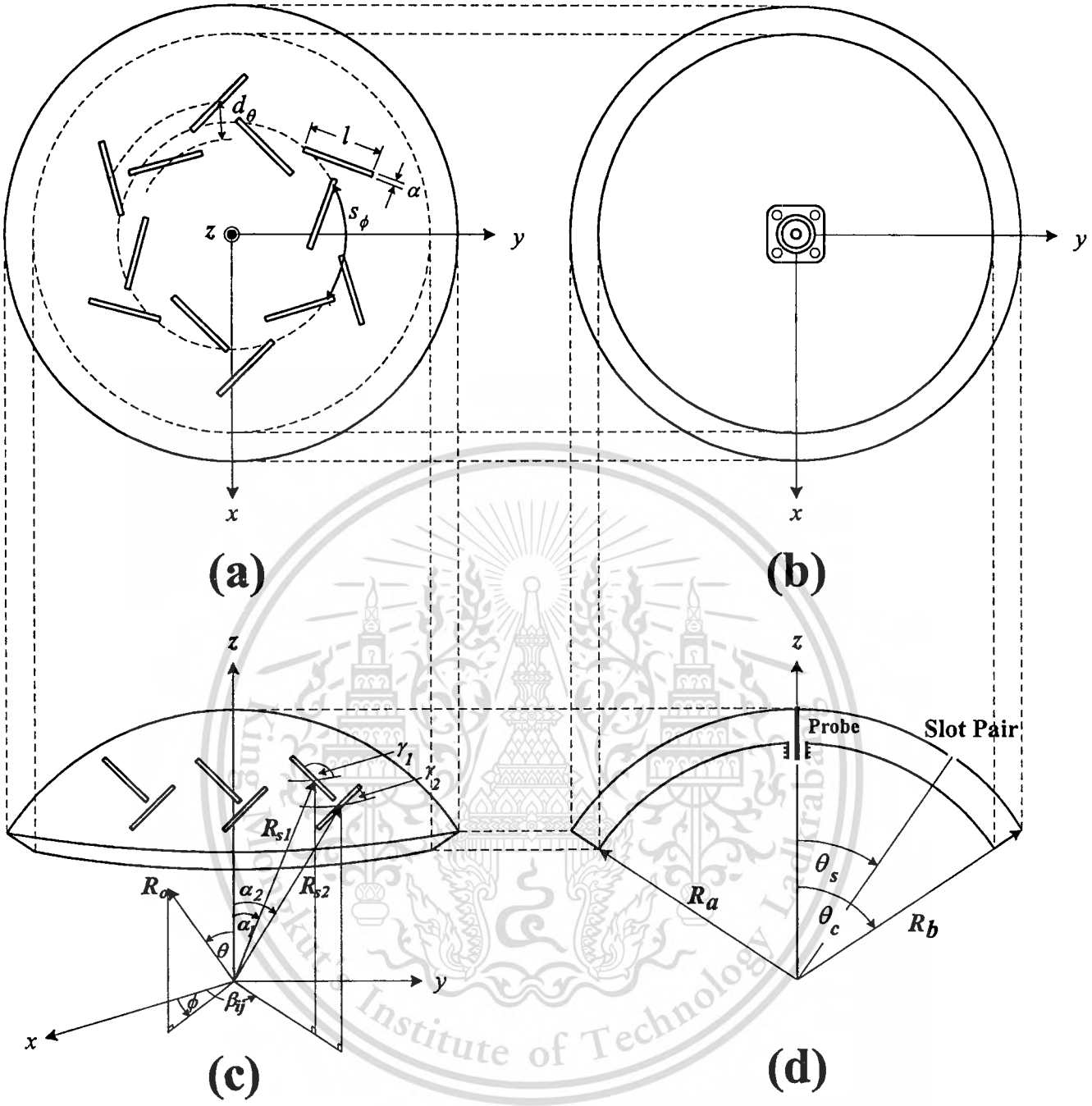

Fig.2.2 A circularly polarized conical beam spherical slot array antenna

(a) top view (b) bottom view

(c) perspective view (d) cross-sectional view

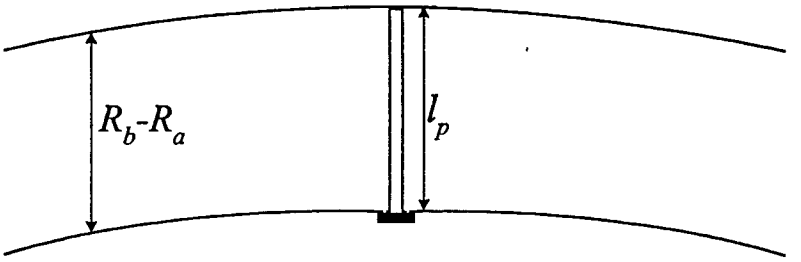

Fig.2.3 Location of the excited probe inside the concentric conducting spherical cavity enclosed by the conducting conical surface

2.3 Principle of the Design of a Circularly Polarized Conical Beam Spherical Slot Array Antenna

From the antenna structure described in the previous section, the antenna parameters will be designed as the initial guidelines for further analysis. By considering the electric dyadic Green's functions [2-1] and the source function directs along the radial direction, it is obvious that the transverse magnetic mode is considerably coupled to the cavity. From the expression of the electromagnetic field simulated from all components in conjunction with the boundary condition that the tangential field vanishes at the conducting surface [2-2]-[2-3], the inner and outer spherical radii, R_a and R_b, can be determined by solving the characteristic equation [2-4]

$$\frac{j_n'(kR_a)}{y_n'(kR_a)} = \frac{j_n'(kR_b)}{y_n'(kR_b)}, \tag{2.1}$$

where $j_n'(*)$ and $y_n'(*)$ denote the derivative with respect to the argument of the spherical Bessel functions of the first and second kinds of order n, respectively. k represents the propagation constant of the medium inside the cavity and the cavity stated in this thesis is air-filled.

The next parameter that is necessary to be designed is the shorted conical angle θ_c of the cavity. It can be calculated by imposing the electric field at the boundary to be vanished, thus

$$P_n^m(\cos\theta)\Big|_{\theta=\theta_c} = 0, \tag{2.2}$$

where $P_n^m(\cos\theta)$ denotes the associated Legendre function of the first kind of order (n,m). Moreover, m represents the number of cycles of field variation in ϕ direction.

After the dimension of the cavity (R_a, R_b, θ_c) is obtained, the location of the slot orientation is subsequently investigated. The position of the center of slot pair θ_s is chosen where the surface current density is maximum. Therefore, it can be found by maximizing

$$\theta_s\Big|_{\theta}^{max} \frac{dP_n^m(\cos\theta)}{d\theta}. \tag{2.3}$$

It is noted that each of two slots is offset from the center line in the elevational plane at the distance $d_\theta/2$. It is expected that each slot in a pair is excited by equal amplitude with the quadrature phase.

Since this structure is excited by the linear electric probe, hence, its location is at an angle where the maximum field in radial direction is satisfied.

$$\theta_p\Big|_{\theta}^{max} P_n^m(\cos\theta) \tag{2.4}$$

To obtain the right-hand circular polarization, we excite two perpendicular slots with identical amplitude but quadrature phase. The phase of slot number *2* leads that of number *1* by *90°*. Since the surface current density that excites the slots is proportional to E_θ and H_ϕ which are proportional to the derivative of the associated Legendre function of cosine of angle θ that is

$$E_\theta, H_\phi \propto \frac{dP_n^m(cos\theta)}{d\theta}, \tag{2.5}$$

therefore, the orientation of these slots are *45°* and *135°* with respect to the horizontal line where the surface current density is maximum. The spacing between the center of these two slots along the elevational plane is adjusted so that phase difference of E_θ is *90°*. The slot array consists of a number of slot pairs arranged in the same manner as described above at the specific position in order that the spacing between the center of each slot pair is equal to $2m\pi/N$ (N is the number of slot pairs).

For a specified directivity, the number of slot pairs, the outer spherical radius and the slot position will be determined. To design a circularly polarized conical beam spherical slot array antenna, the concentric conducting spherical cavity is first designed to excite the slot array. When the number of slot pairs is fixed, the mode number m (the number of cycles along the tangential circumference of the cavity) can be determined to be one half of the number of slot pairs. We found from (2.1) that the spherical radii depend on the mode number n, therefore, n must be appropriately chosen for a particular directivity. Since the field distribution in the cavity depends on the mode of the cavity, hence the dimension, the slot position and the feed probe position are different. Fig 2.4 and Fig 2.5 show the graphical characteristic in the radial and the

elevational direction of the TM_{mn} mode for m is fixed at *3* and n is varied from *6* to *8* and for m = *3,6* with n is fixed at *8*. To estimate the orientation of the slot and the probe position for the TM_{38} mode, the electric and magnetic fields are revealed as depicted in Fig. 2.6 and Fig. 2.7, respectively.

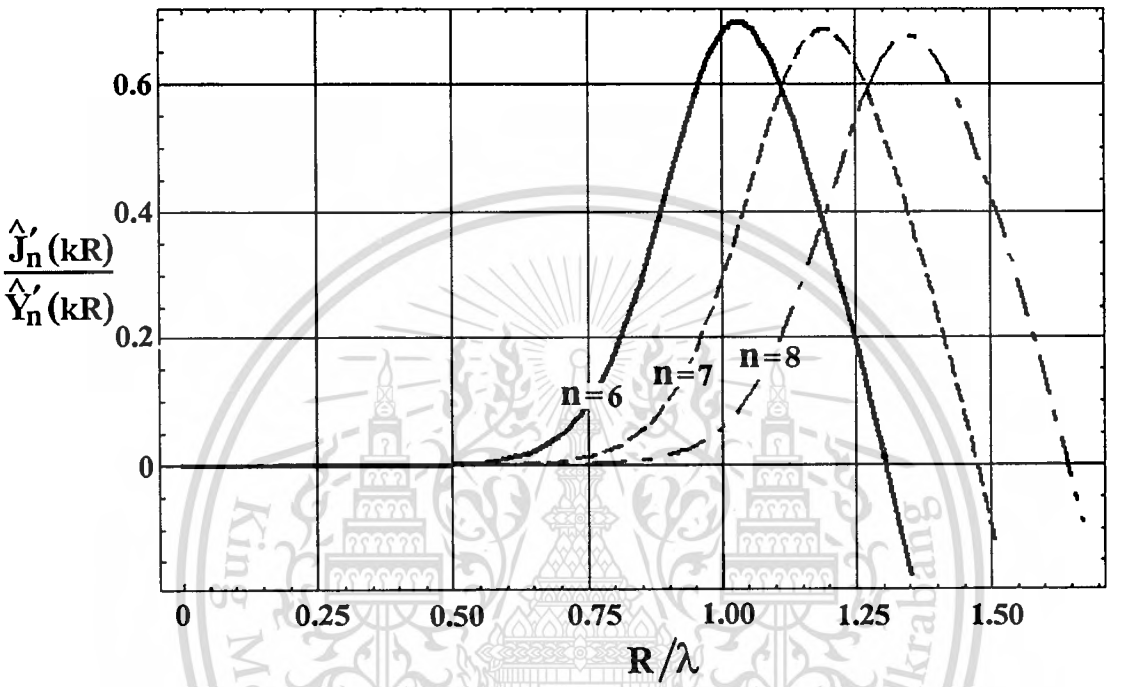

Fig.2.4 Graphical characteristic in the radial direction of the TM_{mn} mode (*n=6,7,8*)

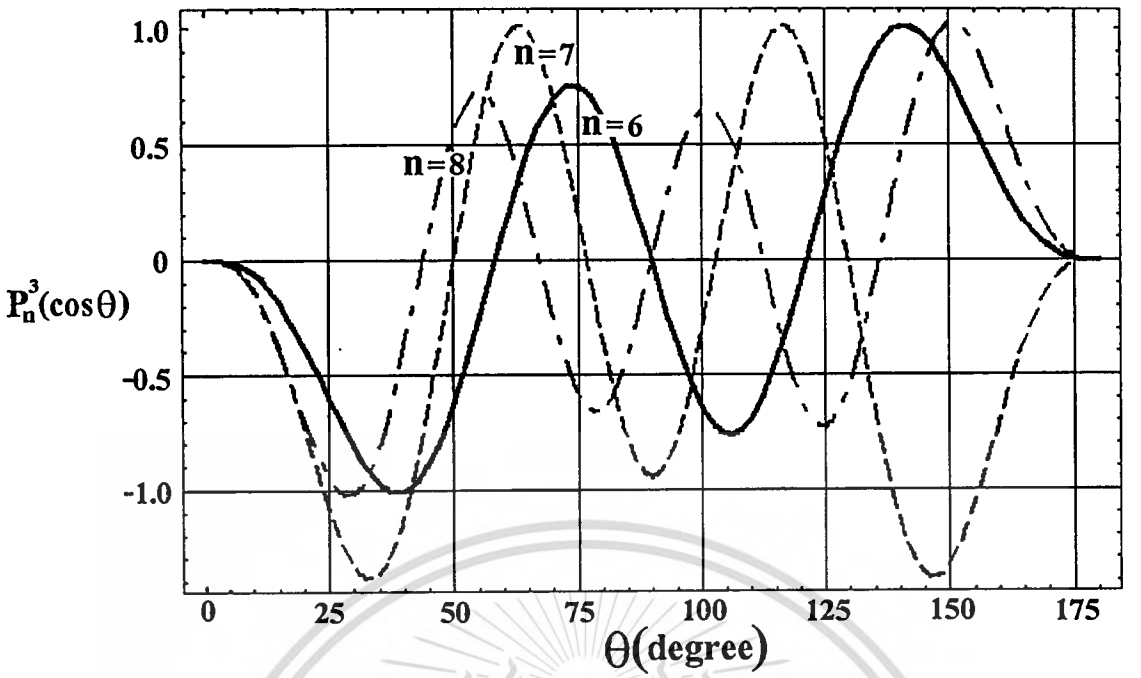

(a)

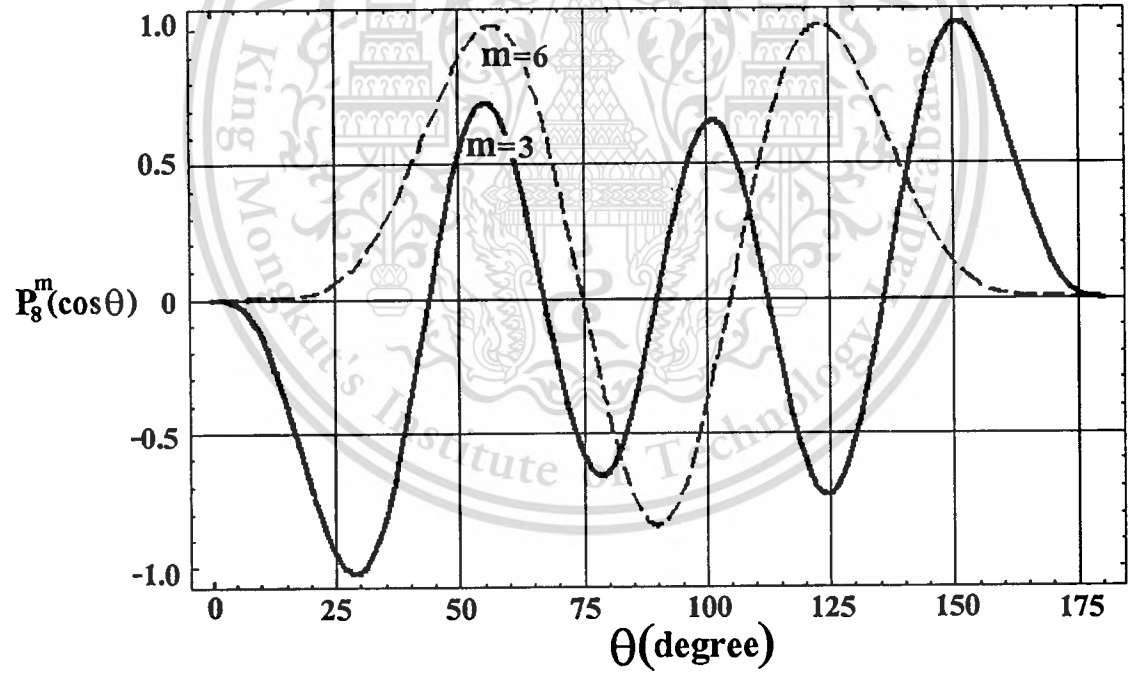

(b)

Fig 2.5 Graphical characteristics in the elevational direction of the TM_{mn} mode ($m=3$, $n=6,7,8$ and $m=3,6$, $n=8$)

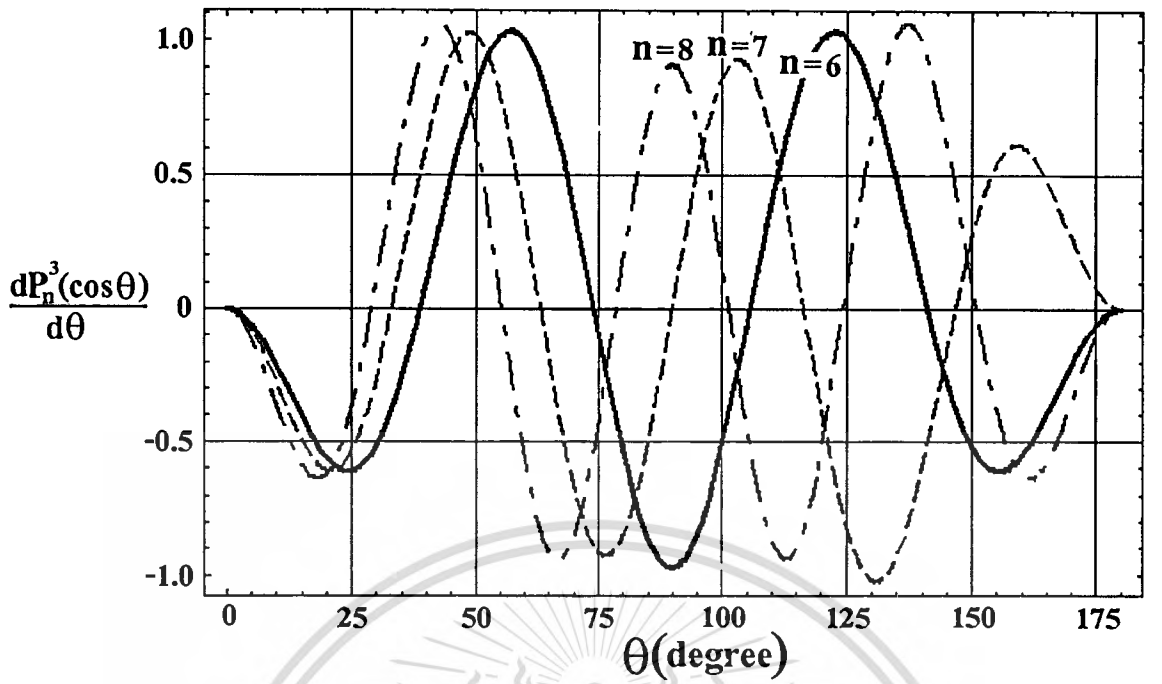

(c)

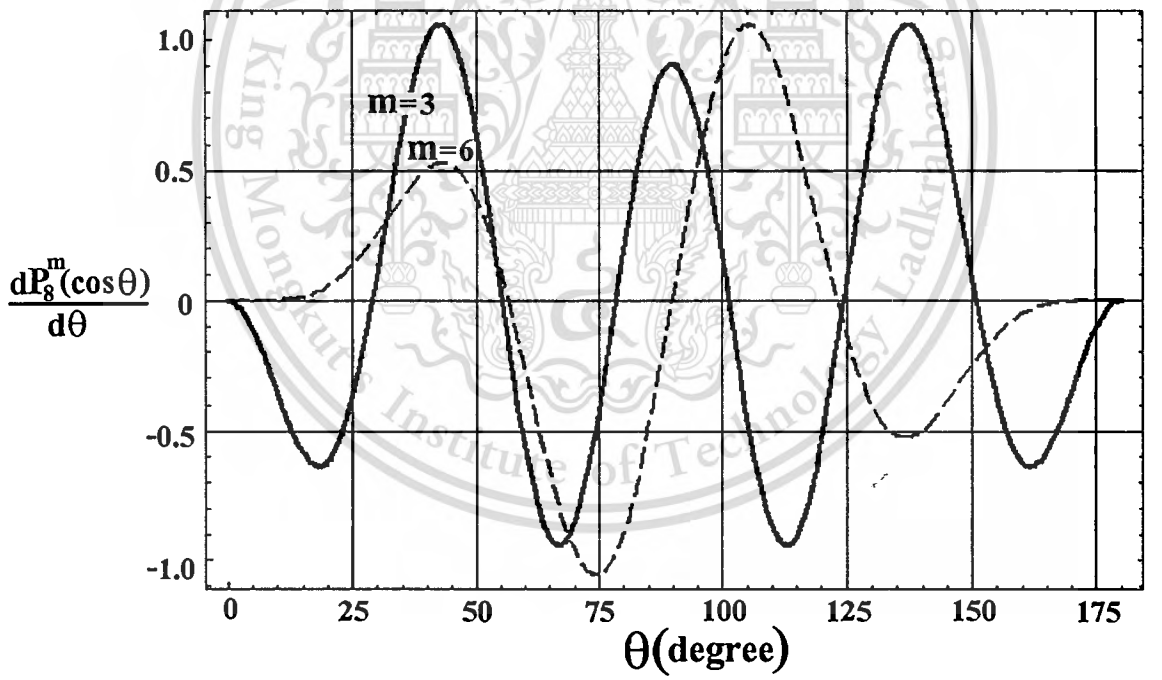

(d)

Fig 2.5 Graphical characteristics in the elevational direction of the TM_{mn} mode ($m=3$, $n=6,7,8$ and $m=3,6$, $n=8$)

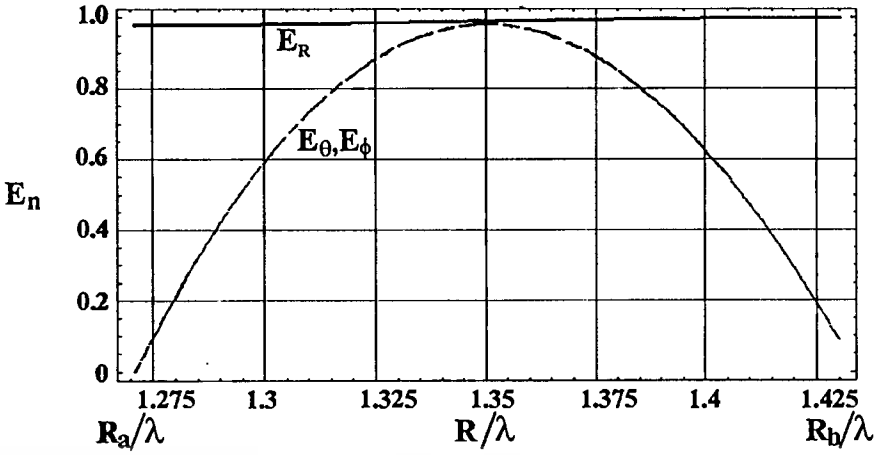

(a)

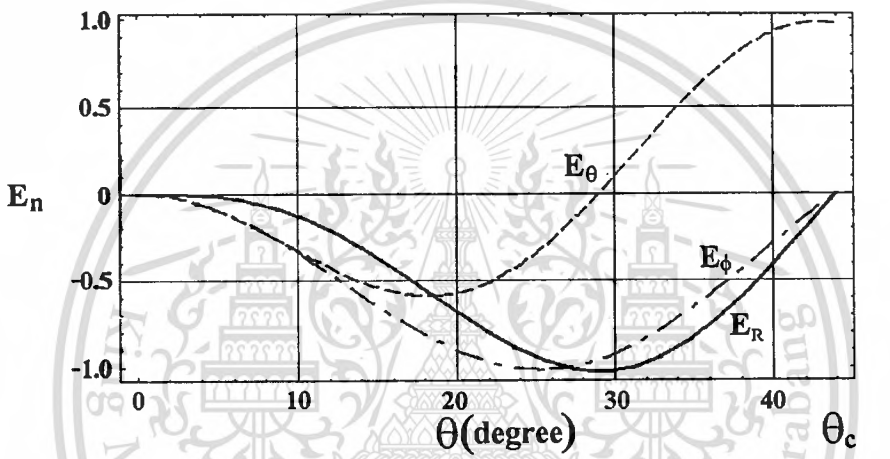

(b)

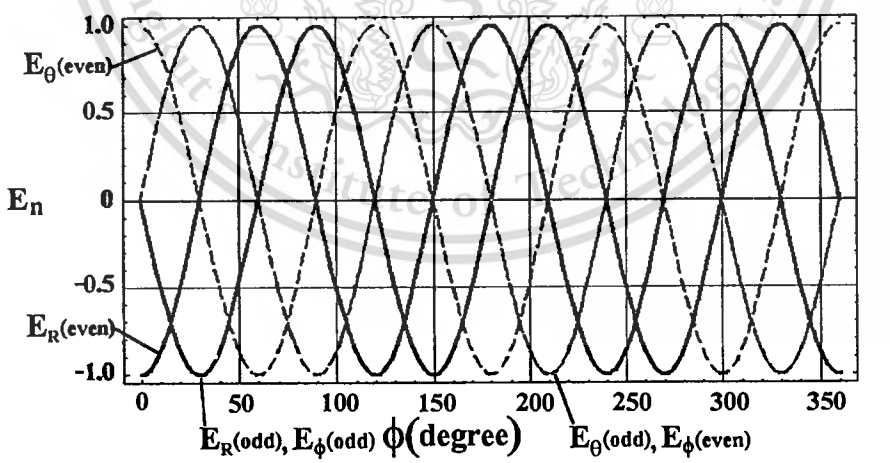

(c)

Fig.2.6 Electric field of TM_{38} mode

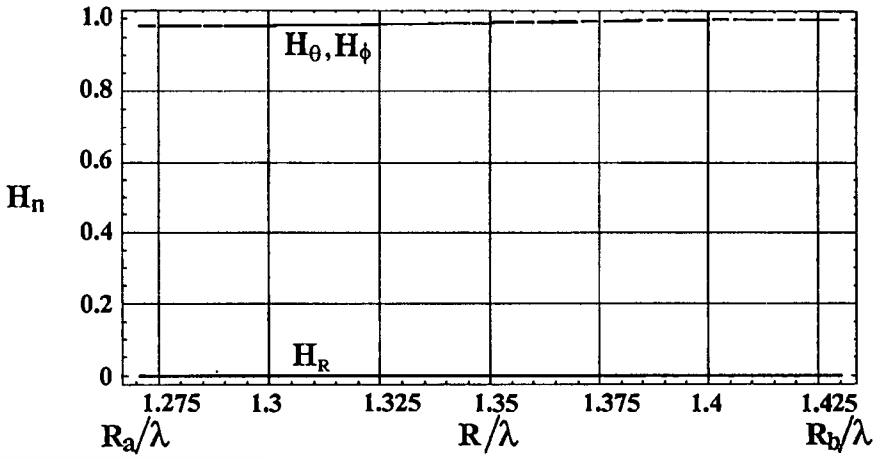

(a)

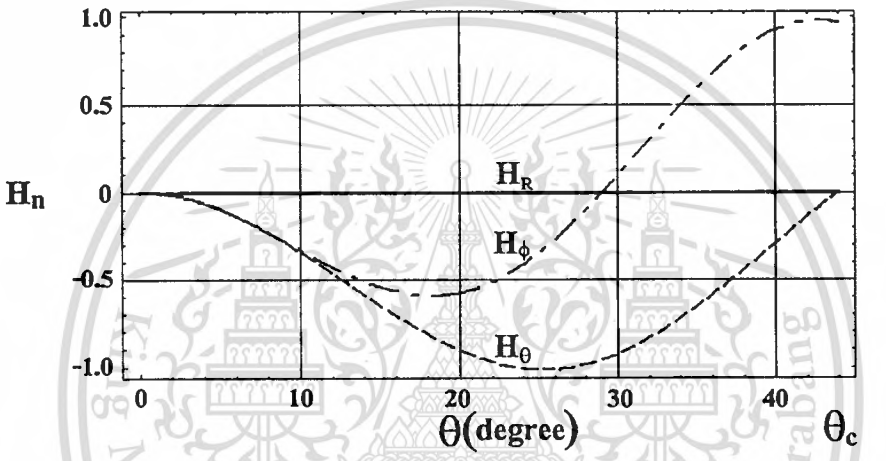

(b)

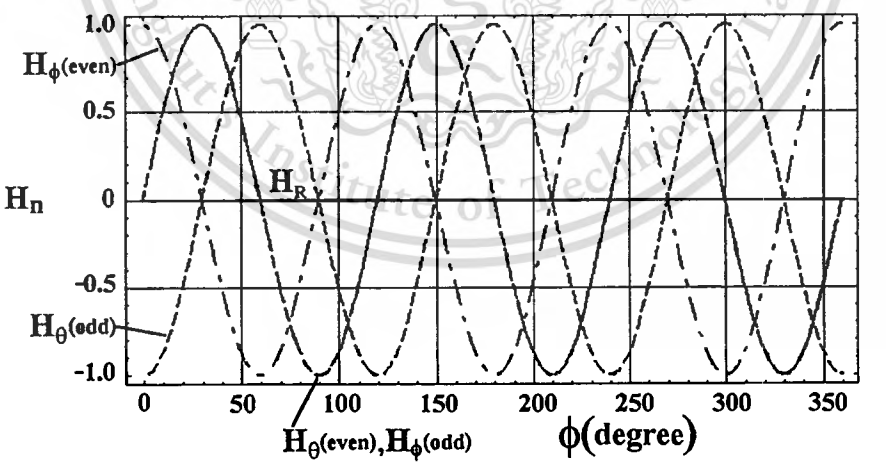

(c)

Fig.2.7 Magnetic field of TM_{38} mode

Table 2.1 summarizes the aforementioned quantity for four different mode cavities. In case of TM_{38}, for instance, the ratio of outer radius to inner radius (R_b:R_a) is *9:8* and the outer spherical radius is 1.43λ. The conical angle can be at 43.96°, 67.34° or 90.00° while the feeding probe position is either at 29.08° or 55.42°. The slot position is either at 16.19°, 42.77° or 64.94°. Let us compare the quantities of TM_{38} and TM_{68} modes surrounded by dashed lines, we can realize that even though they are somewhat different, the outer radius and the slot position (θ_s) are not significantly different. In such case, we can excite the different mode cavities with similar dimension of the outer radius and slot position. Therefore, the number of slot pairs can be increased to provide uniform azimuthal pattern by using the same antenna size.

Table 2.1 Dimensions of a concentric conducting spherical cavity, the feeding probe position and the slot position

mode	R_b:R_a	R_b/λ	$\theta_c(^\circ)$	$\theta_p(^\circ)$	$\theta_s(^\circ)$
TM_{36}	7:6	1.11	58.52	38.83	24.45
			90.00	74.12	57.26
			121.48		90.00
TM_{37}	8:7	1.27	50.16	33.22	20.91
			76.93	63.34	48.91
			103.07		76.64
TM_{38}	9:8	1.43	43.96	29.08	16.19
			67.34	55.42	42.77
			90.00		64.94
TM_{68}	9:8	1.43	75.04	56.79	41.13
			104.96	90.00	74.05

In order to design the antenna with the appropriated dimensions and slot positions, any values of those parameters can be chosen. After the cavity is designed and the probe position is set at $R_a \leq R_f \leq R_a+l_p$, $\theta_f = \theta_p$,$\phi_f = 0°$ then the first slot pair is cut at a position of ϕ equal to $m\pi/N$ away from the probe. The second slot pair is at the position of $2m\pi/N$ .The arrangement of the progressive slot pairs is in the same manner as described above.

2.4 Radiated Fields from the Antenna

The radiation fields of a circularly polarized conical beam spherical slot array antenna designing based on the higher mode of the cavity model are formulated in this section. The radiation patterns of the spherical slot array antenna are determined from the combination of the slots in the pairs, and these slot pairs are arranged as the spherical array, subsequently. Let us consider the slot located at the local coordinate (R_b,ξ,ζ) as shown in Fig.2.8.

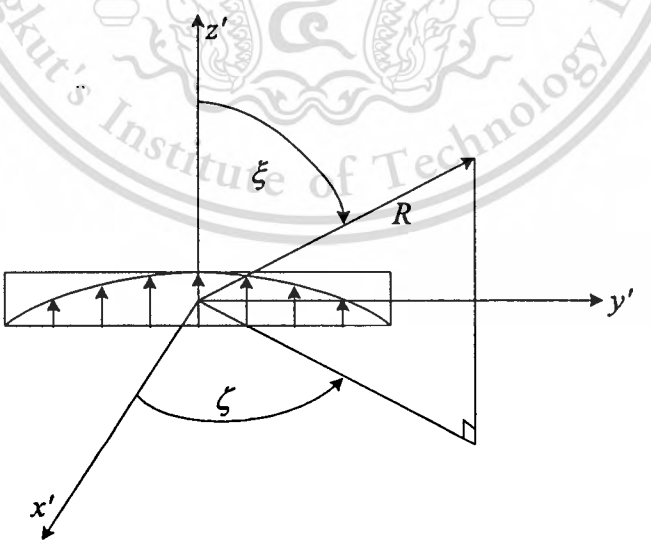

Fig.2.8 Local coordinates of the slot on spherical surface

The radiation pattern of a slot on a spherical conducting surface can be derived by solving the electromagnetic boundary value problem. The aperture field distribution along the slot is reasonably assumed to be sinusoidal to simplify in calculation. The radiation fields can be expressed by the summation of eigenfunctions in the spherical coordinates as follows:

$$f_\xi(R_b,\xi,\zeta)=\sum_{m=0}^{\infty}\sum_{n=m}^{\infty} f_m (j)^n \left[\frac{jA_{mn}^{TE}}{\alpha} \frac{1}{h_n^{(2)}(kR_b)} \frac{dP_n^m(\cos\xi)}{d\xi} + \frac{A_{mn}^{TM}}{\alpha} \frac{kR_b}{\left[kR_b h_n^{(2)}(kR_b)\right]'} \frac{mP_n^m(\cos\xi)}{\sin\xi} \right] \cos(m\zeta) \tag{2.6}$$

$$f_\zeta(R_b,\xi,\zeta)=\sum_{m=0}^{\infty}\sum_{n=m}^{\infty} f_m (j)^n \left[\frac{jA_{mn}^{TE}}{\alpha} \frac{1}{h_n^{(2)}(kR_b)} \frac{mP_n^m(\cos\xi)}{\sin\xi} + \frac{A_{mn}^{TM}}{\alpha} \frac{kR_b}{\left[kR_b h_n^{(2)}(kR_b)\right]'} \frac{dP_n^m(\cos\xi)}{d\xi} \right] \sin(m\zeta) \tag{2.7}$$

The coefficients are given as follows:

$$f_m = \begin{cases} \dfrac{1}{\pi k R_b}(1-\cos(kl)) & ; m=0 \\ \dfrac{1}{\pi R_b}\sin(kl) & ; m=kR_b \\ \dfrac{1}{\pi}\dfrac{2kR_b}{(kR_b)^2-m^2}\left[\cos\left(\dfrac{ml}{R_b}\right)-\cos(kl)\right] & ; \text{elsewhere} \end{cases} \tag{2.8}$$

where $h_n^{(2)}(\cdot)$ denotes the spherical Hankel function of the second kind of order n, and $P_n^m(\cdot)$ denotes the associated Legendre function of order (n,m). The primed bracket designates for the derivative of the function in the bracket with respect to the argument (kR_b). The radiation fields of the spherical slot array antenna can be written as the combination of the field from the total number of slots which are arranged to form the circularly polarized conical beam as [2-5]

$$\overline{E}(\theta,\phi) = \sum_{j=1}^{N}\sum_{i=1}^{2} f(R_b,\xi_{ij},\zeta_{ij})e^{j(kR_b\cos\xi_{ij}+\psi_i)} \tag{2.9}$$

and

$$\begin{aligned} f(R_b,\xi_{ij},\zeta_{ij}) &= f_\xi(R_b,\xi_{ij},\zeta_{ij})[\cos\gamma_i - \sin\gamma_i]\hat{\xi}_{ij} \\ &\quad - f_\zeta(R_b,\xi_{ij},\zeta_{ij})[\cos\gamma_i + \sin\gamma_i]\hat{\zeta}_{ij} \end{aligned} \tag{2.10}$$

where $\hat{\xi}_{ij}$ and $\hat{\zeta}_{ij}$ are unit vectors along the slot local coordinates, respectively, and ψ_i is the phase of the slot number i. It is noted that the phase difference between the two slots (ψ_1-ψ_2) is assumed to be $90°$. Additionally, to express the term of source point (R_b,ξ_{ij},ζ_{ij}) as the term of the observation point (R,θ,ϕ), the contribution of these coordinate transformations are used:

$$\cos\xi_{ij} = \frac{\overline{R}_{si}\cdot\overline{R}_o}{|\overline{R}_{si}||\overline{R}_o|} \tag{2.11a}$$

$$= \sin\alpha_i\sin\theta\cos(\phi-\beta_{ij}) + \cos\alpha_i\cos\theta \tag{2.11b}$$

$$\tan\zeta_{ij} = \frac{\sin\theta\sin(\phi-\beta_{ij})}{\cos\alpha_i\sin\theta\cos(\phi-\beta_{ij})-\sin\alpha_i\cos\theta} \tag{2.12}$$

$$\hat{\xi}_{ij} = -\frac{\sin\alpha_i\cos\theta\cos(\phi-\beta_{ij})-\cos\alpha_i\sin\theta}{\sin\xi_{ij}}\hat{\theta} + \frac{\sin\alpha_i\sin(\phi-\beta_{ij})}{\sin\xi_{ij}}\hat{\phi} \tag{2.13}$$

$$\hat{\zeta}_{ij} = -\frac{\sin\alpha_i\sin(\phi-\beta_{ij})}{\sin\xi_{ij}}\hat{\theta} - \frac{\sin\alpha_i\cos\theta\cos(\phi-\beta_{ij})-\cos\alpha_i\sin\theta}{\sin\xi_{ij}}\hat{\phi} \tag{2.14}$$

where $\overline{R}_O$ is the position vectors of the observation point, $\overline{R}_{si}$ is the position vectors of the location of slot number i, α_i is the elevational angle of the slot number i, and β_{ij} is the azimuthal angle of slot number i in the slot pair number j, respectively.

2.5 Radiation Pattern of the Antenna

From the formulations of the radiated fields determined as described in the prior sections, the radiation pattern of a circularly polarized conical beam spherical slot array antenna will be disclosed in this section. By consideration of the external radiation of the electromagnetic fields from the antenna, it is evident that the parameters impacted on the radiation pattern are the angle of slot pair position and the spherical radius [2-6]. As the initial parameters as tabulated in Table 2.1, the radiation pattern of the antenna for various angles of

slot pair positions are calculated and plotted in Fig.2.9. The outer spherical radius is fixed at 1.43λ. It is found that the elevational beam peak is substantially varied as the angle of the slot pair position is changed. For instance, if the angle of the slot pair position is located at an angle of $20°$, the elevational beam peak directs at an angle of $55°$. It is observed that the elevational beam peak position is higher when the angle of the slot pair position is increased until the certain slot pair position at $45°$. Then the peak position will be very high again even the position of the slot is lower.

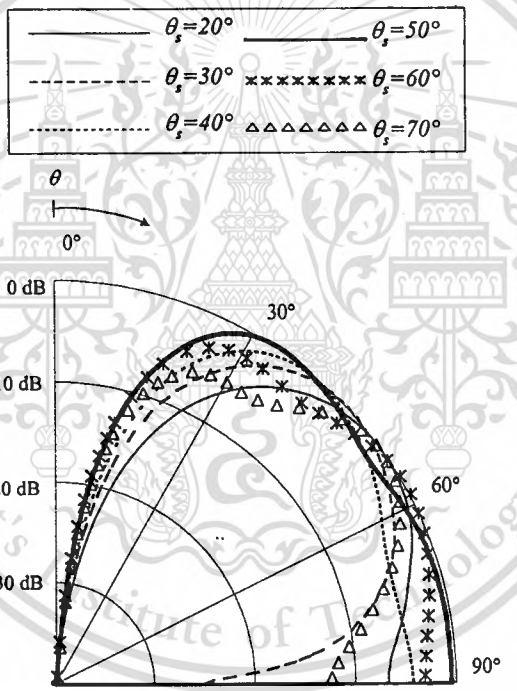

Fig.2.9 Radiation pattern for various angles of slot pairs

In addition, the radiation pattern for various spherical radii is also investigated. It is apparent, in Fig.2.10, that the elevational radiation is changed as a function of the spherical radius. It is found that the larger the spherical radius the higher the elevational beam peak position.

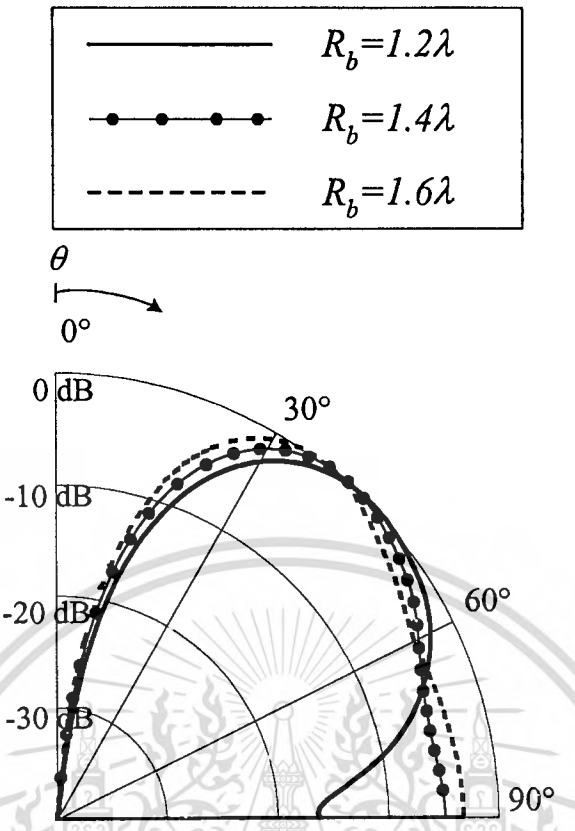

Fig.2.10 Radiation pattern for various spherical radii

Another parameter to be mentioned in this section is the number of elements. It is pointed that for the constant spherical radius and angle of slot pair position, the azimuthal ripple depends on the number of the slot pairs. From Fig.2.11, it is obvious that the there are azimuthal ripples in case of the number of slot pairs is *4*. The level of the ripple is *14* dB. It is noted that the azimuthal ripple is not desirable since the loss of the power occurs when the mobile terminal is moved. It is *1* dB in case of the number of slot pairs is *8*. When the number of slot pairs is increased to *12*, no ripple is observed. This confirms that in order to yield the nondirectional in azimuthal plane, the number of elements should be sufficiently large.

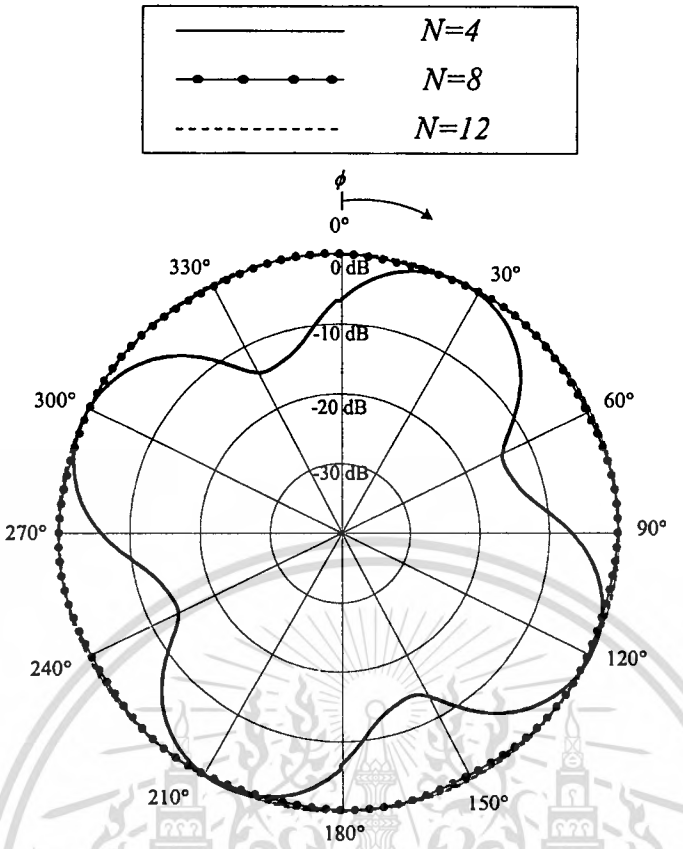

Fig.2.11 Azimuthal pattern for various number of elements

2.6 Conclusion

This chapter shows the antenna configurations. The structure of the antenna is simple and suitable for mass production. The antenna is designed to radiate the conical beam with circular polarization. This structure is very useful to be the antenna for the subscriber unit of the mobile satellite communications and for the base station of the wireless LAN systems. The expressions of the radiated field are determined and the radiation pattern is subsequently investigated. It is obvious that the radiation characteristics of the antenna depend primarily on the outer spherical radius and the angle of the center of slot pair position. These parameters are initially chosen as the guideline for the antenna design.

References

[2-1]C.Phongcharoenpanich, M.Krairiksh and J.Takada, "Dyadic Green's functions of the concentric conducting spherical cavity," *Proceeding of the 1997 Asia-Pacific Microwave Conference*, Hong Kong, vol. 2, pp. 757-760, Dec. 1997.

[2-2]C.Phongcharoenpanich, "Electromagnetic field analysis of the conducting spherical cavity and segment," Master Thesis of King Mongkut's Institute of Technology Ladkrabang, 1998.

[2-3]C.Phongcharoenpanich, E.Khoomwong and M.Krairiksh, "Simulations of EM fields inside the concentric conducting spherical cavity using the FD-TD in spherical coordinates," *Proceedings of the 5th International Symposium on Antennas, Propagation and Electromagnetic Theory*, Beijing, pp.142-145, Aug. 2000.

[2-4]M.Krairiksh, T.Wakabayashi and W.Kiranon, "A spherical slot array applicator for medical applications," *IEEE Trans. Microwave Theory Tech.*, vol.43, no.1, Jan. 1995.

[2-5]C.Phongcharoenpanich, M.Krairiksh and J.Takada, "A concentric conducting spherical cavity-backed slot array antenna radiating circularly polarized conical beam," *Proceedings of the 1999 Progress in Electromagnetics Research Symposium*, Taipei, vol.2, p.708, Mar. 1999.

[2-6]C.Phongcharoenpanich, M.Krairiksh and J.Takada, "Characteristics of a circularly polarized conical beam spherical slot array antenna," *Proceedings of the 2000 Asia-Pacific Microwave Conference*, Sydney, pp.38-41, Dec. 2000.

Chapter 3

Theoretical Formulations of the Antenna Characteristics · Using Method of Moments

3.1 Introduction

In order to conduct the phenomenal electromagnetic fields of the antenna; both inside and outside the cavity, the rigorous formulations of the integral equations taken into account of all the antenna structure are addressed. The dyadic Green's functions are derived to complete the integral equations. The Method of Moments plays a vital tool in solving the integral equations. The entire domain basis functions and Galerkin's method of weighting functions are reasonably selected.

3.2 Analysis Model

From the antenna configuration depicted in the previous chapter, it consists of the slot apertures and a linear electric probe inside the cavity as shown in Fig.3.1(a) again. It is evident that this structure possesses the discontinuities in structure at the slot and the probe. In order to dispose these discontinuities, the Field Equivalent Principle [3-1] is applied by following these conditions:

- For the slot aperture
  - Assuming the perfectly electric conducting surface encloses the original problem as dash lines shown in Fig.3.1(b).
  - The magnetic current $\overline{M}$ is assumed at the slot aperture in both inside and outside of the cavity. They have opposite direction to each other i.e., outside the cavity $\overline{M} = \overline{E} \times \hat{n}$ and inside the cavity

$\overline{M} = \overline{E} \times (-\hat{n})$, as illustrated in Fig.3.1(b), where $\hat{n}$ denotes the unit normal outward vector.

- For the linear electric probe
  - Removing the linear electric probe
  - The electric current $\bar{J}$ is assumed along the linear electric probe.

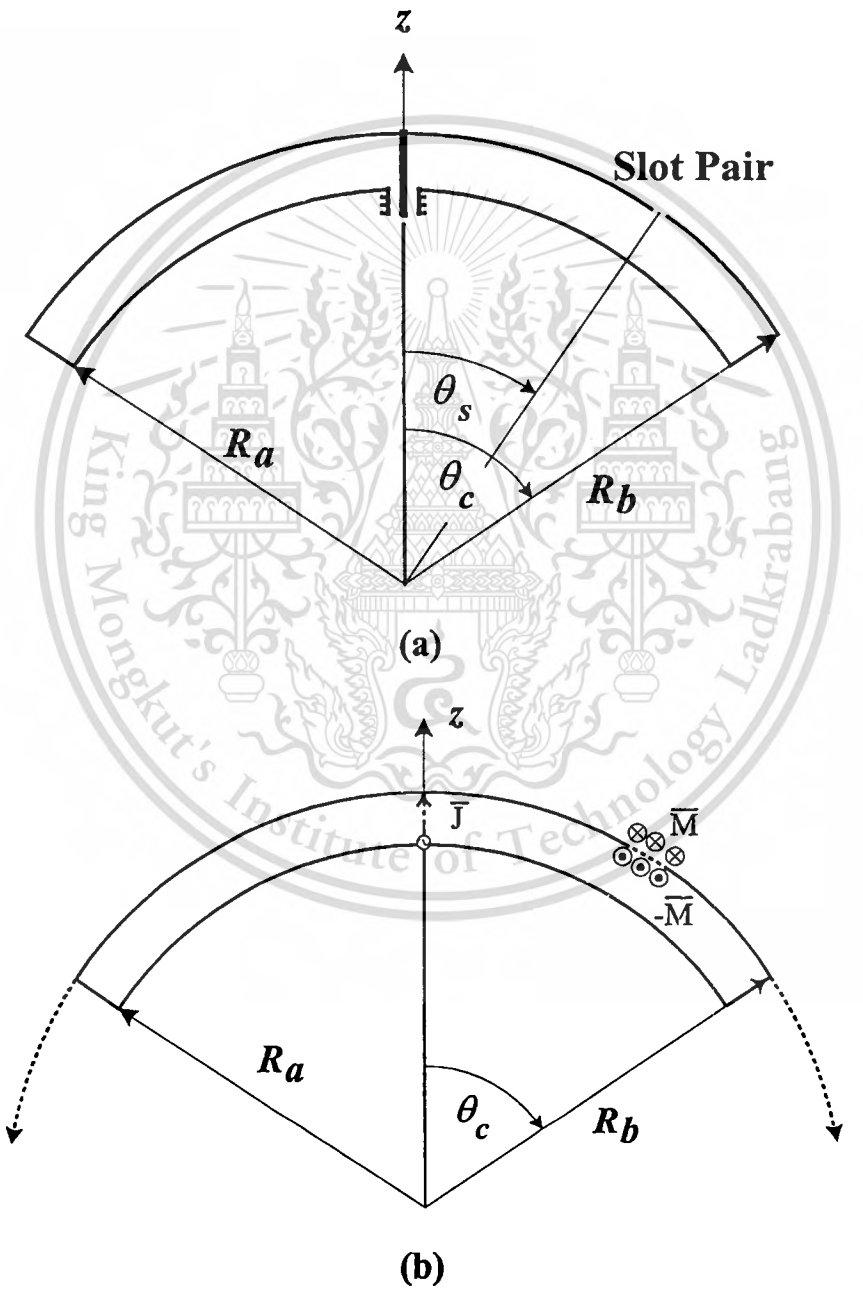

Fig. 3.1 Analysis model for the antenna

(a) original problem (b) equivalent model

In addition, the Field Equivalent Principle is used to divide this analysis model into two canonical regions: external region (*ext*) and internal region (*int*). By following all of above conditions, the equivalent model is established as shown in Fig.3.1(b).

3.3 Integral Equation Formulations

From the analysis model as shown in Fig.3.1, since the discontinuities in the structure were eliminated, the continuous conditions of the tangential magnetic fields are automatically satisfied at the slot aperture.

$$\bar{H}_{tan}^{ext} = \bar{H}_{tan}^{int} \tag{3.1a}$$

$$\bar{H}_{\tan}^{ext} = \bar{H}_{s}^{ext} \times \hat{R} \tag{3.1b}$$

$$\bar{H}_{\tan}^{\text{int}} = \left(\bar{H}_{s}^{\text{int}} + \bar{H}_{p}^{\text{int}}\right) \times \hat{R} \tag{3.1c}$$

$$\bar{H}_{s}^{ext} = \bar{H}_{s}^{int} + \bar{H}_{p}^{int} \tag{3.1d}$$

where $\bar{H}_{tan}^{ext}$ and $\bar{H}_{tan}^{int}$ represent the external and internal tangential magnetic fields, respectively. $\bar{H}_{p}^{int}$ and $\bar{H}_{s}^{int}$ are the internal magnetic fields radiated from the linear electric probe and the slot aperture, respectively. $\bar{H}_{s}^{ext}$ denotes the external magnetic field radiated from the slot aperture. $\hat{R}$ is the unit normal vector to spherical surface.

With the aids of the dyadic Green's functions [3-2]-[3-3], it is feasible to immediately calculate the magnetic field of each term, namely

$$\bar{H}_s^{ext}(\bar{R}) = j\omega\varepsilon_0 \iint_{S_a} \bar{\bar{G}}_{HM}^{ext}\left(\bar{R},\bar{R}'\right)\cdot\left(\bar{E}(\bar{R}')\times\hat{R}\right)dS'$$

$$= j\omega\varepsilon_0 \iint_{S_a} \bar{\bar{G}}_{HM}^{ext}\left(\bar{R},\bar{R}'\right)\cdot\bar{M}(\bar{R}')dS' \qquad (3.2)$$

and

$$\bar{H}_s^{int}(\bar{R}) = j\omega\varepsilon_0 \iint_{S_a} \bar{\bar{G}}_{HM}^{int}\left(\bar{R},\bar{R}'\right)\cdot\left(\bar{E}(\bar{R}')\times-\hat{R}\right)dS'$$

$$= -j\omega\varepsilon_0 \iint_{S_a} \bar{\bar{G}}_{HM}^{int}\left(\bar{R},\bar{R}'\right)\cdot\bar{M}(\bar{R}')dS', \qquad (3.3)$$

$$\bar{H}_p^{int}(\bar{R}) = \iint_{S_f} \bar{\bar{G}}_{HJ}^{int}\left(\bar{R},\bar{R}'\right)\cdot\bar{J}(\bar{R}')dS' \qquad (3.4)$$

where $\bar{\bar{G}}_{HM}^{ext,int}\left(\bar{R},\bar{R}'\right)$ and $\bar{\bar{G}}_{HJ}^{int}\left(\bar{R},\bar{R}'\right)$ denote the magnetic dyadic Green's functions produced by a magnetic current sheet and electric current density, respectively. S_a and S_f are the limit of integration on the surface of slot aperture and on the length of probe, respectively. $\bar{R}$ and $\bar{R}'$ are the location coordinates of field and source point, respectively. In this thesis, the time function $e^{j\omega t}$ is used. Substituting (3.2) (3.3) and (3.4) into (3.1d) the simultaneous equation across the slot can be obtained as:

$$j\omega\varepsilon_0 \iint_{S_a}\left\{\bar{\bar{G}}_{HM}^{ext}\left(\bar{R},\bar{R}'\right)+\bar{\bar{G}}_{HM}^{int}\left(\bar{R},\bar{R}'\right)\right\}\cdot\bar{M}\left(\bar{R}'\right)dS' - \iint_{S_f}\bar{\bar{G}}_{HJ}^{int}\left(\bar{R},\bar{R}'\right)\cdot\bar{J}\left(\bar{R}'\right)dS' = 0 \qquad (3.5)$$

Alternatively, not only is the boundary condition on the tangential electric field along the probe considered, but the delta gap electric field at the bottom of the probe is also considered as the excitation. Therefore,

$$E_{tan}^{int} = 0 \tag{3.6a}$$

For the excitation by probe in R-direction, E_{tan}^{int} can be written as

$$E_{\tan}^{\text{int}} = \left(\bar{E}^{\text{int}} \cdot \hat{R}\right) + E_a \tag{3.6b}$$

where E_a is the applied field, defined by delta gap modeling as

$$E_a = \delta(\bar{R} - \bar{R}') \tag{3.6c}$$

and $\bar{E}^{int}$ denotes the internal scattering field, given as

$$\bar{E}^{int} = \bar{E}_s^{int} + \bar{E}_p^{int} \tag{3.6d}$$

Following (3.6a), (3.6b) can be rearranged as

$$\bar{E}^{int} \cdot \hat{R} = -E_a . \tag{3.7}$$

The complete condition can be stated by using delta gap model as (3.6c)

$$\left(\bar{E}_s^{int} + \bar{E}_p^{int}\right) \cdot \hat{R} = -\delta\left(\bar{R}'\right), \tag{3.8}$$

where $\bar{E}_s^{int}$ and $\bar{E}_p^{int}$ are the internal electric fields radiated from the slot aperture and the probe, respectively. $-\delta(\bar{R}')$ is the assumed voltage source from the delta gap source model.

$$\bar{E}_s^{int}(\bar{R}) = \iint_{S_a} \bar{\bar{G}}_{EM}^{int}(\bar{R},\bar{R}') \cdot \left(\bar{E}(\bar{R}') \times -\hat{R}\right) dS'$$

$$= -\iint_{S_a} \bar{\bar{G}}_{EM}^{int}(\bar{R},\bar{R}') \cdot \bar{M}(\bar{R}') dS' \tag{3.9}$$

$$\bar{E}_p^{int}(\bar{R}) = -j\omega\mu_0 \iint_{S_f} \bar{\bar{G}}_{EJ}^{int}(\bar{R},\bar{R}') \cdot \bar{J}(\bar{R}') dS', \tag{3.10}$$

where $\bar{\bar{G}}_{EM}^{int}(\bar{R},\bar{R}')$ and $\bar{\bar{G}}_{EJ}^{int}(\bar{R},\bar{R}')$ denote the electric dyadic Green's functions produced by magnetic current sheet and electric current density, respectively. Substituting (3.9) and (3.10) into (3.8), the simultaneous integral equation on the probe can be obtained as:

$$-\iint_{S_a} \bar{\bar{G}}_{EM}^{in}(\bar{R},\bar{R}') \cdot \bar{M}(\bar{R}') dS' - j\omega\mu_0 \iint_{S_f} \bar{\bar{G}}_{EJ}^{in}(\bar{R},\bar{R}') \cdot \bar{J}(\bar{R}') dS' = -\delta(\bar{R}'). \tag{3.11}$$

Now the integral equations have been obtained as shown in (3.5) and (3.11). The next step is the unknown evaluation of the magnetic current sheet and electric current density. This can be accomplished by using Method of Moments [3-3]-[3-5].

Next, by following the Method of Moments the basis and weighting functions should be selected. The choice of basis functions should be

physically meaningful bases. Therefore, the natures of electric field on a slot aperture are considered.

- The behavior of aperture electric field distribution is cosinusoidal with respect to the direction of slot length.
- The effect from the width of slot is reasonably considered.

In order to deal with the natures of a slot aperture, the sinusoidal entire domain is appropriate because it is continuous and smooth function throughout a slot aperture. It is easy to include the higher order mode functions into the analysis. Only a few expansion terms are usually adequate to obtain the required accuracy. Accordingly, the expansion of magnetic current can be expressed as following

$$\overline{M}(\overline{R}') = \sum_{sk=1}^{N_{sk}} a_{sk} \overline{m}_{sk}(\overline{R}') \tag{3.12}$$

where $\overline{m}_{sk}(\overline{R}')$ is a basis function for the slot aperture and a_{sk} is the unknown coefficients.

In view of a linear probe, the basis function can be written as

$$\overline{J}(\overline{R}') = \sum_{f=1}^{N_f} b_f \overline{j}_f(\overline{R}') \tag{3.13}$$

where $\overline{j}_f(\overline{R}')$ is a basis function for the probe and b_f is the unknown coefficients.

Additionally, the selection of appropriate weighting function plays an important role to obtain the high accurate result, ease of evaluation of matrix elements and analytically solution. There are many ways to choose the weighting function. However, the Galerkin's method can be effectively

responsible for these requirements. This procedure is to select the weighting function to be the same as the basis functions.

After applying the Galerkin's Method of Moments, the following linear equations for unknown coefficients a_{sk} and b_f are obtained [3-6].

$$j\omega\varepsilon_o \sum_{sk=1}^{N_{sk}} a_{sk} \left\{ \iint_{sl} \iint_{sk} \hat{m}_{sl} \cdot \left(\overline{\overline{G}}_{HM}^{in} + \overline{\overline{G}}_{HM}^{out} \right) \cdot \hat{m}_{sk} dS_{sk} dS_{sl} \right\} + \sum_{f=1}^{N_f} b_f \iint_{sl} \int_f \hat{m}_{sl} \cdot \overline{\overline{G}}_{HJ}^{in} \cdot \hat{j}_f dl_f dS_{sl} = 0 \quad (3.14)$$

$$\sum_{sk=1}^{N_{sk}} a_{sk} \int_f \iint_{sk} \hat{j}_f \cdot \overline{\overline{G}}_{EM}^{in} \cdot \hat{m}_{sk} dS_{sk} dl_f + j\omega\mu_o \sum_{f=1}^{N_f} b_f \int_f \int_f \hat{j}_f \cdot \overline{\overline{G}}_{EJ}^{in} \cdot \hat{j}_f dl_f dl_f = 1 \quad (3.15)$$

where $l=1,2,\ldots,N_{sl}$.

3.4 Dyadic Green's Functions in Each Canonical Region

The dyadic Green's functions, inside and outside the concentric conducting spherical cavity enclosed by the conducting conical surface for electric and magnetic fields due to the electric and magnetic current sources, are derived [3-2], [3-3] to fulfill the requirement of the integral equations. The details of the derivation are described in Appendix B. The results are

$$G_{HM,\theta\theta}^{in} = \frac{1}{k^2} \sum_{l=1}^{\infty} \sum_{m=1}^{\infty} A_m \left[\sum_{\lambda=m}^{\infty} \frac{1}{(\kappa_p^2 - k^2) I_{\lambda p}} \frac{1}{rr'} \Re'_\lambda(r) \Re'_\lambda(r') \Theta'_\lambda(\theta) \Theta'_\lambda(\theta') \Phi_1(\phi) \Phi_1(\phi') \right.$$
$$\left. + \sum_{\mu=m}^{\infty} \frac{\kappa_q^2}{(\kappa_q^2 - k^2) I_{\mu q}} \frac{m^2}{\sin\theta \sin\theta'} \Re_\mu(r) \Re_\mu(r') \Theta_\mu(\theta) \Theta_\mu(\theta') \Phi_2(\phi) \Phi_2(\phi') \right] \quad (3.16)$$

$$G^{in}_{HM,\theta\phi} = \frac{1}{k^2}\sum_{l=1}^{\infty}\sum_{m=1}^{\infty} A_m \left[\mp\sum_{\lambda=m}^{\infty}\frac{m}{(\kappa_p^2-k^2)I_{\lambda p}}\frac{1}{rr'sin\theta'}\Re'_\lambda(r)\Re'_\lambda(r')\Theta'_\lambda(\theta)\Theta_\lambda(\theta')\Phi_1(\phi)\Phi_2(\phi')\right.$$

$$\left. \pm \sum_{\mu=m}^{\infty}\frac{\kappa_q^{\ 2}}{(\kappa_q^2-k^2)I_{\mu q}}\frac{m}{sin\theta}\Re_\mu(r)\Re_\mu(r')\Theta_\mu(\theta)\Theta'_\mu(\theta')\Phi_2(\phi)\Phi_1(\phi')\right] \tag{3.17}$$

$$G^{in}_{HM,\phi\theta} = \frac{1}{k^2}\sum_{l=1}^{\infty}\sum_{m=1}^{\infty} A_m \left[\mp\sum_{\lambda=m}^{\infty}\frac{m}{(\kappa_p^2-k^2)I_{\lambda p}}\frac{1}{rr'sin\theta}\Re'_\lambda(r)\Re'_\lambda(r')\Theta_\lambda(\theta)\Theta'_\lambda(\theta')\Phi_2(\phi)\Phi_1(\phi')\right.$$

$$\left. \pm \sum_{\mu=m}^{\infty}\frac{\kappa_q^{\ 2}}{(\kappa_q^2-k^2)I_{\mu q}}\frac{m}{sin\theta'}\Re_\mu(r)\Re_\mu(r')\Theta'_\mu(\theta)\Theta_\mu(\theta')\Phi_1(\phi)\Phi_2(\phi')\right] \tag{3.18}$$

$$G^{in}_{HM,\phi\phi} = \frac{1}{k^2}\sum_{l=1}^{\infty}\sum_{m=1}^{\infty} A_m \left[\sum_{\lambda=m}^{\infty}\frac{m^2}{(\kappa_p^2-k^2)I_{\lambda p}}\frac{1}{rr'sin\theta sin\theta'}\Re'_\lambda(r)\Re'_\lambda(r')\Theta_\lambda(\theta)\Theta_\lambda(\theta')\Phi_2(\phi)\Phi_2(\phi')\right.$$

$$\left. + \sum_{\mu=m}^{\infty}\frac{\kappa_q^{\ 2}}{(\kappa_q^2-k^2)I_{\mu q}}\Re_\mu(r)\Re_\mu(r')\Theta'_\mu(\theta)\Theta'_\mu(\theta')\Phi_1(\phi)\Phi_1(\phi')\right] \tag{3.19}$$

$$G^{out}_{HM,\theta\theta} = \frac{ik}{2}\sum_{m=1}^{\infty}\sum_{n=m}^{\infty} A_m B_{mn}\left[\frac{1}{k^2rr'}\aleph'_n(r)[\Re'_n(r')+C_n\aleph'_n(r')]\Theta'_n(\theta)\Theta'_n(\theta')\Phi_1(\phi)\Phi_1(\phi')\right.$$

$$\left. \mp \frac{m^2}{sin\theta sin\theta'}\aleph_n(r)[\Re_n(r')+D_n\aleph'_n(r')]\Theta_n(\theta)\Theta_n(\theta')\Phi_2(\phi)\Phi_2(\phi')\right] \tag{3.20}$$

$$G^{out}_{HM,\theta\phi} = \frac{ik}{2}\sum_{m=1}^{\infty}\sum_{n=m}^{\infty} A_m B_{mn}\left[\mp\frac{1}{k^2rr'}\frac{m}{sin\theta'}\aleph'_n(r)\ [\Re'_n(r')\mp C_n\aleph'_n(r')]\Theta'_n(\theta)\Theta_n(\theta')\Phi_1(\phi)\Phi_2(\phi')\right.$$

$$\left. \pm \frac{m}{sin\theta}\aleph_n(r)\ [\Re_n(r')\pm D_n\aleph_n(r')]\Theta_n(\theta)\Theta'_n(\theta')\Phi_2(\phi)\Phi_1(\phi')\right] \tag{3.21}$$

$$G^{out}_{HM,\phi\theta} = \frac{ik}{2}\sum_{m=1}^{\infty}\sum_{n=m}^{\infty} A_m B_{mn}\left[\mp\frac{1}{k^2rr'}\frac{m}{sin\theta}\aleph'_n(r)[\Re'_n(r')\mp C_n\aleph'_n(r)]\Theta_n(\theta)\Theta'_n(\theta')\Phi_2(\phi)\Phi_1(\phi')\right.$$

$$\left. \pm \frac{m}{sin\theta'}\aleph'_n(r)[\Re_n(r')+D_n\aleph_n(r')]\Theta'_n(\theta)\Theta_n(\theta')\Phi_1(\phi)\Phi_2(\phi')\right] \tag{3.22}$$

$$G^{out}_{HM,\phi\phi} = \mp\frac{ik}{2}\sum_{m=1}^{\infty}\sum_{n=m}^{\infty} A_m B_{mn}\Big[\frac{1}{k^2 rr'}\aleph'_n(r)[\Re'_n(r')+C_n\aleph'_n(r')]\frac{m^2}{sin\theta sin\theta'}\Theta_n(\theta)\Theta_n(\theta')\Phi_2(\phi)\Phi_2(\phi') + \aleph_n(r)[\Re_n(r')+D_n\aleph_n(r')]\Theta'_n(\theta)\Theta'_n(\theta')\Phi_1(\phi)\Phi_1(\phi')\Big] \tag{3.23}$$

$$G^{in}_{HJ,\theta r} = \mp\sum_{l=1}^{\infty}\sum_{m=1}^{\infty} A_m\Big[\sum_{\mu=m}^{\infty}\frac{\mu(\mu+1)\kappa_q}{(\kappa_q^2-k^2)I_{\mu q}}\frac{m}{sin\theta}\Re_\mu(r)\Re_\mu(r')\Theta_\mu(\theta)\Theta_\mu(\theta')\Phi_2(\phi)\Phi_1(\phi')\Big] \tag{3.24}$$

$$G^{in}_{HJ,\phi r} = -\sum_{l=1}^{\infty}\sum_{m=1}^{\infty} A_m\Big[\sum_{\mu=m}^{\infty}\frac{\mu(\mu+1)\kappa_q}{(\kappa_q^2-k^2)I_{\mu q}}\Re_\mu(r)\Re_\mu(r')\Theta'_\mu(\theta)\Theta_\mu(\theta')\Phi_1(\phi)\Phi_1(\phi')\Big] \tag{3.25}$$

$$G^{in}_{EM,r\theta} = \mp\sum_{l=1}^{\infty}\sum_{m=1}^{\infty} A_m\Big[\sum_{\mu=m}^{\infty}\frac{\mu(\mu+1)\kappa_q}{(\kappa_q^2-k^2)I_{\mu q}}\frac{m}{sin\theta'}\Re_\mu(r)\Re_\mu(r')\Theta_\mu(\theta)\Theta_\mu(\theta')\Phi_1(\phi)\Phi_2(\phi')\Big] \tag{3.26}$$

$$G^{in}_{EM,r\phi} = -\sum_{l=1}^{\infty}\sum_{m=1}^{\infty} A_m\Big[\sum_{\mu=m}^{\infty}\frac{\mu(\mu+1)\kappa_q}{(\kappa_q^2-k^2)I_{\mu q}}\Re_\mu(r)\Re_\mu(r')\Theta_\mu(\theta)\Theta'_\mu(\theta')\Phi_1(\phi)\Phi_1(\phi')\Big] \tag{3.27}$$

$$G^{in}_{EJ,rr} = \frac{1}{k^2}\Big[-\frac{1}{r^2\sin\theta}\delta(r-r')\delta(\theta-\theta')\delta(\phi-\phi') + \sum_{l=1}^{\infty}\sum_{m=1}^{\infty} A_m\sum_{\mu=m}^{\infty}\frac{\mu^2(\mu+1)^2}{(\kappa_q^2-k^2)I_{\mu q}}\Re_\mu(r)\Re_\mu(r')\Theta_\mu(\theta)\Theta_\mu(\theta')\Phi_1(\phi)\Phi_1(\phi')\Big] \tag{3.28}$$

where the common parameters can be defined as below and other notations have usual meaning as in references [3-2],[3-3].

The expressions of the field in radial direction of the TE and TM modes inside the cavity can be expressed as the spherical Bessel function and its derivative as follows

$$\Re_\mu(r) = b_\mu(\kappa_p r) = j_\mu(\kappa_p r) + A_\mu y_\mu(\kappa_p r), \tag{3.29}$$

$$\Re'_{\lambda}(r)=\frac{\partial[rb_{\lambda}(\kappa_q r)]}{\partial r}=\frac{\partial[r(j_{\lambda}(\kappa_q r)+A_{\lambda}y_{\lambda}(\kappa_q r)]}{\partial r}. \tag{3.30}$$

For the outside the cavity counterpart, the field in radial direction will be

$$\Re_n(r)=b_n(kr)=j_n(kr)+A_n y_n(kr), \tag{3.31}$$

$$\Re'_n(r)=\frac{\partial[rb_n(kr)]}{\partial r}=\frac{\partial[r(j_n(kr)+B_n y_n(kr))]}{\partial r}, \tag{3.32}$$

$$\aleph_n(r)=h_n^{(2)}(kr), \tag{3.33}$$

$$\aleph'_n(r)=\frac{\partial[rh_n^{(2)}(kr)]}{\partial r}. \tag{3.34}$$

The field in θ-direction can be written as

$$\Theta_{\nu}(\theta)=L_{\nu}^{m}(\cos\theta)=P_{\nu}^{m}(\cos\theta)+A_{\nu}^{m}Q_{\nu}^{m}(\cos\theta), \tag{3.35}$$

$$\Theta'_{\nu}(\theta)=\frac{\partial L_{\nu}^{m}(\cos\theta)}{\partial\theta}=\frac{\partial(P_{\nu}^{m}(\cos\theta)+C_{\nu}^{m}P_{\nu}^{m}(\cos\theta)}{\partial\theta}. \tag{3.36}$$

The field in ϕ-direction can be written as

$$\Phi_1(\phi)=\begin{cases}\cos\\ \sin\end{cases}m\phi=\cos m\phi+j\sin m\phi, \tag{3.37}$$

$$\Phi_2(\phi)=\begin{cases}\sin\\ \cos\end{cases}m\phi=\sin m\phi+j\cos m\phi. \tag{3.38}$$

In addition, the modal coefficients can be written as

$$A_m = \frac{2-\delta_m}{2\pi}, \tag{3.39}$$

$$\delta_m = \begin{cases} 1, & m \neq 0 \\ 0, & m = 0 \end{cases}, \tag{3.40}$$

$$B_{mn} = \frac{2n+1}{n(n+1)} \frac{(n-m)!}{(n+m)!}, \tag{3.41}$$

$$C_n = -\frac{j_n(kR_b)}{h_n^{(2)}(kR_b)}, \tag{3.42}$$

$$D_n = \frac{[kR_b j_n(kR_b)]'}{[kR_b h_n^{(2)}(kR_b)]'}, \tag{3.43}$$

$$I_{\upsilon\varsigma} = \frac{1}{\kappa_\varsigma \kappa_\varsigma'} \int_0^{\theta_0} \int_{R_a}^{R_b} \left\{ \upsilon^2 (\upsilon+1)^2 j_\upsilon(\kappa_\varsigma r) j_\upsilon(\kappa_\varsigma' r) [P_\varsigma^m(\cos\theta)]^2 + \frac{\partial[r j_\upsilon(\kappa_\varsigma r)]}{\partial r} \frac{\partial[r j_\upsilon(\kappa_\varsigma' r)]}{\partial r} \left[\left(\frac{\partial P_\varsigma^m(\cos\theta)}{\partial \theta} \right)^2 + \left(\frac{m P_\varsigma^m(\cos\theta)}{\sin\theta} \right)^2 \right] \right\} \sin\theta \, dr d\theta \tag{3.44}$$

3.5 Method of Moments

The following basis/testing functions on the slots $\hat{m}_{sk}$ and on the feeding probe $\hat{j}_f$ are used, assuming that the slots are narrow and the cavity is thin [3-8]:

$$\hat{m}_{sk} = \hat{\zeta}_{sk} f_{sk}(\xi_{sk}) g_{sk}(\zeta_{sk}) = \hat{\zeta}_{sk} \frac{\sin\left\{ k_o \left(\frac{l_{sk}}{2} - R_b |\xi_{sk}| \right) \right\}}{\sin\left(k_o \frac{l_{sk}}{2} \right)} \frac{1}{R_b \sqrt{\left(\frac{\varepsilon_{sk}}{2} \right)^2 - \zeta_{sk}^2}} \tag{3.45}$$

$$\hat{j}_f = \hat{r} \tag{3.46}$$

where l_{sk} and ε_{sk} are the length and the width of slot k, ξ_{sk} and ζ_{sk} are the local co-ordinates originating from the center of the k slot along the length and the width. By utilizing the co-ordinate transformations as in [3-9] and solving the unknown currents, the antenna characteristics can be subsequently determined by using these currents.

3.6 Conclusion

The expressions of the integral equations of two canonical regions of a spherical slot array antenna are formulated by applying the Field Equivalent Principle and the boundary condition in which the magnetic fields are continuous throughout the slot aperture and the delta gap source is modeled at the bottom of the cavity. The dyadic Green's functions are examined by using the eigenfunction expansions. The entire domain basis functions and the Galerkin's Method of Moments are applied to solve those integral equations. The midpoint integration is applied for the numerical integration. The convergent of the numerical solution is obtained by using a few terms of the summation of the basis function. However, the time consumming for the computation is still relatively high.

References

[3-1]C.A. Balanis, *Advanced Engineering Electromagnetics*, New York: Wiley and Sons. 1989.

[3-2]C.Phongcharoenpanich, M.Krairiksh and J.Takada, "Dyadic Green's functions of the concentric conducting spherical cavity," *Proceedings of the*

1997 Asia-Pacific Microwave Conference, Hong Kong, vol. 2, pp. 757-760, Dec. 1997.

[3-3]C.T.Tai, *Dyadic Green Function in Electromagnetic Theory*, 2nd Ed. New York: IEEE Press, 1993.

[3-4]R.F.Harrington, *Field Computation by Moment Methods*, Rebert E. Krieger Publishing, Inc., 1968.

[3-5]A.R.Djordjevic and T.K.Sarkar "A theorem on the Moment Methods," *IEEE Trans. Antennas Propagat.*, vol. AP-35, no. 3, pp. 353-355, Mar. 1987.

[3-6]J.H. Richmond "On the variational aspects of the Moment Method," *IEEE Trans. Antennas Propagat.*, vol. 39, no. 4, pp. 473-479, Apr. 1991.

[3-7]J.Takada, N.Araoka and A.Tanisho "Method of moments analysis of small aperture radial line slot slot antenna using the rectangular cavity Green's function." *IEE Proc.-Microw. Antennas Propag.*, vol. 144, no. 6, pp. 498-500, Dec. 1997.

[3-8]J.Takada, "A study of the slot design for Radial Line Slot Antennas," Doctoral Dissertation of Tokyo Institute of Technology, Dec. 1991.

[3-9]C.Phongcharoenpanich, M.Krairiksh and J.Takada, "MoM analysis of a circularly polarized conical beam spherical slot array antenna," *Proceedings of the 2000 International Symposium on Antennas and Propagation*, Fukuoka, vol.4, pp.1625-1628, Aug. 2000.

Chapter 4

Radiation Characteristics of the Antenna

4.1 Introduction

The radiation characteristics such as radiation pattern and directivity of the spherical slot array antenna are primarily investigated in this chapter. The radiation characteristics for various parameters such as the outer spherical radius and the angle of the slot pair position are investigated. The parameters that yield the conical beam radiation are analyzed. The elevation angle of the conical beam is necessarily examined. The directivity is calculated to find the condition that meets the requirement of the applications.

4.2 Radiation Pattern

By applying Method of Moments to solve the integral equations, the unknown coefficients of the current density are examined. Subsequently, the electromagnetic fields outside the concentric conducting spherical cavity-backed slot antenna can be determined by integrating the Green's functions outside the cavity and the magnetic current sheet along the slot. The resultant electric field can be expressed as [4-1]

$$\overline{E}(\overline{R}) = \int_{S_a} \overline{\overline{G}}_{EM}(\overline{R},\overline{R}') \cdot \overline{M}(\overline{R}') dV' . \tag{4.1}$$

For the magnetic field counterpart, it should be

$$\overline{H}(\overline{R}) = \int_{S_a} \overline{\overline{G}}_{HM}(\overline{R},\overline{R}') \cdot \overline{M}(\overline{R}') dV' . \tag{4.2}$$

The far-field expression of these electromagnetic fields can be carried out by utilizing the asymptotic expression of the spherical Hankel functions and its derivative with the large arguments as follows [4-2]

$$h_n^{(2)}(kr) \sim \frac{j^{n+1}}{kr} e^{-jkr} \tag{4.3}$$

and

$$\left(krh_n^{(2)}(kr)\right)' \sim j^{n+1}\left(\frac{(n+1)}{kr} - j\right)e^{-jkr}. \tag{4.4}$$

The far zone expression of the spherical slot array antenna can be found by combining the field from all of the two-slot (slot pair) around the ring. The total radiated electric field can be written as [4-3]

$$\overline{E}_T(\theta,\phi) = \sum_{j=1}^{N_s}\sum_{i=1}^{2}\overline{E}_{ij}(\theta,\phi), \tag{4.5}$$

where i is the index of the slot number in a pair and j denotes the number of the slot pairs around a ring, respectively.

It is pointed that the far zone magnetic field is related to the electric field by the relation

$$\overline{E}_T(\theta,\phi) = \eta\overline{H}_T(\theta,\phi). \tag{4.6}$$

As previously mentioned that the spherical slot array antenna in this thesis is designed to radiate the circularly polarized pattern, the co-polarized pattern is

significantly contributed to the application. The co-polarized field in the sense of clockwise rotation or right-hand circular polarization can be determined by employing [4-4]

$$E_{co}(\theta,\phi) = \overline{E}_T(\theta,\phi)\cdot\frac{\hat{\theta}+j\hat{\phi}}{\sqrt{2}} \tag{4.7}$$

The cross-polarized field will be characterized in the next chapter as the information of the polarization characteristics.

To illustrate the radiation pattern of a circularly polarized conical beam spherical slot array antenna, let us demonstrate a model of the slot array oriented at an angle of slot position (θ_s) of 40° on the spherical cavity of the radius (R_b) of 1.43λ and the azimuthal spacing (s_ϕ) of 0.481λ. Other antenna parameters used in the model is tabulated in Table 4.1.

Table 4.1 Antenna parameters used to find the numerical results

Slot length (l_s)	0.5λ
Slot width (w_s)	0.017λ
Outer spherical radius (R_b)	1.43λ
Inner spherical radius (R_a)	1.27λ
Shorted conical angle (θ_c)	67.34°
Center of slot pair angle (θ_s)	40.00°
Azimuthal spacing between slot pair (s_ϕ)	0.481λ
Elevational distance between slot in pair (d_θ)	0.22λ
Number of slot pairs (N_s)	12

It can be seen that the elevational radiation pattern possesses the null in the boresight direction and the beam peak is at $40°$ as shown in Fig.4.1 by the solid line. Fig.4.2 shows the azimuthal radiation pattern at $\theta = 40°$. It is evident that the omnidirectional radiation is obtained. The directivity of this antenna is about *6.1* dBi.

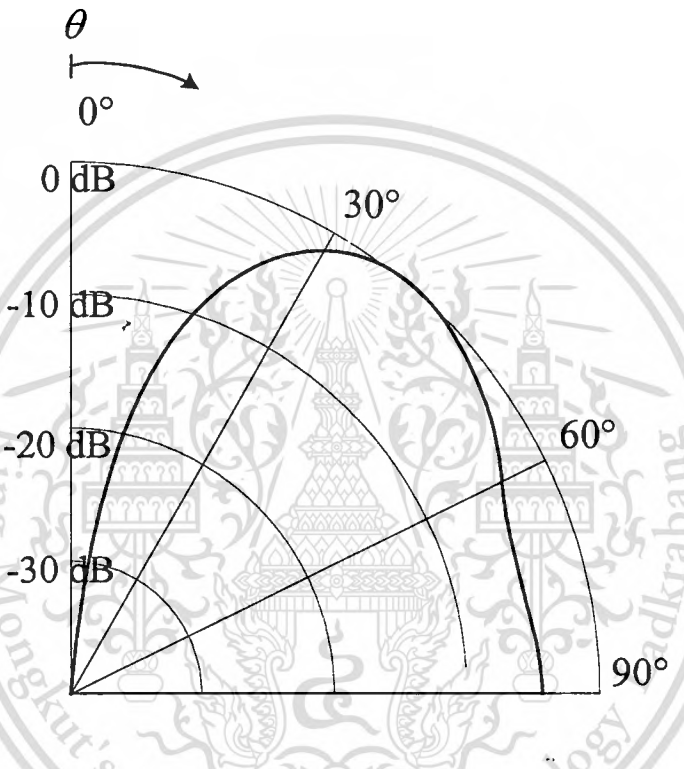

Fig.4.1 Simulation results of elevational radiation pattern

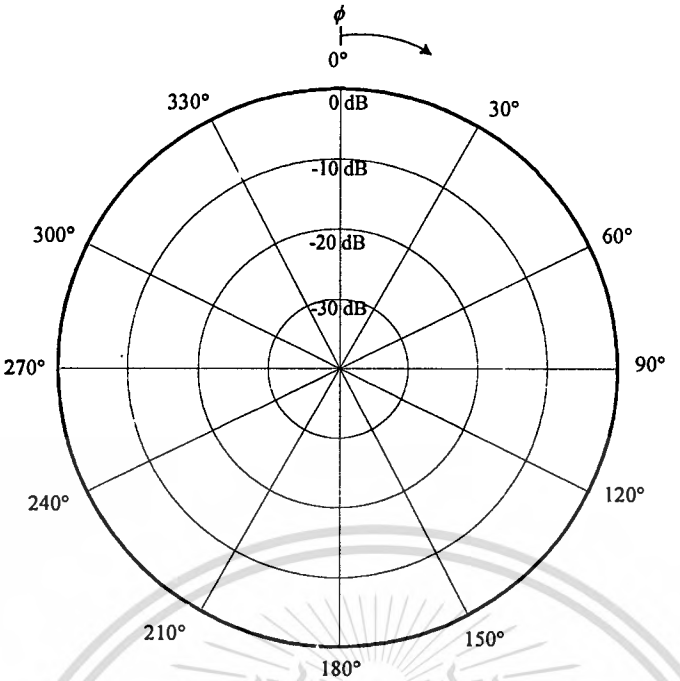

Fig.4.2 Simulation results of azimuthal radiation pattern at $\theta=40^\circ$

4.3 Elevation Angle

The elevation angle of the conical beam antenna is another significant parameter to use this antenna to practical application. The desirable elevational beam peak is different corresponding the location of the installation unit. For the mobile satellite application, the lower of the elevational beam peak is useful for the mobile subscriber unit located far from the equator. For the wireless LAN system, the antenna that provides the low elevational beam peak can enhance the coverage service area but it was done at the expense of the weak field strength in the boresight direction of the antenna. Therefore, this parameter can be arbitrarily chosen according to several aspects of the actual applications. The elevational beam peak can be determined by determining the maximum radiation pattern in elevation plane as

$$\theta_{max}(\text{degree}) = \theta_{max}\left|\begin{matrix}\max \\ \theta\end{matrix} E_{co}(\theta,\phi)\right. . \tag{4.8}$$

Fig.4.3 shows the elevational beam peak position as a function of the outer spherical radius for various angles of slot pair positions. It can be seen that when the radius is larger, the elevational beam peak position tends to be higher. There is no trend observed in the case of θ_s equals $50°$. However, when we compare among the different θ_s it is found that when θ_s is increased θ_{max} will be getting lower until θ_s equals $50°$. θ_{max} will turn to be higher and it will be lower again due to the increment of θ_s. From this information, we can say that the elevational beam peak position is changed as the function of the spherical radius and angle of slot pair position.

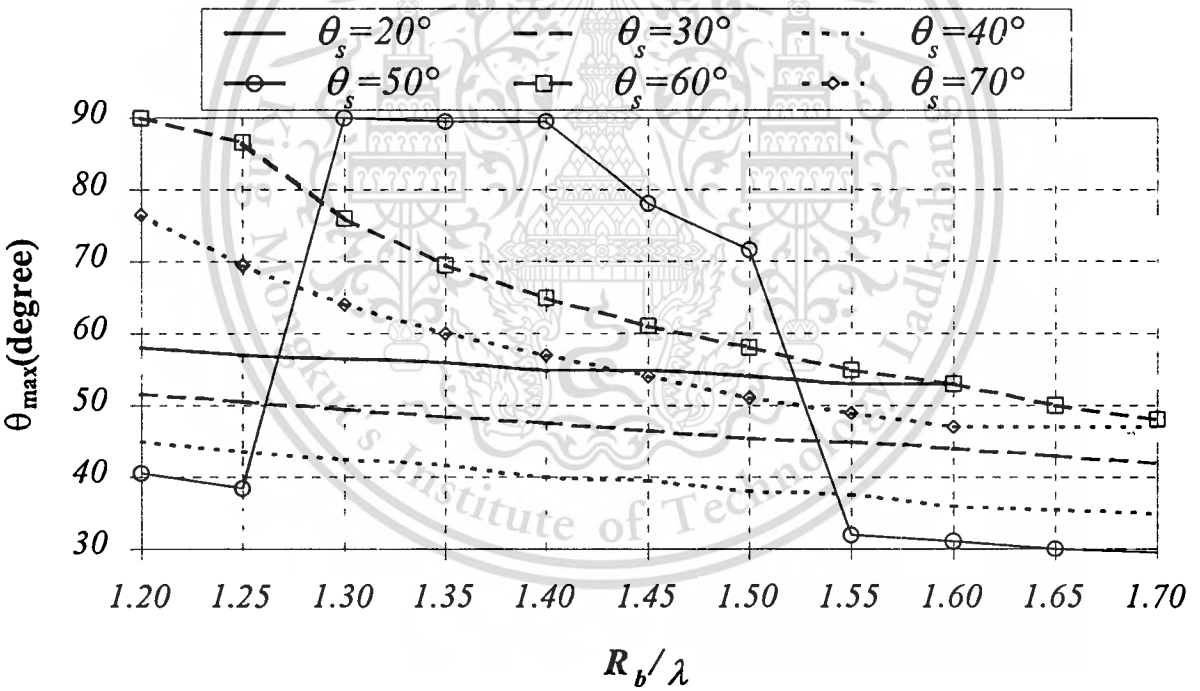

Fig.4.3 Simulation results of elevational beam peak position as a function of the outer spherical radius for various angles of slot pair positions

The elevational beam peak position as a function of the angles of slot pair positions for various outer spherical radii is illustrated in Fig.4.4. We can

explicitly observe that for all different spherical radii the elevational beam peak position will be lower as the descending of the angles of the slot pair positions except for the angle of around $45°$-$55°$ that the variation is inverse. Hence, we have to investigate the relation between the elevational beam peak as the function of the angle of the slot pair position and spherical radius in order that we can make the antenna design.

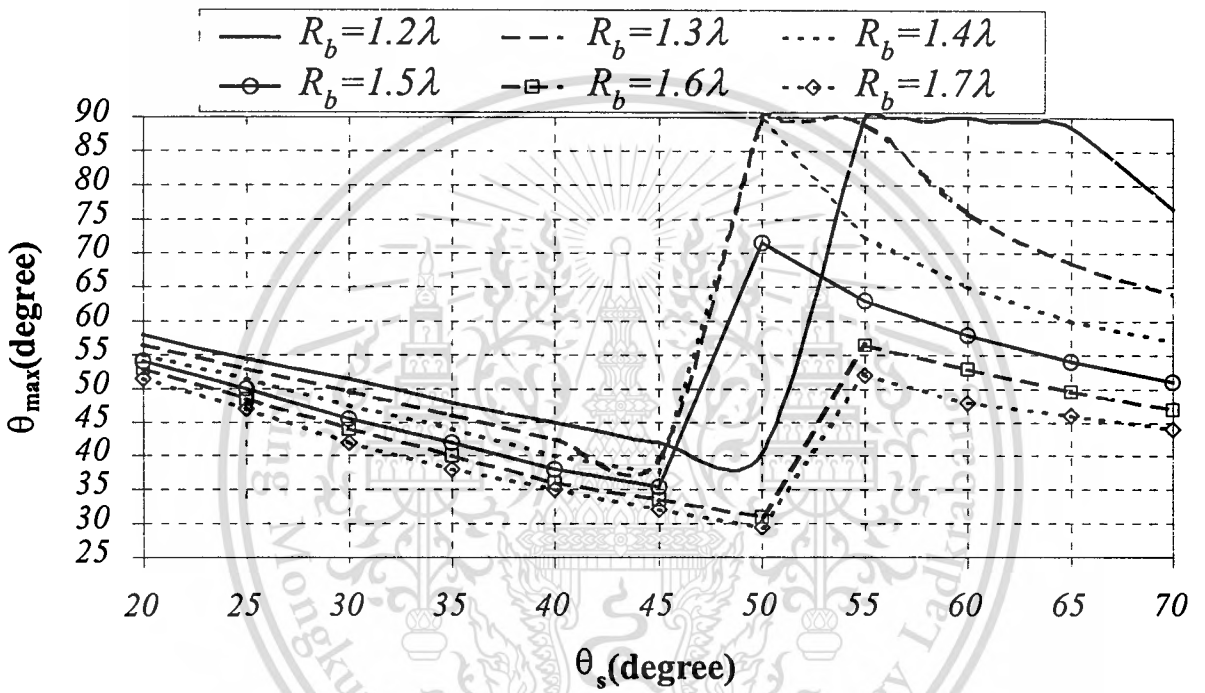

Fig.4.4 Simulation results of elevational beam peak direction as a function of the angles of slot pair positions for various outer spherical radii

To extend the explanation about the radiation characteristics, the half power beamwidth of the antenna is also investigated. The half power beamwidth as a function of the spherical radius and angle of the slot pair position are illustrated in Fig.4.5 and Fig.4.6, respectively. We can see that the wide beamwidth is observed when θ_s is $50°$. The result of the beamwidth is also influenced to the elevational beam peak and the directivity.

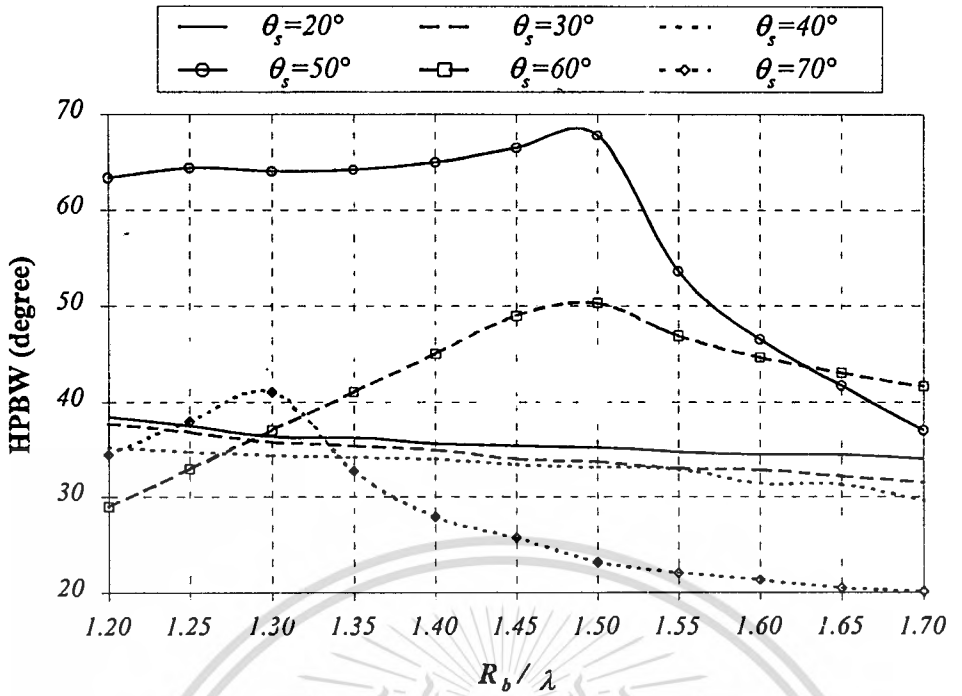

Fig.4.5 Simulation results of half-power beamwidth as a function of the outer spherical radius for various angles of slot pair positions

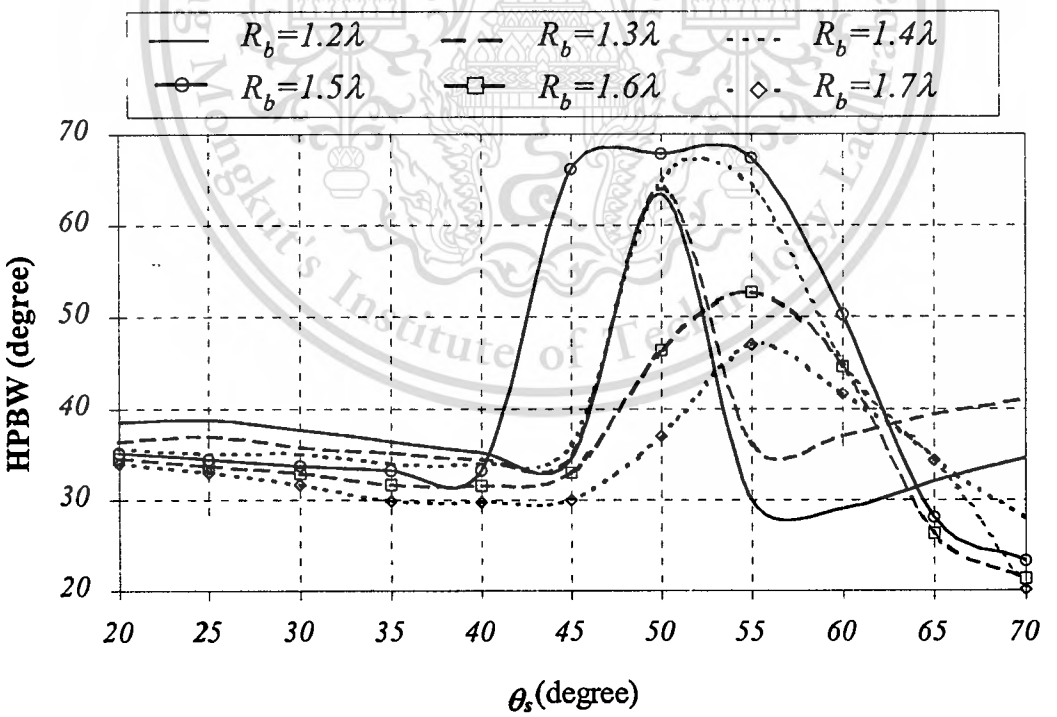

Fig.4.6 Simulation results of half-power beamwidth Directivity as a function of angles of **slot** pair positions for various outer spherical radii

4.4 Directivity

Directivity is another characteristic that is used to evaluate the merit of the antenna. Directivity can be calculated as the ratio of the radiation intensity of the antenna to the radiation intensity of isotropic source [4-5]. The directivity of the circularly polarized conical beam spherical slot array antenna can be estimated by using

$$\text{Directivity(dBi)} = 10\log\left|\frac{4\pi\left(\mathrm{E}_{co}(\theta,\phi)\big|_{max}\right)^2}{\int_0^{2\pi}\int_0^{\pi}\left|\mathrm{E}_T(\theta,\phi)\right|^2\sin\theta\,\mathrm{d}\theta\,\mathrm{d}\phi}\right| \tag{4.9}$$

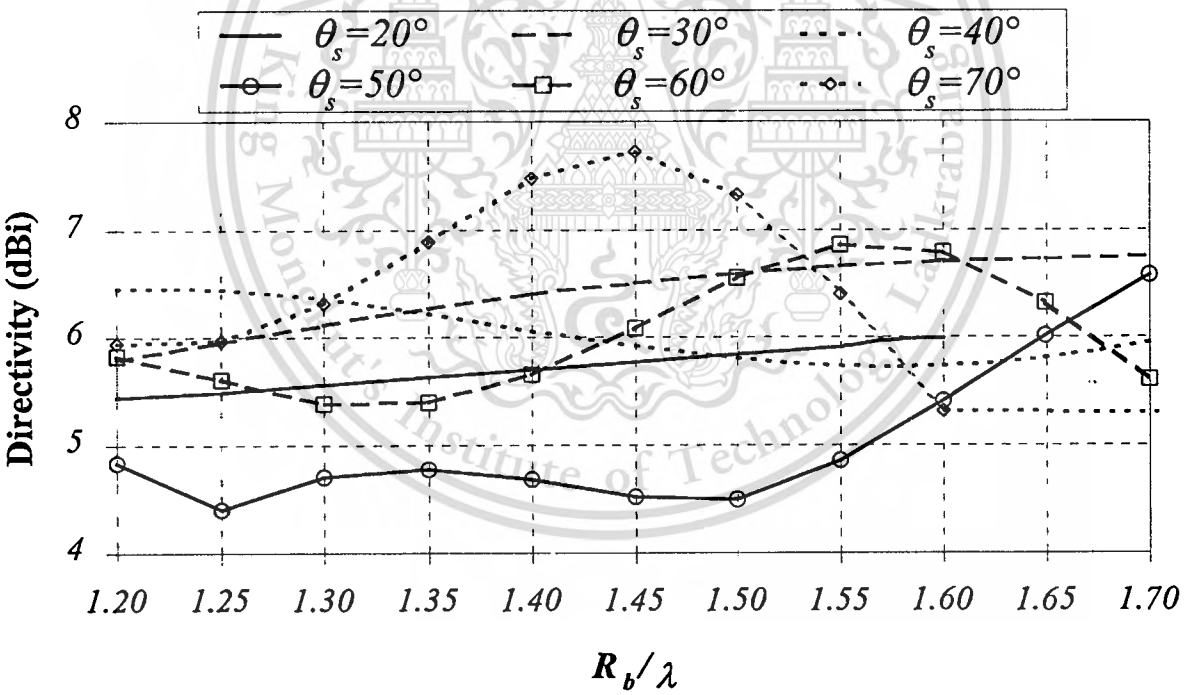

Fig. 4.7 Simulation results of directivity as a function of the outer spherical radius for various angles of slot pair positions

Fig.4.7 shows the directivity of the antenna as a function of the outer spherical radius for various angles of slot pair positions. It is apparent that the directivity is not significantly changed much when we adjust the radius of the sphere because the azimuthal spacing is slightly changed. However, it can be found that the directivity of the antenna with the radius between 1.2λ and 1.7λ is around *4.5-7.0* dBi.

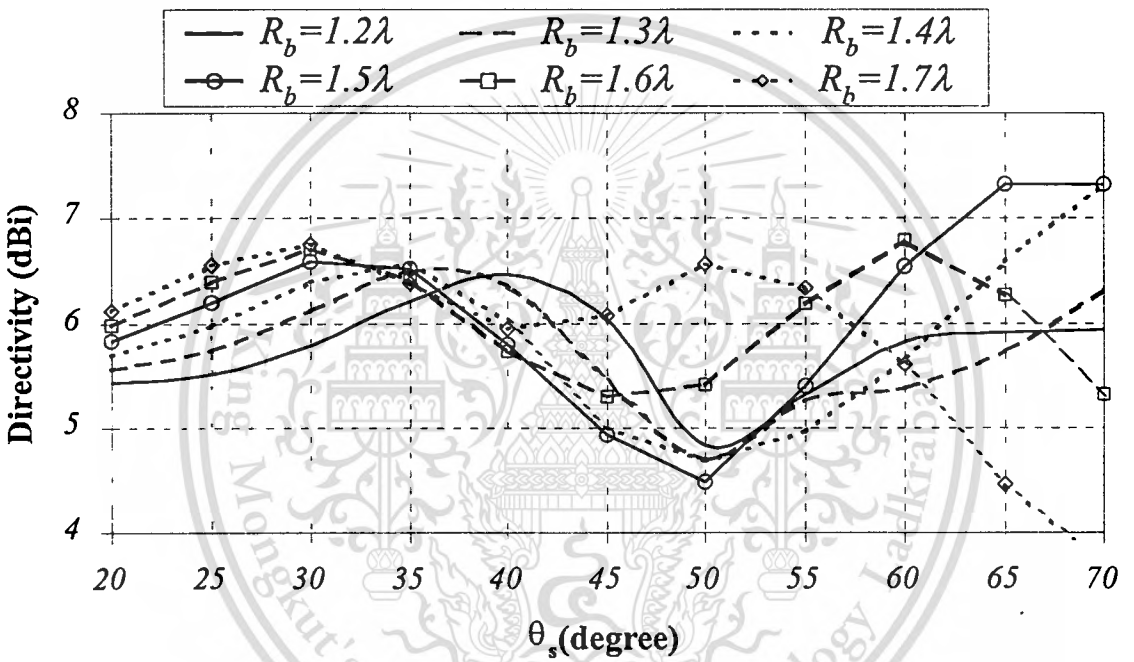

Fig. 4.8 Simulation results of directivity as a function of angles of slot pair positions for various outer spherical radii

Fig.4.8 illustrates the directivity as a function of angles of slot pair positions for various outer spherical radii. It is evident that the directivity is almost the same for different spherical radii. When the angle of the slot pair position is varied, it can be observed that the directivity is declined in the case of the angle ranged from *45°* to *55°*. This phenomenon is caused by the dilation of the beamwidth for these angles. Thus, if the high directivity is necessary the

angle of the slot pair position should be appropriately chosen to be around *30°-35°*.

4.5 Azimuthal Ripple

The azimuthal ripple is the notable parameter of the antenna to form the conical beam pattern. If the azimuthal ripple occurs, the conical beam cannot be completely realized. Hence, the antenna parameters should be appropriately chosen to keep away from the azimuthal ripple. The azimuthal ripple can be determined by

$$\text{Azimuthal Ripple (dB)} = 20\log\left(\frac{E_{co}(\theta_{max},\phi)|_{max}}{E_{co}(\theta_{max},\theta)|_{min}}\right) \quad (4.10)$$

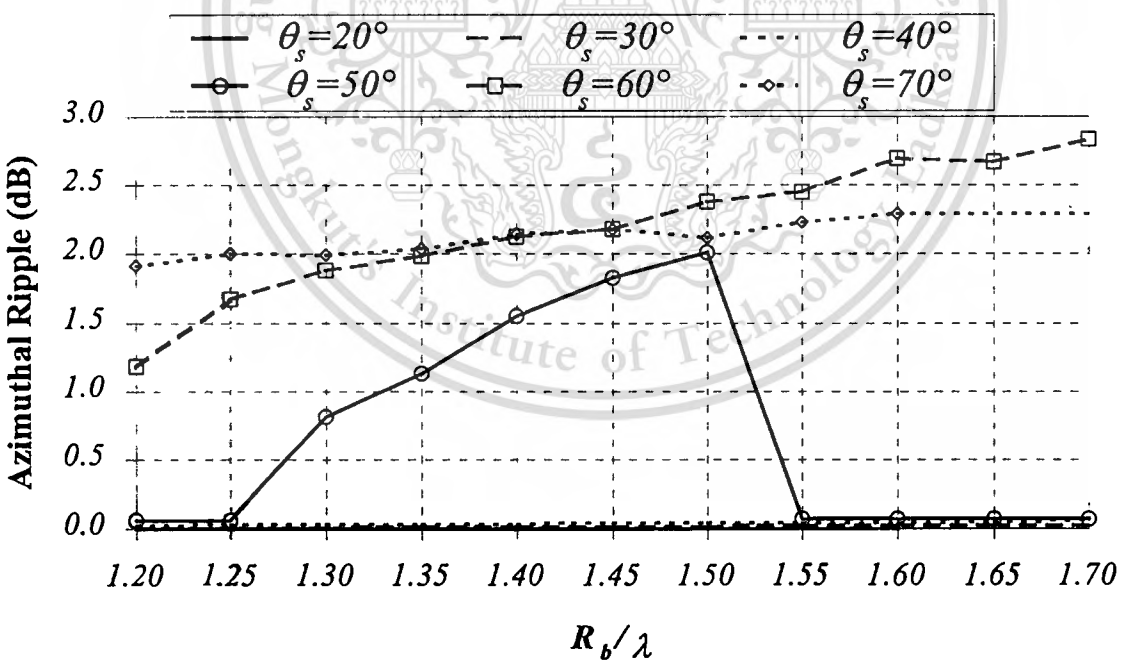

Fig.4.9 Simulation results of zimuthal ripples as a function of the outer spherical radius for various angles of slot pair positions

From Fig.4.9, the azimuthal ripple is observed for the case that the angle of the slot pair position exceeds $50°$. The variation of the spherical radius does not notably affect to the azimuthal ripple such as the angle of the slot pair position. This is because the azimuthal ripple will be occurred in case of the azimuthal spacing is not sufficiently small to be greater than 0.5λ and the angle of the slot pair position has more pronounceable contribution than the spherical radius.

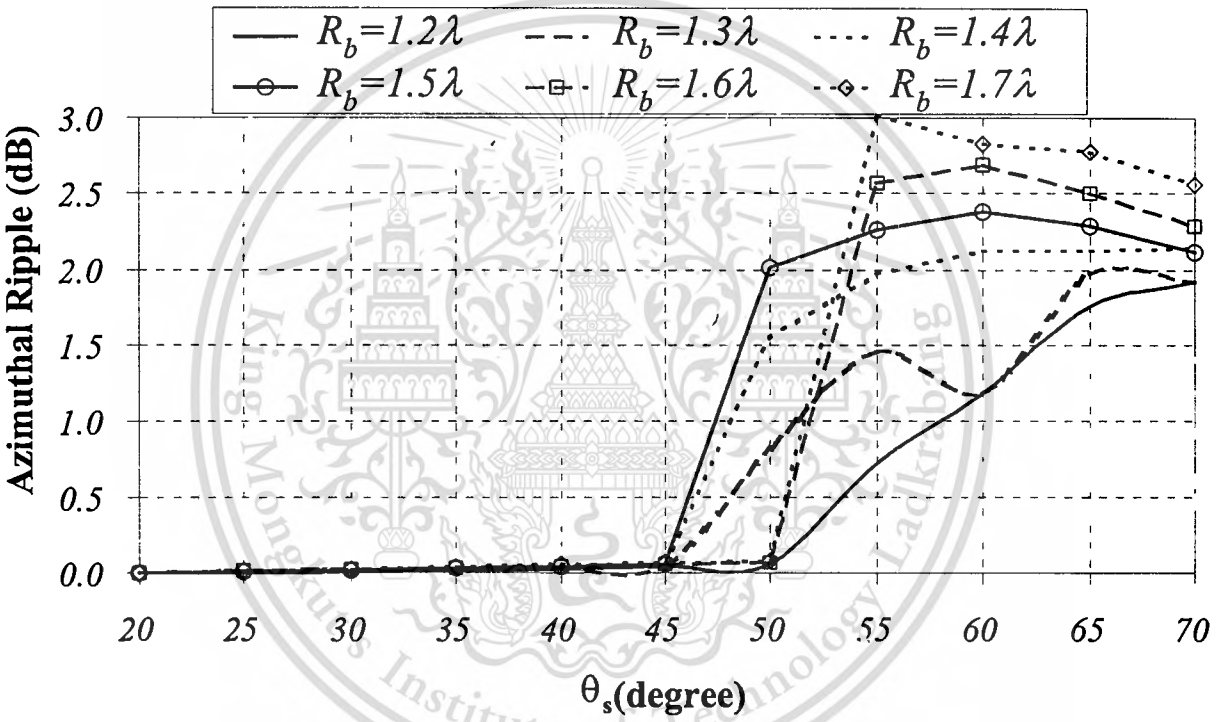

Fig.4.10 Simulation results of azimuthal ripple as a function of angles of slot pair positions for various outer spherical radii

The azimuthal ripple as a function of the angles of the slot pair positions for various outer spherical radii is plotted as shown in Fig.4.10. It can be found that for most of the spherical radii, the azimuthal ripple appears when the angle of the slot pair position is more than $45°$. Accordingly, the conical beam pattern can be realized for θ_s less than $45°$ for the radius 1.2λ and 1.7λ.

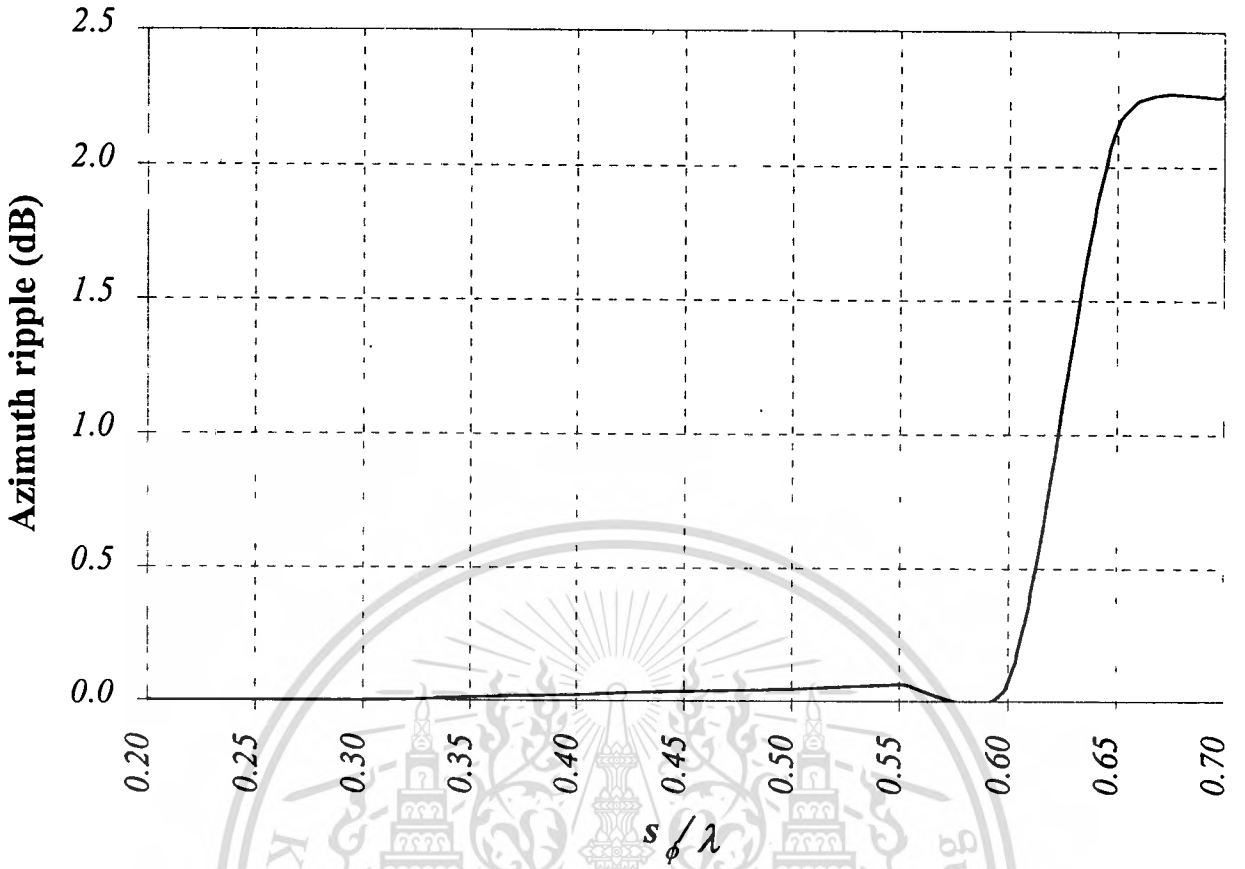

Fig.4.11 Simulation results of azimuthal ripple as a function of azimuthal spacing

Fig.4.11 illustrates the results of the azimuthal ripple as a function of azimuthal spacing. We found that the azimuthal ripples will be absent when the azimuthal spacing is less than around 0.6λ. This condition should consider for the antenna design to realize the conical beam pattern.

4.6 Back Lobe Ratio

Back lobe ratio is defined as the ratio of the maximum field radiated in the front side of the antenna to the maximum field radiated in the rear side of the antenna. It is desirable for the antenna to posses the low back lobe ratio since it should radiate as less as possible in the back side. However, this circumstance is difficult to avoid since the spherical cavity has the finite radius. The back lobe ratio will be infinity or it can be no back lobe only if the radius

of the sphere is infinite extent and the spherical surface becomes the plane. The back lobe ratio can be determined by using

$$\text{Back Lobe Ratio (dB)}=20\log\left|\frac{E_{co}(0\le\theta\le\pi/2,\phi)|_{max}}{E_{co}(\pi/2<\theta\le\pi,\phi)|_{max}}\right| \qquad (4.11)$$

To extend the investigations of the effect of the finite radius of the sphere, the back lobe ratio for various sizes of the sphere is plotted as shown in Fig.4.12. As expected, the larger the radius of the sphere the larger the value of the back lobe ratio. The constraint of the back lobe ratio is that the values become infinity (no back lobe) when the radius of the sphere is infinity (spherical surface becomes planar surface).

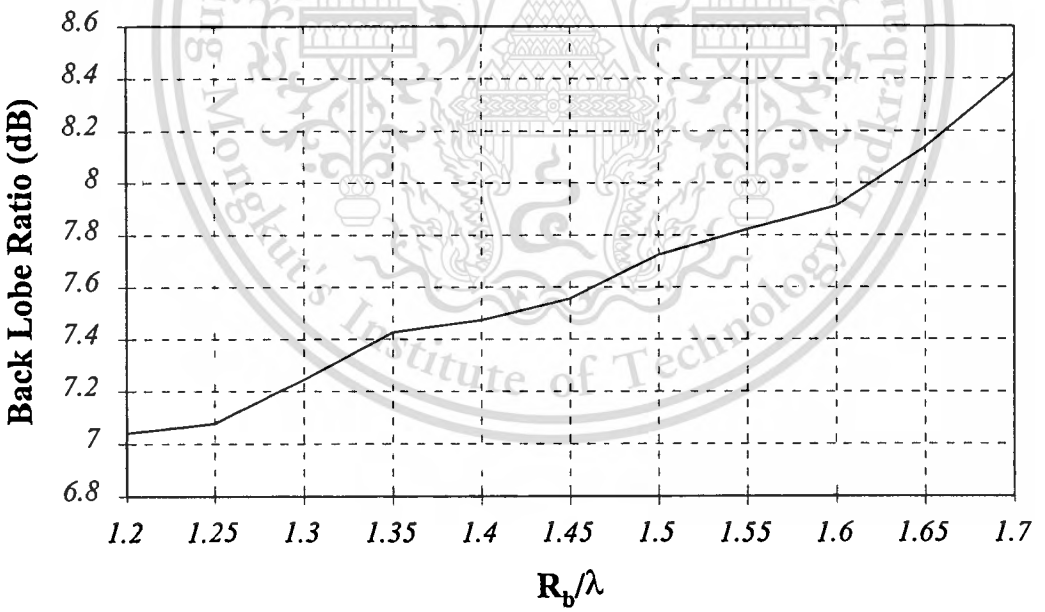

Fig.4.12 Simulation results of Back lobe ratio as a function of the outer spherical radius

It is noted that the back lobe ratio is calculated under the assumption that the dyadic Green's function outside the cavity is the free space dyadic Green's function with the presence of whole sphere. Therefore, in the actual situation the accuracy of this results is not reasonable due to the truncation at the edge of the cavity and the diffracted field has more pronounce effect. So, the reality back lobe ratio can be further obtained from the measurement and it is left for further investigations.

4.7 Design Criteria

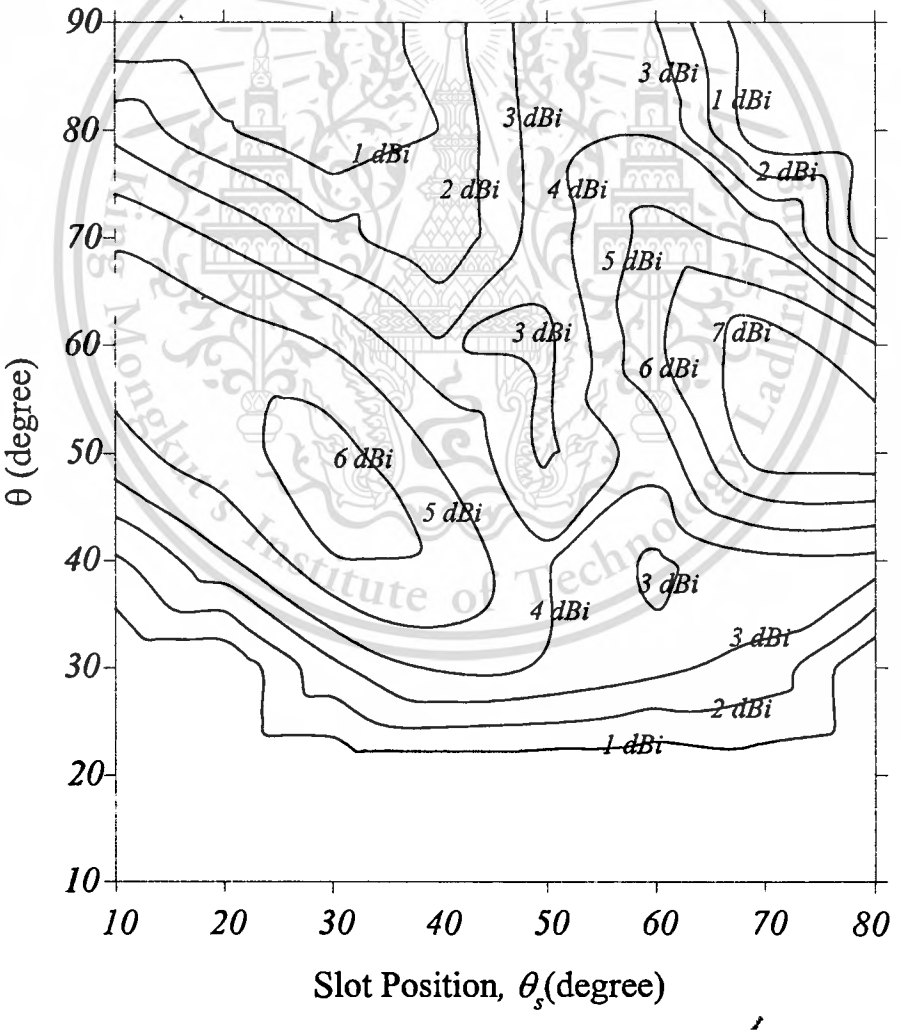

Fig.4.13 Simulation results of contour of directivity as a function of the angle of slot pair position ($R_b = 1.43\lambda$)

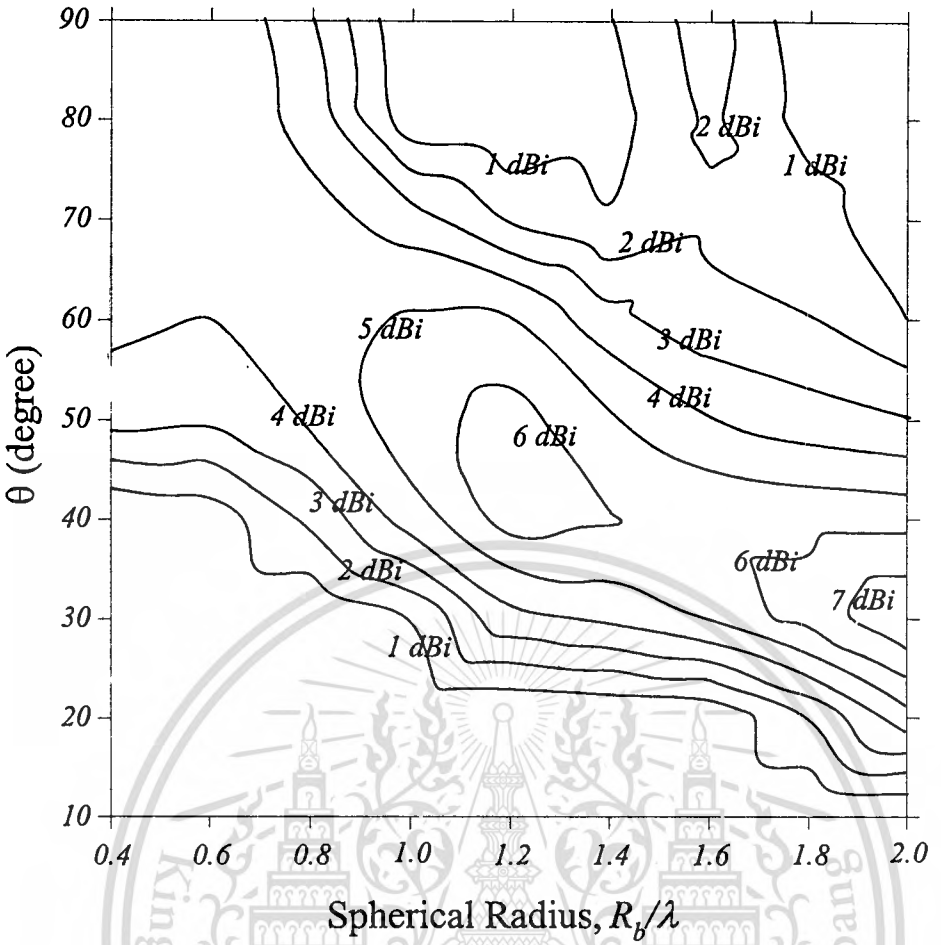

Fig.4.14 Simulation results of contour of directivity as a function of the spherical radius ($\theta_s = 40°$)

To design the circularly polarized conical beam spherical slot array antenna, the design criteria are provided. The contour of directivity as a function of the angle of slot pair position (θ_s) and the spherical radius (R_b) are shown in Figs.4.13 and 4.14, respectively. These contours are plotted in case of the azimuthal spacing is fixed to be 0.481λ. Other design parameters are listed in Table 4.1 [4-6]. By this way, to design a circularly polarized conical beam spherical slot array antenna for a specified directivity, the angle of slot pair position (θ_s) and the spherical radius (R_b) can be determined by using Fig.4.13 and Fig.4.14, respectively. Fig.4.13 shows the contour of directivity when R_b is

fixed at 1.43λ. From this graph, we can observe that the antenna provides a *6.5* dBi directivity at an angle (θ) of 45° when the angle of slot pair position is at 30°. For example, when the desired directivity is *7* dBi, an appropriate angle (θ) of 60° at an angle of slot pair position (θ_S) less than 75° can be chosen. Fig.4.14 shows the contour of directivity when θ_S equals 40°. If one chooses the spherical radius of 1.2λ, a 6 dBi directivity can be obtained at an angle around 40° to 55°. However, when the azimuthal spacing is fixed, the angle of slot position (θ_s) and spherical radius (R_b) cannot be arbitrarily varied because the number of slot pairs should be discrete value as the integer. Accordingly, the directivity in a particular direction can be designed from these contours of directivity.

4.8 Conclusion

The radiation pattern of the antenna appears to be the conical beam radiation i.e., the null occurs in boresight axis, the elevational beam peak varies between *20-80* degrees (measured with respect to the horizontal line) and the azimuthal pattern possesses the identical field strength. The elevation angle can be adjusted by varying the radius of the cavity and the angle of the slot pair position. The directivity of the antenna is determined to fulfill the specification of the actual applications. The contour plots of the directivity for various elevational beam directions as the functions of the spherical radius and the angle of the slot pair position are illustrated as the guideline for the antenna design.

References

[4-1]C.T.Tai, *Dyadic Green Function in Electromagnetic Theory*, 2nd Ed. New York: IEEE Press, 1993.

[4-2]M.Abramowitz and I.A.Stegun (eds.), *Handbook of Mathematical Functions with Formulas, Graphs and Mathematical Tables*, Dover Publications, New York, 1970.

[4-3]C.Phongcharoenpanich, M.Krairiksh and J.Takada, "Investigations of radiation characteristics of a circularly polarized conical beam spherical slot array antenna," *IEICE Trans. Electronics*, vol. E82-C, no.7, pp.1242-1247, July 1999.

[4-4]P.S.Kildal, *Foundation of Antennas: A Unified Approach*, Lund, Sweden: Studentlitteratur, 2000.

[4-5]*IEEE Standard Definitions Terms for Antennas*, IEEE Std 149-1979, published by IEEE, Inc., 1993, distributed by Wiley-Interscience.

[4-6]C.Phongcharoenpanich, M.Krairiksh, K.Meksamoot and J.Takada, "Radiation characteristics of a circularly polarized conical beam spherical slot array antenna," *Proceeding of the 1998 Asia-Pacific Microwave Conference*, Yokohama, vol. 3, pp. 1229-1232, Dec. 1998.

Chapter 5

Impedance, Polarization Characteristics and Bandwidth of the Antenna

5.1 Introduction

This chapter presents the impedance, polarization characteristics and bandwidth of a circularly polarized conical beam spherical slot array antenna. The initial parameters from the previous chapter are used for characterizing the impedance characteristics. The parameters yielding the optimum matching condition will be clarified. The axial ratio is investigated to show the circularity of the pattern radiated from the antenna. The theoretical bandwidth of the antenna is also included.

5.2 Impedance Characteristics

The input impedance at the feeding point is the most significant parameter to clarify the matching condition between the antenna and the transmission line. The input impedance is defined as the ratio of the voltage excitation to the current excitation. From the known current distribution of the feeding probe that is obtained from Chapter 3, and with the reference at the feeding point, the input impedance is inversely proportional to the current excitation while the voltage is set to be unity to simplify the calculation. It can be written as [5-1]

$$Z_{in} = \frac{V_{in}}{I_{in}} \tag{5.1a}$$

or

$$Z_{in} = \frac{1}{J(R_f' = R_a, \theta_f = 0°, \phi_f = 0°)} \tag{5.1b}$$

The other impedance characteristics which is also necessary to be specified are the reflection coefficient and the standing wave ratio. The formulations to determine the reflection coefficient and the standing wave ratio can be written as [5-2]

$$\Gamma = \frac{Z_{in} - Z_o}{Z_{in} + Z_o} \tag{5.2}$$

where Γ is the reflection coefficient, Z_{in} is the input impedance of the antenna and Z_o is the characteristic impedance of the transmission line.

$$\text{Reflection Coefficient (dB)} = 20\log|\Gamma| \tag{5.3}$$

and

$$SWR = \frac{1+|\Gamma|}{1-|\Gamma|} \tag{5.4}$$

5.3 Impedance Bandwidth

Impedance bandwidth is the frequency range that the sufficient matching condition is obtained. To realize the impedance bandwidth, the standing wave ratio less than *2.0* is used as the indicating value. The antenna should possess the standing wave ratio less than *2.0* over these frequency ranges. The impedance bandwidth of the antenna is obtained from the following formula:

$$\text{Impedance Bandwidth (\%)} = \frac{f_H(\text{SWR} \le 2.0) - f_L(\text{SWR} \le 2.0)}{f_o} \times 100 \qquad (5.5)$$

where f_o is the operating frequency.

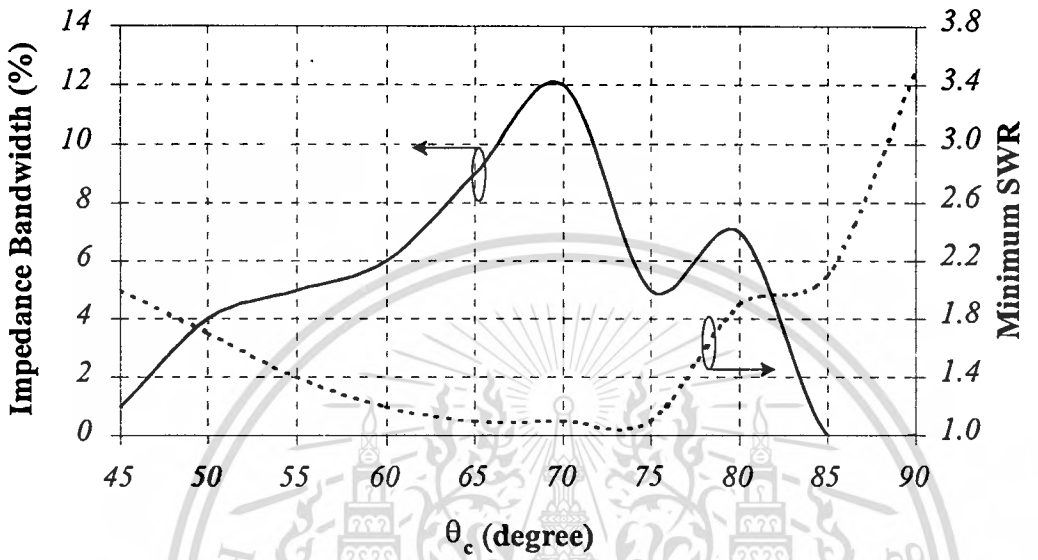

Fig.5.1 Impedance bandwidth and minimum SWR as a function of the shorted conical angle

Since this antenna is designed by using the preliminary parameters as determined in chapter 2, the radiation characteristics are first investigated to reveal the parameters that affect to the radiation pattern, elevation angle, directivity and azimuthal ripple. It can be clarified that these radiation characteristics depend on the angle of the slot pair position and the spherical radius. In addition, the angle of the slot pair of 40° and the spherical radius of 1.43λ are used as the design parameters to obtain the conical beam pattern with the elevational beam peak of 40° and the directivity of *6.1* dBi. However, the shorted conical angle is fixed at 64° as the initial parameter. From the investigation, it is obvious that this parameter is another parameter that can be adjusted to meet the optimum impedance matching. Fig.5.1 shows the

impedance characteristics such as the impedance bandwidth and minimum SWR as a function of the shorted conical angle. It is apparent that the shorted conical angle of $70°$ yields the minimum SWR and widest impedance bandwidth. Therefore, this parameter is also used to be the design parameter for further investigation.

From the antenna parameters selected in the previous section, the result of the input impedance for various frequencies is shown in Fig.5.2. It is found that the impedance exhibits as the capacitive reactance when the frequency is lower than $0.94f_o$ and it becomes inductive reactance when the frequency is higher. The impedance at the operating frequency (f_o) is $40.9 + j0.1\ \Omega$.

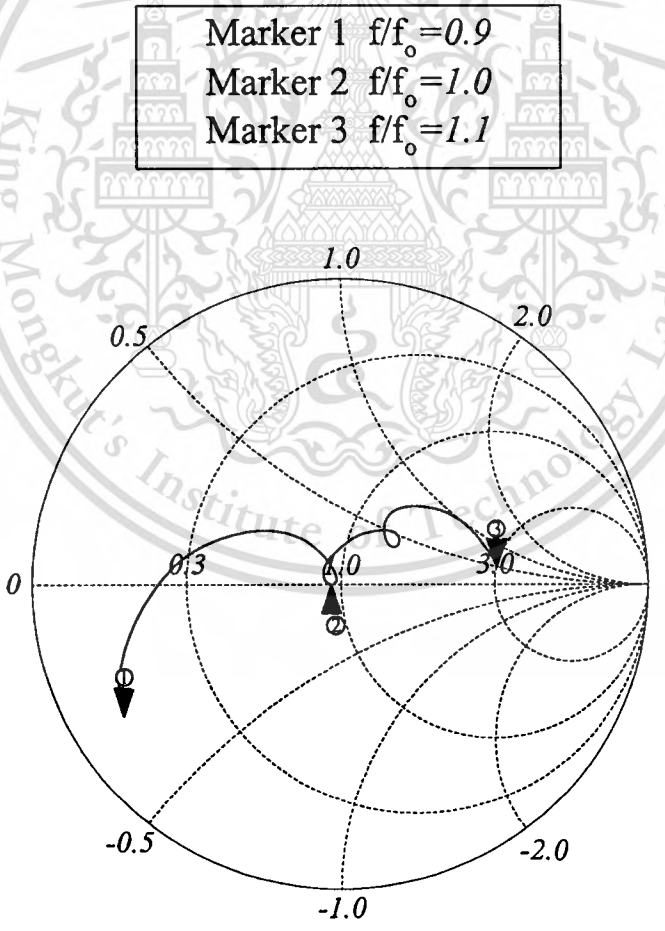

Fig. 5.2 Input impedance of the antenna

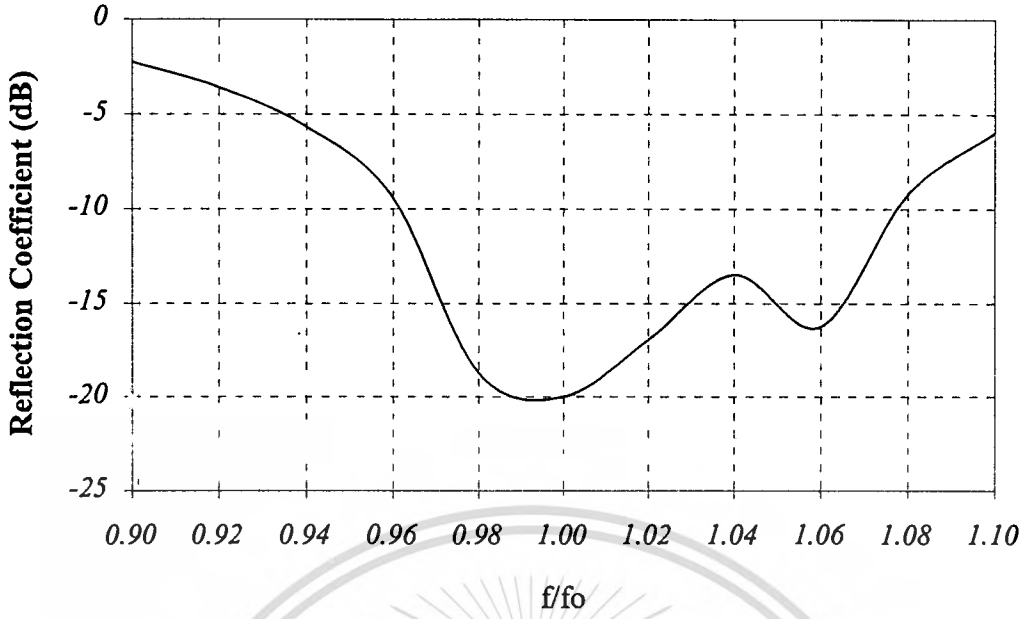

Fig.5.3 Frequency response of the reflection coefficient

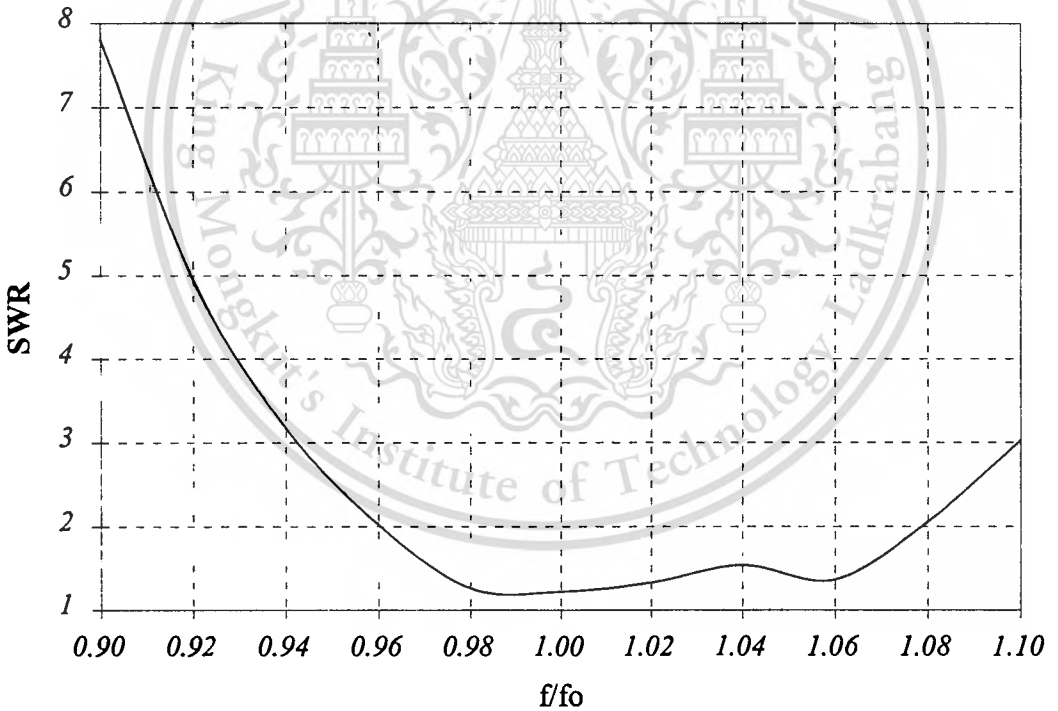

Fig.5.4 Frequency response of the standing wave ratio

Fig.5.3 and Fig.5.4 illustrate the frequency response of the reflection coefficient and the standing wave ratio. From these two graphs, we can find the impedance bandwidth that the reflection coefficient is not greater than *–9.542*

dB or the standing wave ratio is less than *2.0*. Seemingly, the impedance bandwidth of *12%* is observed [5-3].

5.4 Polarization Characteristics

Principally, a spherical slot array antenna is designed to radiate the conical beam with the right-hand circular polarization. In this event, the component of the field in the left-hand circularly polarized rotation should be substantially examined. This field component is referred to as the cross-polarized pattern. It can be found by using [5-4]

$$E_{xp}(\theta,\phi) = \bar{E}_T(\theta,\phi)\cdot\frac{\hat{\theta} - j\hat{\phi}}{\sqrt{2}} \tag{5.6}$$

The next parameter that expresses the polarization circularity is the axial ratio. The axial ratio is defined as the maximum field component (major axis of polarization ellipse) to the minimum field component (minor axis of polarization ellipse) radiated from the antenna. The axial ratio can be determined from

$$\text{Axial Ratio (dB)} = 20\log\left|\frac{|E_{co}| + |E_{xp}|}{|E_{co}| - |E_{xp}|}\right| \tag{5.7}$$

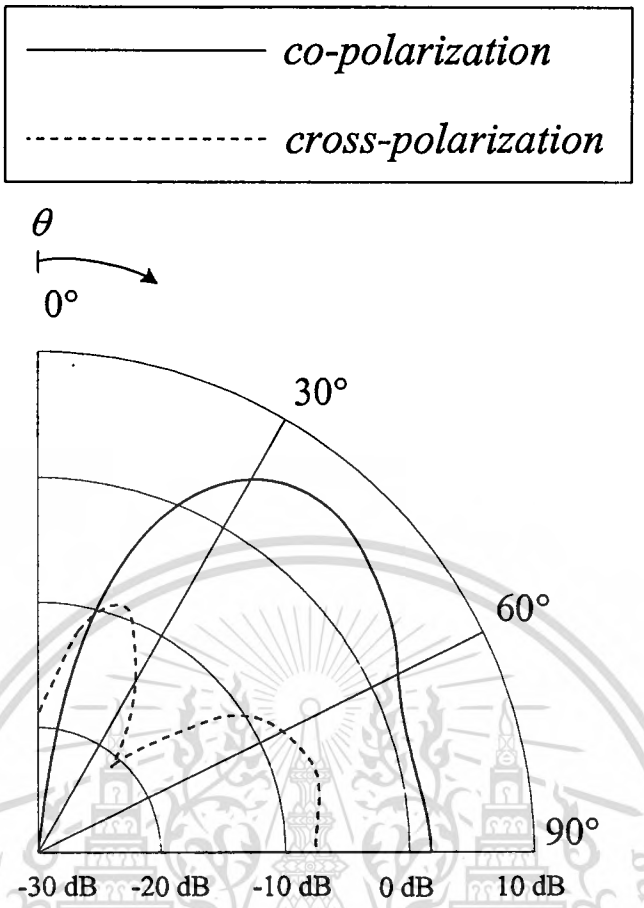

Fig.5.5 Cross-polarized pattern

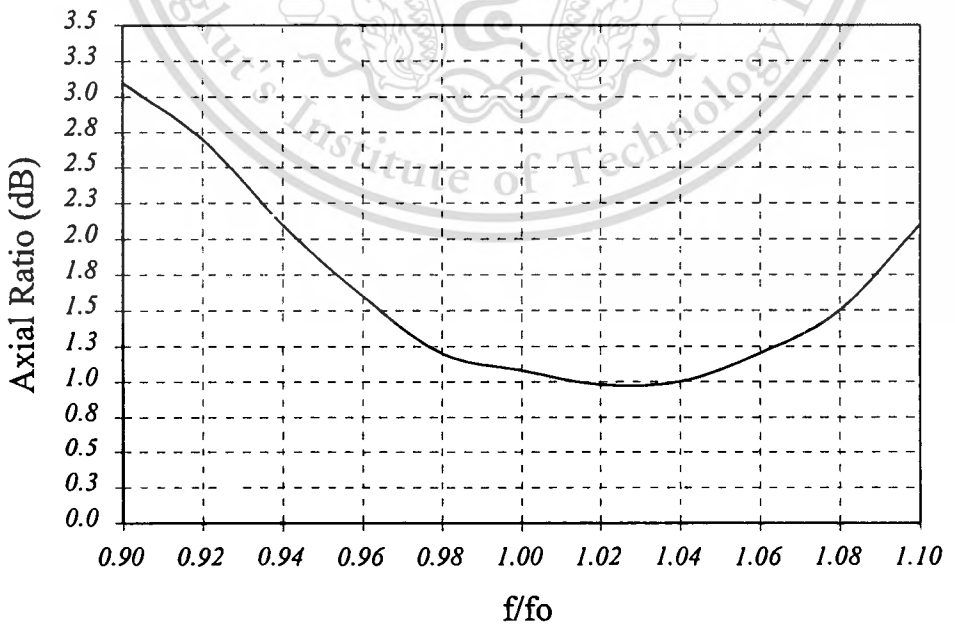

Fig.5.6 Frequency response of the axial ratio

The cross-polarized pattern is shown in Fig.5.5. It can be inspected that the cross-polarized level is *–26* dB less than the co-polarized one at the elevational beam peak. The axial ratio of this antenna is also estimated to perform the polarization characteristics. Fig.5.6 shows the axial ratio at the elevational beam peak as a function of the frequency. At the operating frequency, the axial ratio of *1.1* dB is attained by this antenna. Moreover, the purity of the circular polarization can be realized by optimized the slot design such as the slot length and slot location. This topic is under investigation.

5.5 Polarization Bandwidth

Polarization bandwidth of the antenna radiating circularly polarized pattern is the frequency range that the polarization circularity is still acceptable. Normally, the nominal value of *3* dB axial ratio is extensively used as the standard, therefore, the axial ratio over this frequency range must be less than *3* dB. Theoretically, the polarization bandwidth of this antenna can be found by using

$$\text{Polarization Bandwidth (\%)} = \frac{f_H(\text{3 dB axial ratio}) - f_L(\text{3 dB axial ratio})}{f_o} \times 100 \quad (5.8)$$

Illustrated in Fig.5.6, the axial ratio of the antenna is lower than *3.0* dB over the frequency range between $0.9f_o$ and $1.1f_o$. Therefore, from the viewpoint of the polarization characteristics, the bandwidth of *20%* is obtained with the less than *3* dB axial ratio [5-5].

5.6 Pattern Bandwidth

The pattern bandwidth is the frequency range in which the pattern is applicable in view of the applications. In case of a spherical slot array antenna, it is designed to radiate the conical beam pattern. In the dynamic range of the operating bandwith, the conical beam pattern should be obtained. For instance, the elevational beam peak directs to the desired direction, and the azimuthal ripple should be as small as possible or it is nearly zero. The directivity should be high enough for the application requirements. Fig.5.7 shows the radiation patterns, both elevational and azimuthal patterns, of the antenna for various frequencies. It can be observed that the conical beam is procured for over a wide range of the frequencies. The elevational beam peaks are different when the frequency is changed. The azimuthal pattern is completely circle. Hence, this antenna can provide the conical beam pattern over the frequency range as portrayed in Fig.5.7. For further application, the pattern bandwidth of the antenna is restricted by the deviation of the elevational beam peak from the desired one. For example, if the antenna is installed at the location where the elevational beam peak of 30° is required and the deviation of the beam peak should be less than 5°, the frequency range that enables the beam peak between 25° and 35° will be termed the pattern bandwidth.

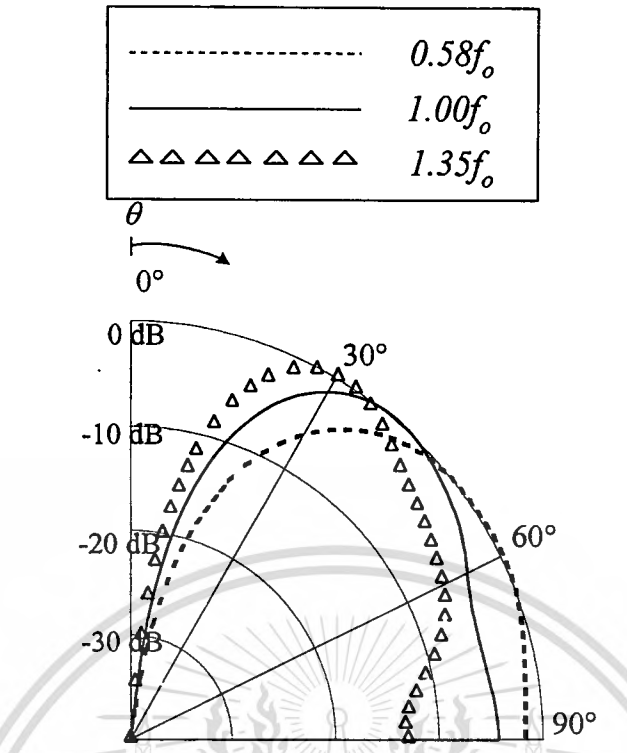

(a) Elevational pattern

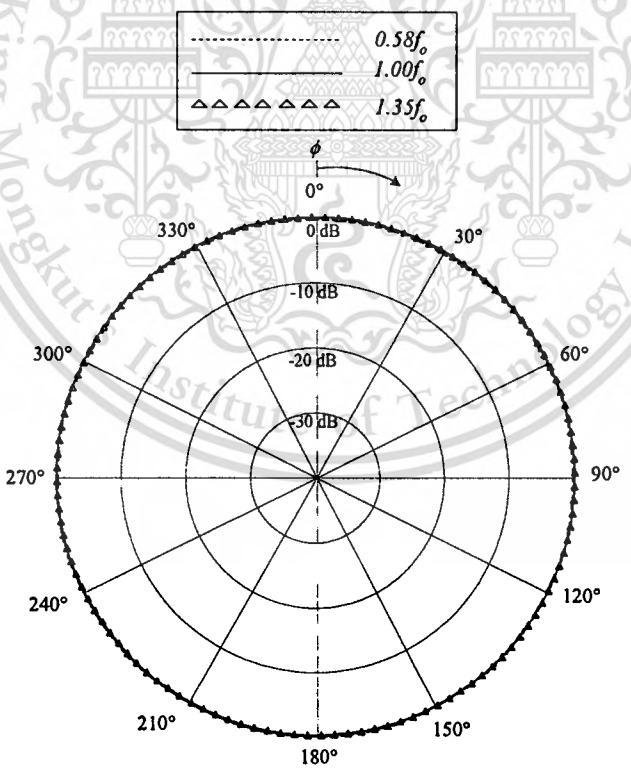

(b) Azimuthal pattern

Fig.5.7 Radiation patterns for various frequencies

Fig.5.8 shows the frequency response of the elevational beam peak. From this graph, it is obvious that the elevational beam peak varies proportionally to the frequency. The higher the frequency, the higher the elevational beam peak.

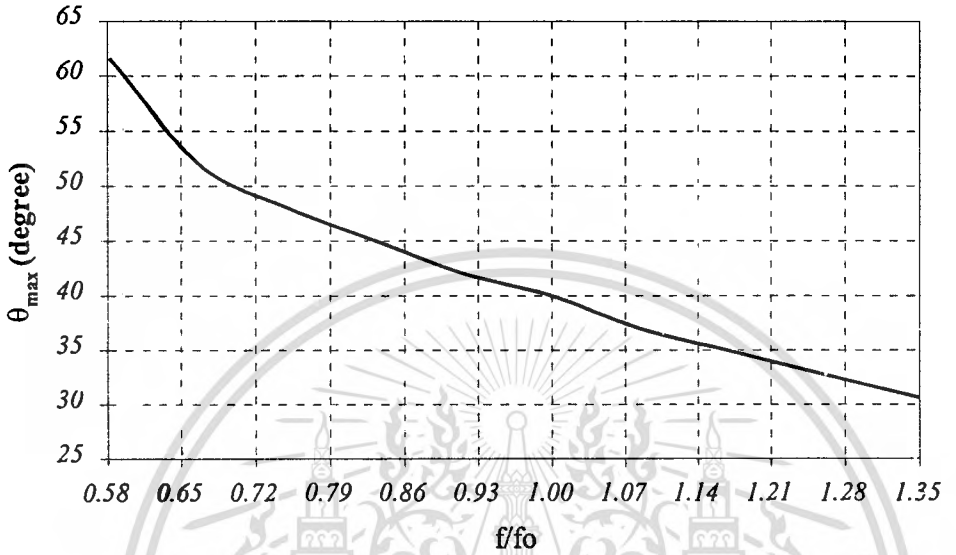

Fig.5.8 Frequency response of the elevational beam peak

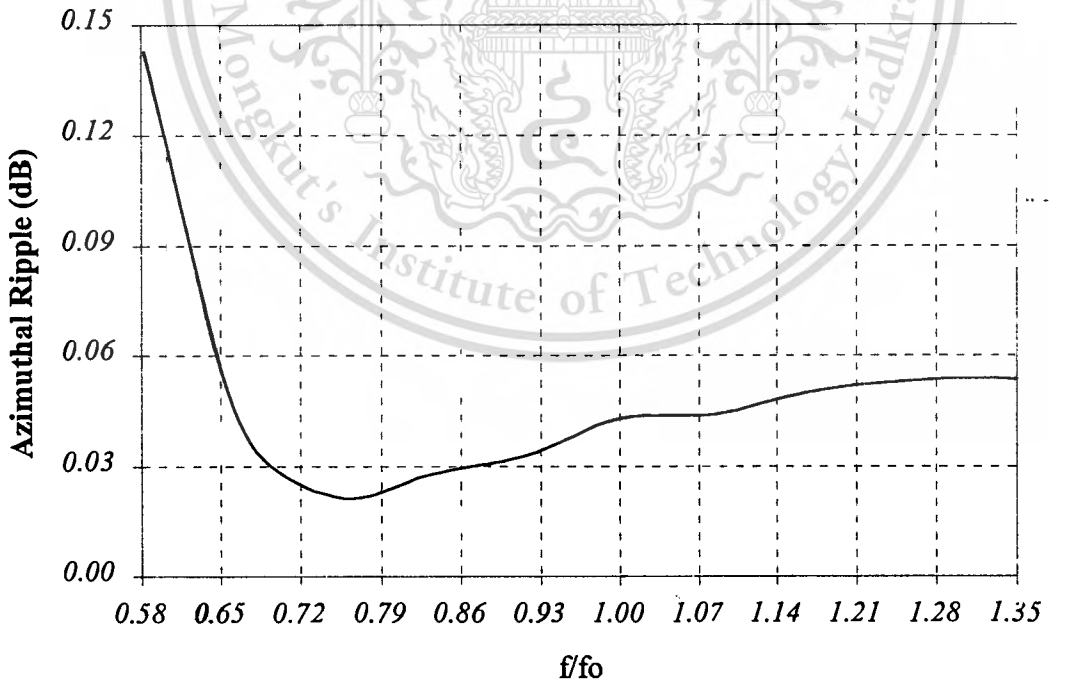

Fig.5.9 Frequency response of the azimuthal ripple

Fig.5.9 shows the azimuthal ripple as a function of the frequency range. Obviously, the level of the azimuthal ripple is relatively low over a wide range of the frequencies.

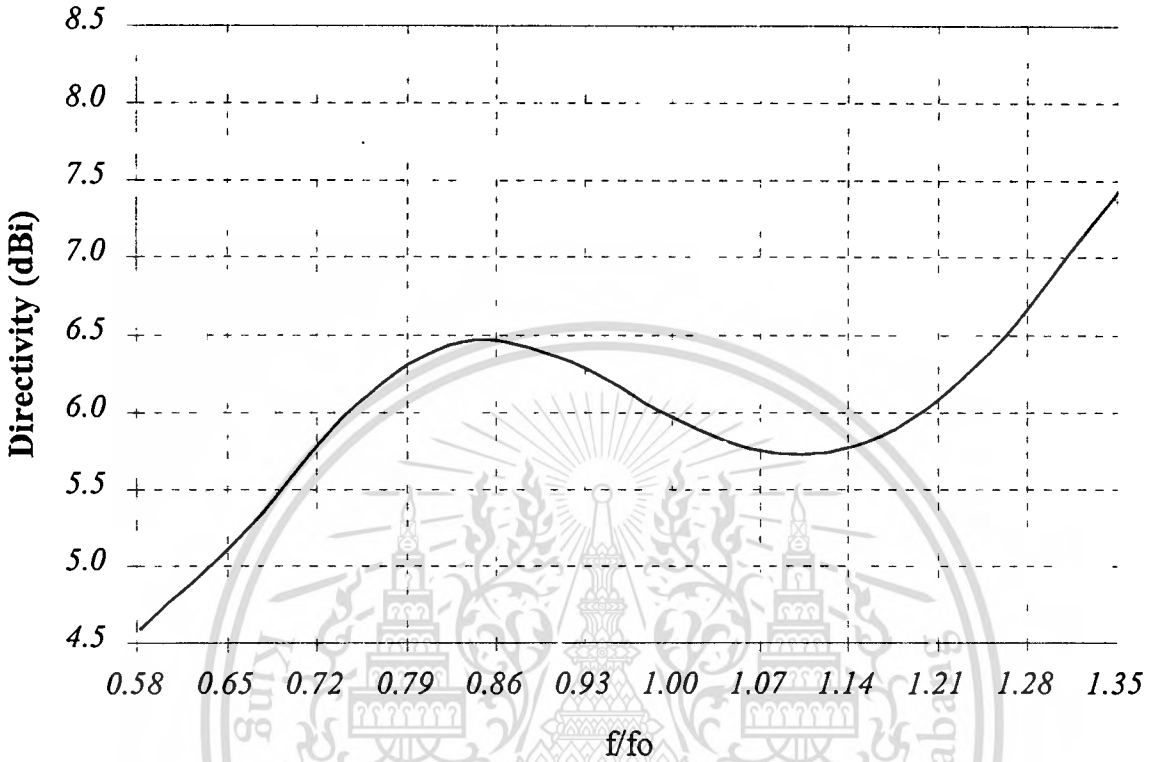

Fig.5.10 Frequency response of the directivity

Fig.5.10 shows the frequency response of the directivity. It is found that the directivity of *5.7-7.5* dBi can be obtained over the frequency ranging from $0.72f_o$ to $1.35f_o$ of the operating frequency with which this antenna can fulfill the requirement of the mobile satellite communication system.

5.7 Conclusion

The impedance characteristics of the antenna are analyzed to clarify matching condition of the antenna when connected to the transmission line. The matching condition can be improved by adjusting the distance between the position of the slot pairs and the location of the shorted conical angle. The

bandwidth of the antenna for many of shorted conical angles is investigated. The axial ratio is calculated to find the optimum condition of the circularly polarized radiation. According to the results of the analysis, the antenna with the acceptable properties can be designed. The experimental verification will be presented in the next chapter.

References

[5-1]C.A. Balanis, *Advanced Engineering Electromagnetics*, New York: Wiley and Sons. 1989.

[5-2]J.Helszajn, *Microwave Engineering: Passive, Active and Non-Reciprocal Circuits*, McGrawHill: Cambridge. 1992.

[5-3]C.Phongcharoenpanich, M.Krairiksh and J.Takada, "Impedance characteristics of a circularly polarized conical beam spherical slot array antenna," *Proceedings of the AP2000 Millennium Conference on Antennas and Propagation*, Davos, vol.1, p.203, Apr. 2000.

[5-4]P.S.Kildal, *Foundation of Antennas: A Unified Approach*, Lund, Sweden: Studentlitteratur, 2000.

[5-5]C.Phongcharoenpanich, M.Krairiksh and J.Takada, "Polarization characteristics of a circularly polarized conical beam spherical slot array antenna," *Proceedings of the 5th International Symposium on Antennas, Propagation and Electromagnetic Theory*, Beijing, pp. 638-641, Aug. 2000.

Chapter 6

Antenna Measurements

6.1 Introduction

To verify the proposed principles that have been explained in the preceding chapters, the prototypes of the antenna that the parameters are optimized as mentioned in the previous chapter were fabricated. The antenna measurements were set up to test the characteristics of a circularly polarized conical beam spherical slot array antenna. The radiation patterns in both elevational and azimuthal directions are measured. The impedance characteristics such as the input impedance are tested by using the Network Analyzer. The axial ratio is experimented by using the circular component method.

6.2 Antenna Fabrication

To verify the conical beam radiation, the experiment was set up at the frequency of *2.4* GHz (standard frequency of land mobile satellite communication) to measure the elevational and azimuthal radiation patterns. The dimensions of the circularly polarized conical beam spherical slot array antenna are summarized in Table 6.1 [6-1].

Table 6.1 Antenna dimension used for fabrication

Slot length (l_s)	*6.25* cm
Slot width (w_s)	*0.21* cm
Outer spherical radius (R_b)	*17.88* cm
Inner spherical radius (R_a)	*15.88* cm
Shorted conical angle (θ_c)	*70.00°*
Center of slot pair angle (θ_s)	*40.00°*
Azimuthal spacing between slot pair (s_ϕ)	*6.01* cm
Elevational distance between slot in pair (d_θ)	*2.75* cm
Numbers of slot pairs (N_s)	*12*

The fabricated antenna consists of two parts of conductors; the outer spherical conductor with a number of slots cut on it and the inner surface with the ring of the shorted conical conductor. The metal plates of those two parts are projected from the spherical prototype, and they are duplicated to the curve surface by compressing with the mold. The slots on the outer spherical surface are cut by using the computer-numerically controlled (CNC) machine. The tolerance of the machine used to fabricate is ± *0.1* μm. The probe of *1.6* cm in length, made of the metallic conductor is connected via N-type connector to feed the antenna at the center of the cavity. The photograph of the prototype antenna is depicted in Fig.6.1.

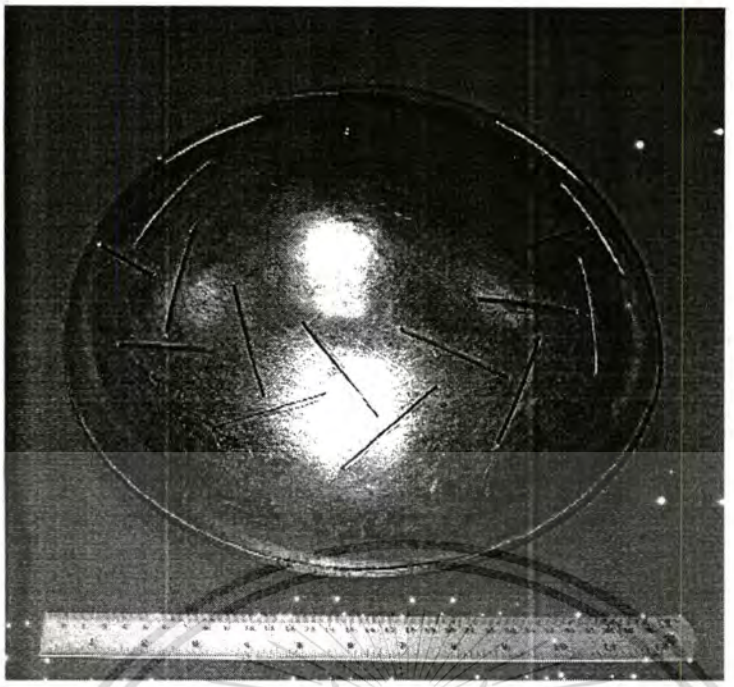

Fig 6.1 Prototype of a circularly polarized conical beam spherical slot array antenna

6.3 Radiation Pattern

The outdoor field test was done at the deck of the campus building, and the far-field range of *6* m is used [6-2]-[6-3]. A *10*-turn helical antenna with the axial ratio of *0.4* dB was employed to transmit a right-hand circularly polarized wave, and the antenna under test was rotated to receive the transmitted wave at *10°* per step until the angle of *90°*. These angles of measurement are chosen in order that the elevational beam peak can be determined and this characteristic is very important for the practical applications. Therefore, the co-polarized pattern of the angles between *0°* and *90°* is measured. The measurements set up to test the elevational and azimuthal co-polarized patterns are depicted in Fig.6.2. and Fig.6.3, respectively. After the elevational pattern is measured, the elevational beam peak is determined. The azimuthal pattern measurement is set up where the angle between the transmitting and the receiving antennas is equal

to the angle of the elevational beam peak. Then, the antenna under test is rotate $10°$ per step from $0°$ to0 $360°$. It is noted that the azimuthal pattern has to be measured for full circle because the field strength of the conical beam pattern should be identical to all directions of the antenna. This characteristic is necessary because the tracking system will no longer necessary.

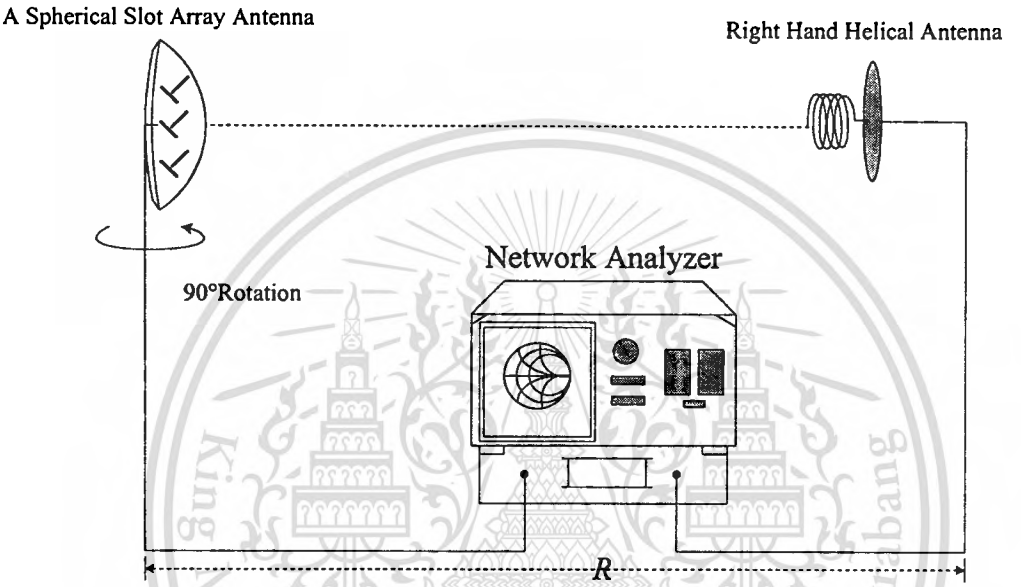

Fig.6.2 Measurement set up of the elevational co-polarized pattern

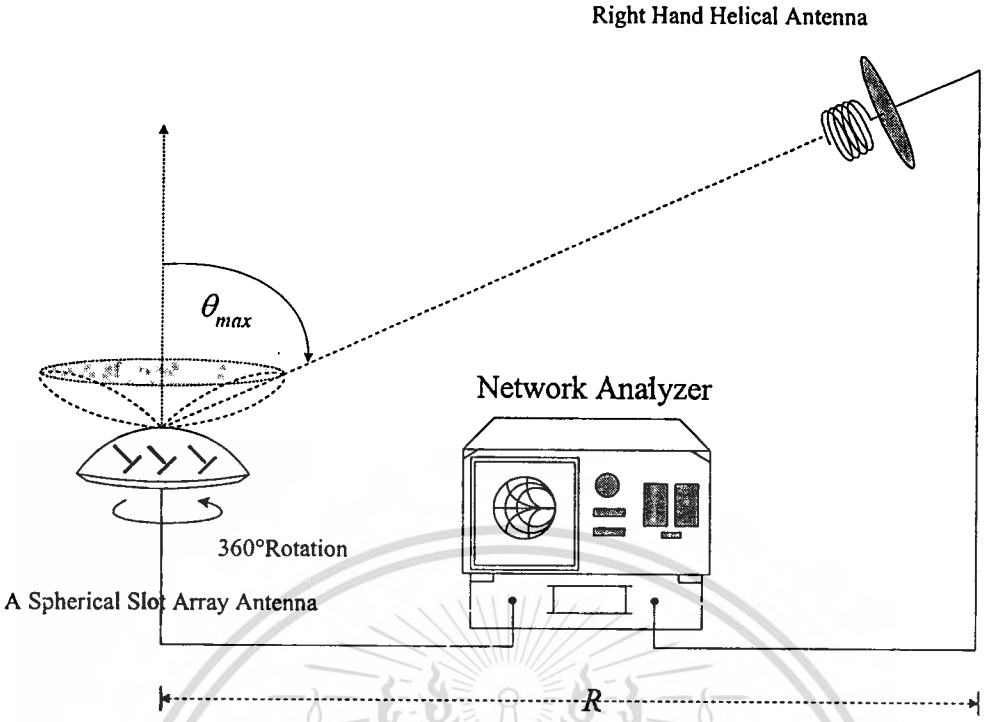

Fig.6.3 Measurement set up of the azimuthal co-polarized pattern

Experimental result of radiation pattern in the elevational plane is plotted and compared with the calculation as shown in Fig. 6.4. From this comparison, we can see that these results are in good agreement i.e., the beam peak is at *40°*; however, there are some errors on account of the diffraction at the edge of the cavity, the imperfect fabrication and the test-site situations [6-4]. Fig. 6.5 shows the azimuthal pattern of the antenna at the elevational beam peak direction (θ=*40°*). The theoretical and experimental results are comparatively illustrated. These results agree very well and are completely omnidirectional.

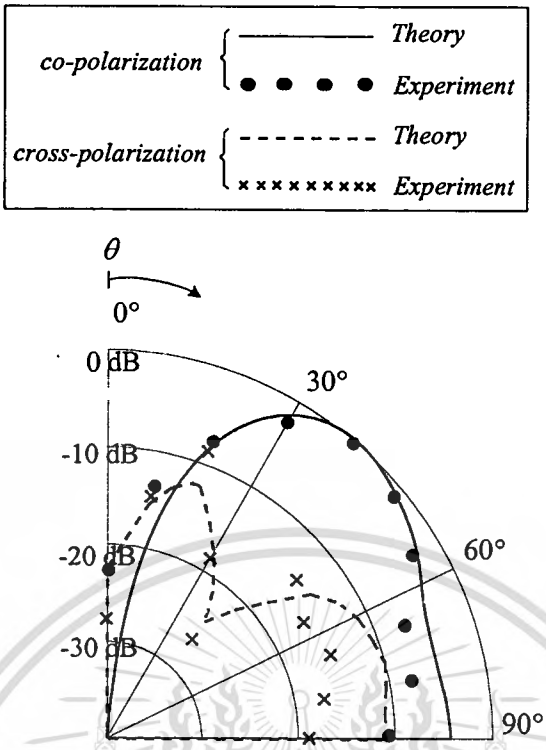

Fig.6.4 Elevational radiation pattern

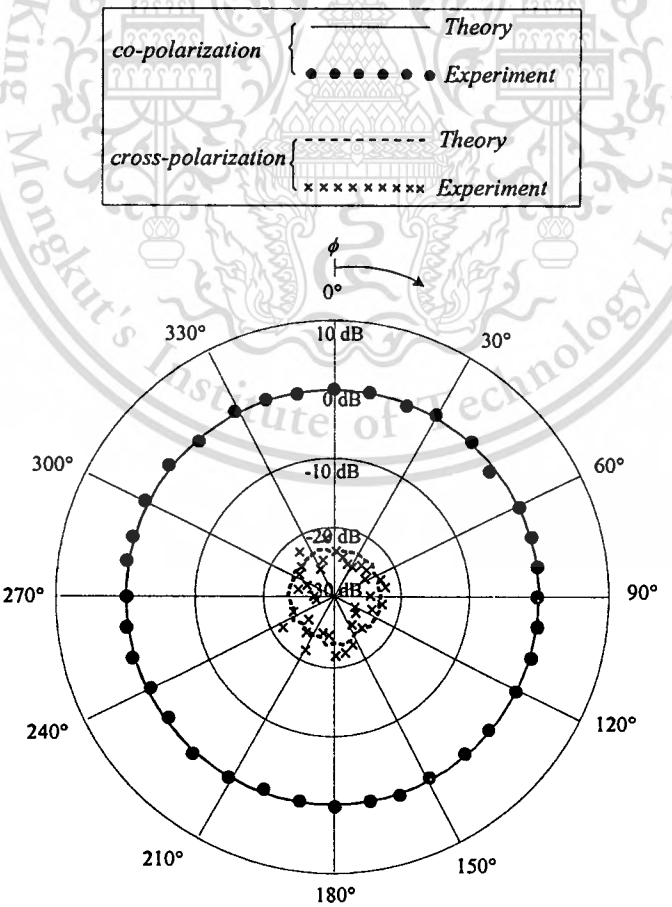

Fig.6.5 Azimuthal radiation pattern at $\theta=40°$

6.4 Input Impedance

To measure the input impedance of the antenna, the experiment is set up as shown in Fig.6.6. The measured results are plotted and compared with the theoretical one as figured in Fig.6.7. It is obvious that the theoretical results are coincided with the experimental ones. However, the experimental result and theoretical results are different in that the bandwidth of VSWR ≤ 2 of experimental results is slightly less in narrow than the theoretical ones due to the use of the finite series of the basis function of the Method of Moments.

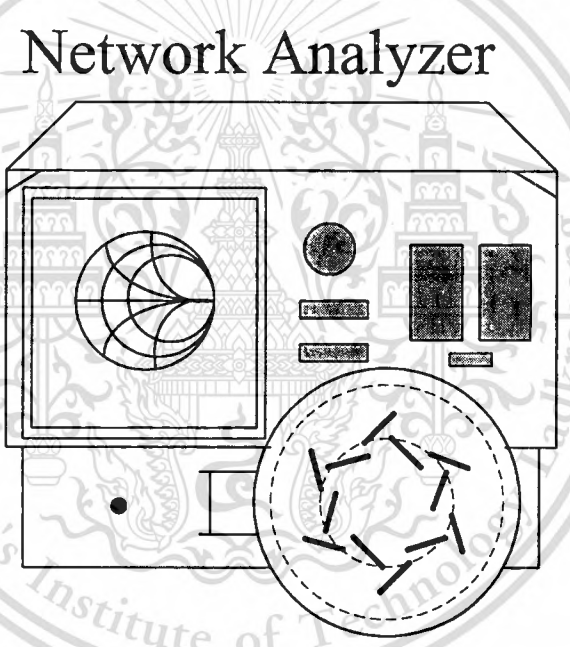

Fig.6.6 Measurement set up of the impedance characteristics

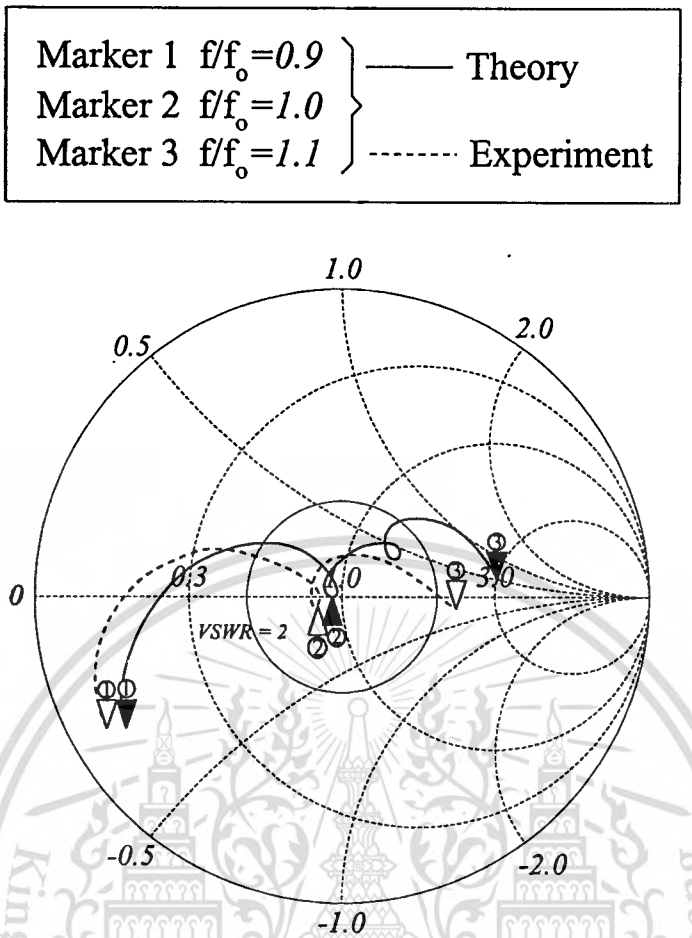

Fig. 6.7 Input impedance of the antenna

6.5 Cross Polarization and Axial Ratio

The measurements of the cross-polarized pattern and the axial ratio are carried out by using circular component method [6-5]. The cross-polarized field components in elevational and azimuthal planes were measured by replacing the right-hand circularly polarized antenna with the left hand one as illustrated in Fig.6.8 and Fig.6.9. The result of the cross-polarized pattern is shown in the same graph as the co-polarized pattern in Fig.6.4 and Fig.6.5, respectively, for elevational and azimuthal radiation patterns. It can be seen that the maximum cross-polarized level at an elevational angle of $20°$ is -9 dB below the co-polarized one. The cross polar level at azimuthal direction is relatively low that

is not greater than *–21* dB. Then, we calculate the measured axial ratio by using (5.7). Fig.6.10 shows the axial ratio at θ equals 40° and ϕ equals 0° for various frequencies. Obviously, the experimental result of axial ratio at the operating frequency is around *1.2* dB. The experimental polarization bandwidth of *16%* can be observed. Obviously, it is narrower than the theoretical one. The difference between the experimental and numerical results is because of the incompleteness in polarization of the transmitting antenna for which the helical antenna of the axial ratio of *0.4* dB is employed in the measurement.

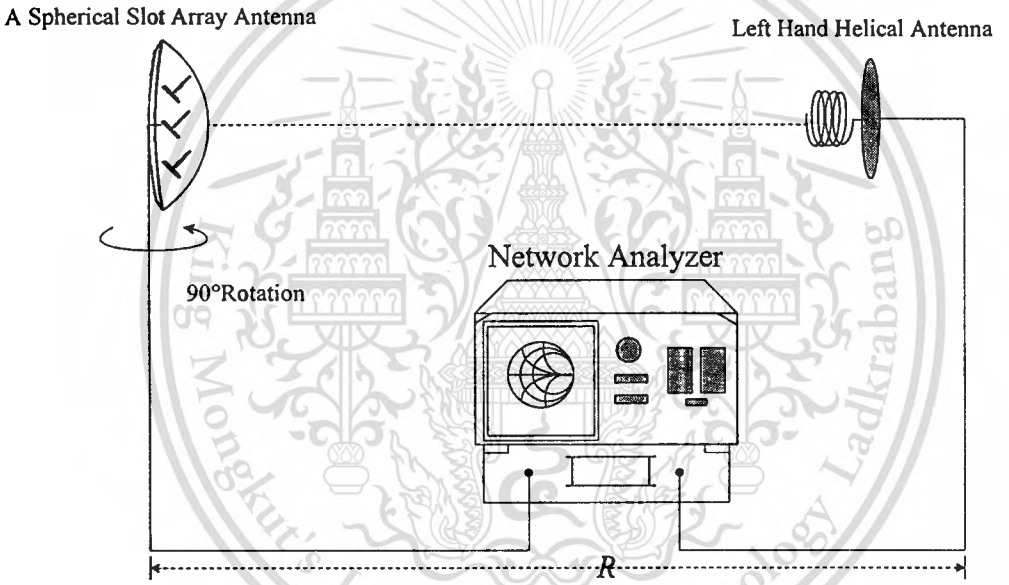

Fig.6.8 Measurement set up of the azimuthal cross-polarized pattern

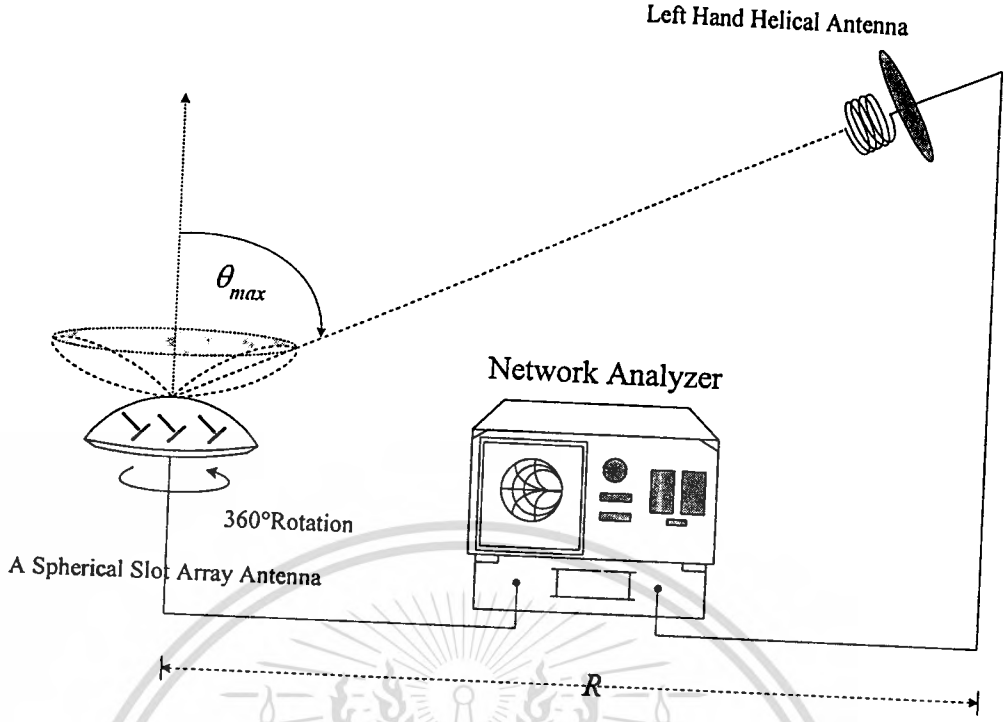

Fig.6.9 Measurement set up of the azimuthal cross-polarized pattern

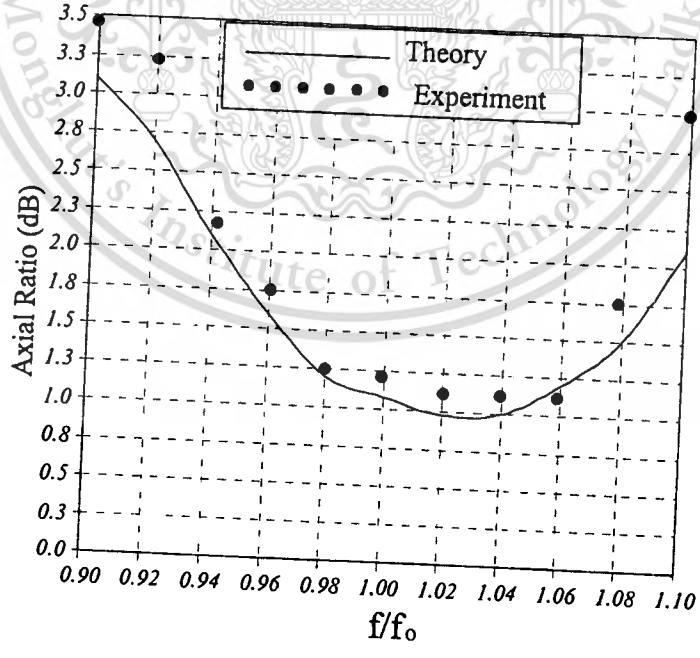

Fig. 6.10 Frequency characteristics of the axial ratio (θ=40°, ϕ=0°)

6.6 Antenna Bandwidth

The bandwidth of the antenna means the frequency range in which the antenna can be well-operated. In the case of a circularly polarized conical beam spherical slot array antenna, the characteristics that have to be considered consist of the radiation pattern, the impedance matching and the polarization circularity. The pattern should be the conical beam with the desired elevational beam peak. The impedance condition must be well-matched viz., the standing wave ratio with no more than *2.0*. The polarization circularity should possess the axial ratio with no greater than *3.0*. The frequency band that meets all of these requirements is nominated to be the bandwidth of the antenna. From the information as described above, it is obvious that the antenna bandwidth is constrained by the impedance bandwidth that is around *12%* of the operating frequency [6-6].

6.7 Conclusion

The experiments of the radiation pattern, input impedance and axial ratio were set up to verify the antenna characteristics that are theoretically investigated. It is apparent that the theoretical and experimental are reasonably meet in agreement. These results exhibit that the antenna can work well in the practical situation. In addition, the circularly polarized conical beam spherical slot array antenna is suitable for applying to the mobile satellite communications and wireless LAN systems.

References

[6-1]C.Phongcharoenpanich, M.Krairiksh, and J.Takada, "Theory and experiment of a circularly polarized conical beam spherical slot array antenna," *Proceedings of the 2001 IEEE International Symposium on*

Antennas and Propagation and USNC/URSI National Radio Science Meeting, Boston, vol.3, pp.380-383, July 2001.

[6-2]*IEEE Standard Test Procedures for Antennas*, IEEE Std 149-1979, published by IEEE, Inc., 1979, distributed by Wiley-Interscience.

[6-3]J.S.Hollis, T.J.Lyon, and L.Clayton, Jr., *Microwave Antenna Measurements*, Scientific-Atlanta, Inc., Atlanta, Georgia, July 1970.

[6-4]G.E.Evans, *Antenna Measurement Techniques*, Artech House, Norwood, MA, 1990.

[6-5]J.D.Kraus, *Antennas*, McGraw-Hill, New York, 1988.

[6-6]C.Phongcharoenpanich, M.Krairiksh and J.Takada, "Performance of a circularly polarized conical beam spherical slot array antenna," *Proceedings of the 2000 Asia-Pacific Symposium on Broadcasting and Communications*, Bangkok, pp.145-150, Dec.2000.

Chapter 7

Discussions and Conclusions

Synopses of this thesis and discussions of the future studies are included in this chapter.

7.1 Summary of Preceding Chapters

As mentioned in the first chapter, this thesis proposes the so-called Spherical Slot Array Antenna. This antenna type is categorized into the group of conformal antenna. The advantage of this antenna type is that its structure is simple since the power divider and the feeding structure are integrated into a single structure. Furthermore, this thesis is concentrated on the design of this antenna type to radiate circularly polarized conical beam pattern for applying to the land mobile satellite communications and wireless LAN system.

Then, the preliminary principle of the antenna design is illustrated in Chapter 2. The antenna structure is revealed and the principle of the antenna design is addressed. The electromagnetic field radiated from the antenna is primarily investigated. The radiation of the antenna appears to be the conical beam radiation. Moreover, the radiation pattern of the antenna substantially depended on the angle of the slot pair position and the radius of the sphere. The rigorously theoretical investigation is subsequently conducted in Chapter 3.

In Chapter 3, the integral equation is first established by using the Field Equivalent Principle and the boundary conditions. The equivalent model of the analysis is shown. The dyadic Green's functions are readily derived to fulfill the integral equations. Method of Moments is served as a vital tool in solving the integral equations. The entire domain basis functions and the Galerkin's

method of weighting functions are reasonably selected in order to determine the unknown currents.

Chapter 4 shows the radiation characteristics of the antenna. The radiation patterns both elevational and azimuthal ones are obtained. The elevational angle is also shown to clarify the feasibility of the antenna applications for different locations of the land mobile satellite communications. It is obvious that the elevational beam peak significantly varies as the angle of the slot pair positions. The outer spherical radius of the cavity is the second parameter that affects the elevational angle. The directivity of this antenna is calculated to find the optimum parameters that is sufficient for using in practical applications. The azimuthal ripple is characterized to find the parameters in which the conical beam is completely realized. The back lobe ratio is determined to illustrate the field radiated in the rearward direction. Ultimately, the contour plots of the directivity as the function of the elevational beam angle for various angles of the slot pair positions and the spherical radii are provided for further guideline of the antenna design.

Chapter 5 expresses the impedance characteristics such as the input impedance, reflection coefficient and standing wave ratio to characterize the situation of the connection between the antenna and the transmission line. The bandwidth of the antenna is calculated and found to be wide enough for the possible applications. The polarization characteristics such as cross polarization and axial ratio are investigated to find the polarization circularity. The angle of the shorting cone is adjusted to improve circularly polarized purity.

Chapter 6 verifies the principle and theory presented in the previous chapters. With the appropriate parameters, the antenna prototype is fabricated to test its characteristics. The experiments were set up to measure the radiation pattern, the input impedance and axial ratio of the antenna. The reasonably agreement between the theoretical and experimental results are acquired. From

the comparison, it confirms that this antenna is very useful and serviceable for the applications of mobile satellite communications and wireless LAN systems.

Finally, the summary of the material in this thesis and the discussion for the future studies are included in chapter 7, the last chapter.

Appendices consist of, the first, includes the spherical Bessel function and the associated Legendre function, and the second describes derivation of the dyadic Green's functions.

7.2 Remark for Future Studies

Since the aim of this thesis is to study the spherical slot array antenna, the antenna characteristics are investigated and analyzed. The ultimate goal of this thesis is to design the antenna to radiate the circularly polarized radiation for the specific application as previously described. However, there are many strategies to design this antenna for various aspects of the applications. Therefore, the antenna feature will be different from one presented in this thesis, for example it is possible to employ this antenna to radiate the steerable beam that is out of scope of this thesis. However, the antenna design to radiate the linear polarization is also left for further study.

In addition, this thesis is mainly concerned with the investigation of the spherical slot array antenna. The feasibility for applications of the mobile satellite and wireless LAN system are offered. Nevertheless, to really apply this antenna to these systems, the propagation model taken into account that the environment should be significantly conducted. This is left for further works as well.

Moreover, the radome that is very useful to prevent this antenna from any environmental damage is another topic that is open for other researchers.

In the theoretical viewpoint, since the assumption of the calculation is based on the entire sphere of the external dyadic Green's functions, the effect

of the shadow region of the sphere is neglected. Therefore, the diffraction effect of the finite spherical surface should be taken into consideration to get more precise results. This work is left for future investigations.

Last but not least, the wall thickness of the concentric conducting spherical cavity enclosed by the conducting conical surface in this thesis is ideally assumed to be very thin and disregarded. For more accurate results, this phenomenon should be taken into account in the calculations.

Appendices

Appendix A

Special Functions in Spherical Coordinates

A-1 Spherical Bessel Functions

One set of the Bessel and Hankel functions, referred to as the ordinary spherical Bessel and Hankel functions, is satisfied the ordinary spherical Bessel's differential equation

$$\frac{d^2}{dx^2}[xb_n(x)] + [1 - \frac{n(n+1)}{x^2}]xb_n(x) = 0 \qquad \text{(A.1)}$$

where $b_n(x)$ are

$j_n(x)$: ordinary spherical Bessel function of the first kind of order n,

$y_n(x)$: ordinary spherical Bessel function of the second kind of order n,

$h_n^{(1)}(x)$: ordinary spherical Hankel function of the first kind of order n and

$h_n^{(2)}(x)$: ordinary spherical Hankel function of the second kind of order n.

The ordinary spherical Bessel and Hankel functions are related to the regular (cylindrical) Bessel function as

$$b_n(x) = \sqrt{\frac{\pi}{2x}} B_{n+\frac{1}{2}}(x) \qquad \text{(A.2)}$$

where $B_n(x)$ is the regular Bessel function of order n.

Another set of the Bessel and Hankel functions which are usually used in determining the electromagnetic field in the spherical geometry are refered to as the Schelkunoff spherical Bessel and Hankel functions satisfied the Schelkunoff spherical Bessel's differential equation

$$\frac{1}{\hat{B}_n(x)}\{x^2\frac{d^2\hat{B}_n(x)}{dx^2}\}+x^2-n(n+1)\ =\ 0 \qquad \text{(A.3)}$$

where $\hat{B}_n(x)$ are

$\hat{J}_n(x)$: Schelkunoff spherical Bessel function of the first kind of order n,

$\hat{Y}_n(x)$: Schelkunoff spherical Bessel function of the second kind of order n,

$\hat{H}_n^{(1)}(x)$: Schelkunoff spherical Hankel function of the first kind of order n and

$\hat{H}_n^{(2)}(x)$: Schelkunoff spherical Hankel function of the second kind of order n.

The Schelkunoff spherical Bessel and Hankel functions are related to the regular Bessel function and the ordinary spherical Bessel function as

$$\hat{B}_n(x)\ =\ \sqrt{\frac{\pi x}{2}}B_{n+\frac{1}{2}}(x)\ =\ xb_n(x) \qquad \text{(A.4)}$$

A-2 Associated Legendre Functions

Associated Legendre functions are the function satisfied the associated Legendre's differential equation as

$$(1-x^2)\frac{d^2L_n^m(x)}{dx^2}-2x\frac{dL_n^m(x)}{dx}+[n(n+1)-\frac{m^2}{1-x^2}]L_n^m(x)\ =\ 0 \qquad \text{(A.5)}$$

where the solution $L_n^m(x)$ is

$$L_n^m(x)\ =\ A_1P_n^m(x)+B_1Q_n^m(x) \qquad \text{(A.6)}$$

where

$P_n^m(x)$: the associated Legendre function of the first kind of order *(n,m)* and

$Q_n^m(x)$: the associated Legendre function of the second kind of order *(n,m)*.

The relationship between the associated Legendre function and the ordinary Legendre function is

$$L_n^m(x) = (-1)^m (1-x^2)^{m/2} \frac{d^m L_n(x)}{dx^m} \tag{A.7}$$

where $L_n(x)$ are

$P_n(x)$: the ordinary Legendre function of the first kind of order *n* and

$Q_n(x)$: the ordinary Legendre function of the second kind of order *n*.

Appendix B

Dyadic Green's Function Derivations

From the structure of the concentric conducting spherical cavity in the spherical coordinate system (R,θ,ϕ) illustrated in Fig.3.1, the cavity consists of two parts of concentric conducting spheres of which the inner and outer spherical radii are R_a and R_b, respectively. This structure is enclosed by a part of a conducting cone with the conical angle of θ_c.

The eigenfunction expansion method is used for determining the electromagnetic field in the source region. A lossless homogeneous medium is considered and the time convention $e^{j\omega t}$ is omitted. The scalar eigenfunction ($\varphi_{\substack{e\\o}mn}(\kappa_\zeta)$) is a solution of the homogeneous Helmholtz equation [B-1]

$$\nabla^2\varphi+\kappa_\zeta^{\,2}\varphi=0. \tag{B.1}$$

In the spherical coordinate system, it is considered in the form of

$$\varphi_{\substack{e\\o}mn}(\kappa_\zeta)=b_\xi(\kappa_\zeta R)L_\xi^m(\cos\theta)\begin{Bmatrix}\cos\\ \sin\end{Bmatrix}m\phi, \tag{B.2}$$

where $b_\xi(\kappa_\zeta R)$ denotes the linear combination of the spherical Bessel function of the first kind ($j_\xi(\kappa_\zeta R)$) and the second kind ($y_\xi(\kappa_\zeta R)$) of order ξ. It satisfies the spherical Bessel differential equation [B-1]

$$\frac{d^2}{dx^2}[xb_\xi(x)]+[1-\frac{\xi(\xi+1)}{x^2}]xb_\xi(x)=0, \tag{B.3}$$

where x is $\kappa_\zeta R$, with the unknown normalized coefficient $A_\xi(\kappa_\zeta)$:

$$b_\xi(\kappa_\zeta R) = j_\xi(\kappa_\zeta R) + A_\xi(\kappa_\zeta) y_\xi(\kappa_\zeta R). \tag{B.4}$$

κ_ζ is either κ_p or κ_q corresponding to TE and TM mode, respectively.

By applying the boundary condition that the tangential electric field in the radial direction vanishes, the unknown coefficient $A_\xi(\kappa_\zeta)$ can be determined from the characteristic equation [B-1]. For TM mode

$$A_\xi(\kappa_\zeta) = -\frac{j'_\xi(\kappa_\zeta R_a)}{y'_\xi(\kappa_\zeta R_a)} = -\frac{j'_\xi(\kappa_\zeta R_b)}{y'_\xi(\kappa_\zeta R_b)}, \tag{B.5}$$

where the prime denotes the differentiation with respect to the argument. This characteristic equation gives the solution

$$\kappa_\zeta R_a = x'_{\zeta,\alpha} \tag{B.6}$$

and

$$\kappa_\zeta R_b = x'_{\zeta,\beta} \tag{B.7}$$

such that

$$\kappa_\zeta (R_a - R_b) = x'_{\zeta,\gamma}, \tag{B.8}$$

where x' denotes the roots of zero of derivative of the ordinary spherical Bessel function ratio and γ is the interval between the roots α and β. γ is equal to α-β

corresponding to the order of the root interval. For TE mode counterpart, the characteristic equation becomes

$$A_\xi(\kappa_\zeta) = -\frac{j_\xi(\kappa_\zeta R_a)}{y_\xi(\kappa_\zeta R_a)} = -\frac{j_\xi(\kappa_\zeta R_b)}{y_\xi(\kappa_\zeta R_b)} \quad . \tag{B.9}$$

The solution of the above equation are

$$\kappa_\zeta R_a = x_{\zeta,\alpha} \tag{B.10}$$

and

$$\kappa_\zeta R_b = x_{\zeta,\beta} \tag{B.11}$$

such that

$$\kappa_\zeta (R_a - R_b) = x_{\zeta,\gamma}, \tag{B.12}$$

where x denotes the roots of zero of the ordinary spherical Bessel function ratio and α, β, γ are the same as declared before.

The function $L_\xi^m(cos\theta)$ denotes the linear combination of the associated Legendre function of the first kind ($P_\xi^m(cos\theta)$) and the second kind ($Q_\xi^m(cos\theta)$) of order (ξ,m) which satisfies the associated Legendre differential equation [B-1]

$$\frac{1}{sin\theta}\frac{d}{d\theta}[sin\theta\frac{d}{d\theta}L_\xi^m(cos\theta)] + [\xi(\xi+1) - \frac{m^2}{sin^2\theta}]L_\xi^m(cos\theta) = 0 \tag{B.13}$$

with the unknown normalized coefficient B_ξ^m :

$$L_\xi^m(cos\theta) = P_\xi^m(cos\theta) + B_\xi^m Q_\xi^m(cos\theta). \tag{B.14}$$

The unknown coefficient B_ξ^m can be obtained by enforcing the finite condition of the dyadic at θ equals $180°$ as [B-2]

$$B_\xi^m = -\frac{2}{\pi} tan[\pi(\xi + m)] \ . \tag{B.15}$$

In the event of the concentric conducting spherical cavity enclosed by the conducting conical surface at $\theta = 0°$ and θ_c, because $\theta = 0°$ is contained, hence $B_\xi^m = 0$ is caused by the integer of ξ.

The eigenvalues m is determined from the dimension in the azimuthal direction of the cavity. ξ is either μ or λ and can be determined from the auxiliary equation [B-1]

$$\frac{dL_\lambda^m(cos\theta)}{d\theta}\Big|_{\theta=\theta_c} = 0 \tag{B.16}$$

and

$$L_\mu^m(cos\theta)\Big|_{\theta=\theta_c} = 0. \tag{B.17}$$

They satisfy the field in the TE and TM mode, respectively.

The eigenvalues κ_ζ is κ_p or κ_q that after being multiplied by the certain radii of concentric conducting spheres of the spherical coordinate system are the roots of the indical equation [B-1]

$$b_\xi(\kappa_p R)\Big|_{R=R_a} = b_\xi(\kappa_p R)\Big|_{R=R_b} = 0, \tag{B.18}$$

for TE mode, and

$$\frac{d[\kappa_q R b_\xi(\kappa_q R)]}{d(\kappa_q R)}\Big|_{R=R_a} = \frac{d[\kappa_q R b_\xi(\kappa_q R)]}{d(\kappa_q R)}\Big|_{R=R_b} = 0 \tag{B.19}$$

for TM mode.

In the method of magnetic dyadic Green's function ($\overline{\overline{G}}_m$), for the configuration of the conducting spherical cavity, the eight sets of solenoidal spherical vector wave functions with discrete eigenvalues are required. They are

$$\overline{M}_{\substack{e\\o}mn}(\kappa_\zeta) = \nabla\times[\varphi_{\substack{e\\o}mn}(\kappa_\zeta)\overline{R}], \tag{B.20}$$

$$\overline{N}_{\substack{e\\o}mn}(\kappa_\zeta) = \frac{1}{\kappa_\zeta}\nabla\times\nabla\times[\varphi_{\substack{e\\o}mn}(\kappa_\zeta)\overline{R}]. \tag{B.21}$$

Where ξ and ζ can be either μ or λ and p or q, respectively. Both of these functions are the solutions of the vector wave equation

$$\nabla\times\nabla\times\overline{F} - \kappa_\zeta^2\overline{F} = 0, \tag{B.22}$$

where $\overline{F}$ is $\overline{M}$ or $\overline{N}$, satisfying the symmetrical relationships

$$\overline{N}_{o_{e_o}^{m\xi}}(\kappa_\zeta) = \frac{1}{\kappa_\zeta}\nabla\times\overline{M}_{o_{e_o}^{m\xi}}(\kappa_\zeta) \tag{B.23}$$

and

$$\overline{M}_{o_{e_o}^{m\xi}}(\kappa_\zeta) = \frac{1}{\kappa_\zeta}\nabla\times\overline{N}_{o_{e_o}^{m\xi}}(\kappa_\zeta) \quad . \tag{B.24}$$

By substituting the eigenfunction into (B.23) and (B.24), the complete expressions of the vector wave function will be obtained and written in the form of

$$\overline{M}_{o_{e_o}^{m\xi}}(\kappa_\zeta) = \mp\frac{m}{\sin\theta}b_\xi(\kappa_\zeta R)L_\xi^m(\cos\theta)\begin{Bmatrix}\sin\\\cos\end{Bmatrix}m\phi\hat{\theta} - b_\xi(\kappa_\zeta R)\frac{\partial L_\xi^m(\cos\theta)}{\partial\theta}\begin{Bmatrix}\cos\\\sin\end{Bmatrix}m\phi\hat{\phi}, \tag{B.25}$$

$$\overline{N}_{o_{e_o}^{m\xi}}(\kappa_\zeta) = \frac{\xi(\xi+1)}{\kappa_\zeta}b_\xi(\kappa_\zeta R)L_\xi^m(\cos\theta)\begin{Bmatrix}\cos\\\sin\end{Bmatrix}m\phi\hat{R} + \frac{1}{\kappa_\zeta R}\frac{\partial[Rb_\xi(\kappa_\zeta R)]}{\partial R}[\frac{\partial L_\xi^m(\cos\theta)}{\partial\theta}\begin{Bmatrix}\cos\\\sin\end{Bmatrix}m\phi\hat{\theta}$$
$$\mp\frac{m}{\sin\theta}L_\xi^m(\cos\theta)\begin{Bmatrix}\sin\\\cos\end{Bmatrix}m\phi\hat{\phi}]. \tag{B.26}$$

To derive the dyadic Green's function of the structure under consideration, the method of $\overline{\overline{G}}_m$ approach will be applied. The magnetic type of dyadic Green's function was first derived by using [B-1]

$$\nabla\times\nabla\times\overline{\overline{G}}_{m2}(\overline{R},\overline{R}') - k^2\overline{\overline{G}}_{m2}(\overline{R},\overline{R}') = \nabla\times[\overline{\overline{I}}\delta(\overline{R}-\overline{R}')], \tag{B.27}$$

where $\overline{\overline{G}}_{m2}$ denotes the magnetic dyadic Green's function of the second kind that satisfies the boundary condition

$$\overline{n}\times\nabla\times\overline{\overline{G}}_{m2}(\overline{R},\overline{R'})=0 \tag{B.28}$$

at R equals R_a and R_b, θ equals 0° and θ_c for the concentric conducting spherical cavity. k is the propagation constant of the medium which equals $\sqrt{\mu\varepsilon}$, ω is the operating angular frequency, μ and ε are the permeability and permittivity of the medium, respectively, $\overline{\overline{I}}$ is the Idem factor and $\delta(\overline{R}-\overline{R'})$ is the three dimensional delta function.

According to Ohm-Rayleigh method, the source function in case of the concentric conducting spherical cavity is expanded in the form of solenoidal vector wave functions

$$\nabla\times[\overline{\overline{I}}\delta(\overline{R}-\overline{R'})]=\sum_{l,m}[\sum_{\lambda}\overline{N}_{\substack{e\\o}ml\lambda}(\kappa_p)\overline{C}_{\substack{e\\o}ml\lambda}(\kappa_p)+\sum_{\mu}\overline{M}_{\substack{e\\o}ml\mu}(\kappa_q)\overline{D}_{\substack{e\\o}ml\mu}(\kappa_q)], \tag{B.29}$$

where the number l represents the numerical number for the discrete eigenvalues κ_p and κ_q. $\overline{C}_{\substack{e\\o}ml\lambda}(\kappa_p)$ and $\overline{D}_{\substack{e\\o}ml\mu}(\kappa_q)$ are two unknown vector coefficients to be determined. By taking the anterior scalar product of (B.29) with $\overline{N'}_{\substack{e\\o}ml'\lambda'}(\kappa'_p)$ and $\overline{M'}_{\substack{e\\o}ml'\mu'}(\kappa'_q)$, respectively, integrating the resultant equation throughout the cavity configuration domain and using the orthogonal relationship between the vector wave function, one obtains

$$\overline{C}_{\substack{e\\o}ml\lambda}(\kappa_p)=\frac{(2-\delta_m)\kappa_p}{2\pi I_{\lambda p}}\overline{M'}_{\substack{e\\o}ml\lambda}(\kappa_p) \tag{B.30}$$

and

$$\overline{D}_{e_{o}m\mu}(\kappa_q) = \frac{(2-\delta_m)\kappa_q}{2\pi I_{\mu q}} \overline{N'}_{e_{o}m\mu}(\kappa_q), \tag{B.31}$$

where

$$I_{\xi\zeta} = \frac{1}{\kappa_\zeta \kappa'_\zeta} \int_0^{\vartheta_c} \int_{R_a}^{R_b} \{\xi^2(\xi+1)^2 j_\xi(\kappa_\zeta R) j_\xi(\kappa'_\zeta R)[P_\xi^m(cos\theta)]^2 + \frac{\partial[Rj_\xi(\kappa_\zeta R)]}{\partial R} \frac{\partial[Rj_\xi(\kappa'_\zeta R)]}{\partial R} [(\frac{\partial P_\xi^m(\cos\theta)}{\partial\theta})^2 + (\frac{mP_\xi^m}{\sin\theta})^2]\} sin\theta dR d\theta. \tag{B.32}$$

$\xi\zeta$ is λp and μq, respectively, and δ_m represents the Kronecker delta function. To find $\overline{\overline{G}}_{m2}$, we will expand $\overline{\overline{G}}_{m2}$ by using the same expression of the source function as shown in (B.29), but the two different scalar unknown coefficients $E(\kappa_p)$ and $F(\kappa_q)$ as

$$\overline{\overline{G}}_{m2}(\overline{R}, \overline{R'}) = \sum_{l,m} \frac{2-\delta_m}{2\pi} [\sum_\lambda \frac{\kappa_p}{I_{\lambda p}} E(\kappa_p) \overline{N}_{e_{o}m\lambda}(\kappa_p) \overline{M'}_{e_{o}m\lambda}(\kappa_p) + \sum_\mu \frac{\kappa_q}{I_{\mu q}} F(\kappa_q)\ \overline{M}_{e_{o}m\mu}(\kappa_q) \overline{N'}_{e_{o}m\mu}(\kappa_q)] \tag{B.33}$$

By substituting (B.33) in (B.27), the unknown coefficients $E(\kappa_p)$ and $F(\kappa_q)$ can be determined

$$E(\kappa_p) = \frac{1}{(\kappa_p^2 - k^2)} \tag{B.34}$$

$$F(\kappa_q) = \frac{1}{(\kappa_q^2 - k^2)} \tag{B.35}$$

and $\overline{\overline{G}}_{m2}$ can be written in the form

$$\overline{\overline{G}}_{m2}(\overline{R},\overline{R'}) = \sum_{l,m} \frac{2-\delta_m}{2\pi} [\sum_{\lambda} \frac{\kappa_p}{(\kappa_p^2 - k^2) I_{\lambda p}} \overline{N}_{e\,m\lambda}(\kappa_p) \overline{M'}_{e\,m\lambda}(\kappa_p) + \sum_{\mu} \frac{\kappa_q}{(\kappa_q^2 - k^2) I_{\mu q}} \overline{M}_{e\,m\mu}(\kappa_q) \overline{N'}_{e\,m\mu}(\kappa_q)] \tag{B.36}$$

After $\overline{\overline{G}}_{m2}$ was derived, by considering the singularities of the source point and using the Maxwell's coupled differential equation in dyadic form,

$$\nabla \times \overline{\overline{G}}_{m2} = \overline{\overline{I}} \delta(\overline{R} - \overline{R'}) + k^2 \overline{\overline{G}}_{el}, \tag{B.37}$$

where $\overline{\overline{G}}_{el}$ denotes the electric dyadic Green's function of the first kind that satisfies the boundary condition

$$\overline{n} \times \overline{\overline{G}}_{el}(\overline{R},\overline{R'}) = 0. \tag{B.38}$$

$\overline{\overline{G}}_{el}(\overline{R},\overline{R'})$ could be derived as [B-3]

$$\begin{aligned} \overline{\overline{G}}_{el}(\overline{R},\overline{R'}) = -\frac{1}{k^2} \overline{\overline{I}} \delta(\overline{R} - \overline{R'}) + \frac{1}{k^2} \sum_{l,m} \frac{2-\delta_m}{2\pi} [\sum_{\lambda} \frac{\kappa_p^{\,2}}{(\kappa_p^2 - k^2) I_{\lambda p}} \overline{M}_{e\,m\lambda}(\kappa_p) \overline{M'}_{e\,m\lambda}(\kappa_p) \\ + \sum_{\mu} \frac{\kappa_q^{\,2}}{(\kappa_q^2 - k^2) I_{\mu q}} \overline{N}_{e\,m\mu}(\kappa_q) \overline{N'}_{e\,m\mu}(\kappa_q)]. \end{aligned} \tag{B.39}$$

Based on the electric dyadic Green's function of the first kind, the primed functions ($\overline{M'}$ and $\overline{N'}$) are the excitation functions and the unprimed functions ($\overline{M}$ and $\overline{N}$) are the field functions. The former and the latter terms correspond to the transverse electric and transverse magnetic modes, respectively.

Alternatively, by using the symmetrical relationship between the electric and magnetic dyadic Green's functions, the electric dyadic Green's function of the second kind and the magnetic dyadic Green's function of the first kind can be expressed as

$$\overline{\overline{G}}_{e2}(\overline{R},\overline{R'}) = -\frac{1}{k^2}\overline{\overline{I}}\delta(\overline{R}-\overline{R'}) + \frac{1}{k^2}\sum_{l,m}\frac{2-\delta_m}{2\pi}\Big[\sum_{\lambda}\frac{\kappa_p^{\,2}}{(\kappa_p^2-k^2)I_{\lambda p}}\overline{N}_{e\,m\lambda}(\kappa_p)\overline{N'}_{e\,m\lambda}(\kappa_p) + \sum_{\mu}\frac{\kappa_q^{\,2}}{(\kappa_q^2-k^2)I_{\mu q}}\overline{M}_{e\,m\mu}(\kappa_q)\overline{M'}_{e\,m\mu}(\kappa_q)\Big]. \tag{B.40}$$

and

$$\overline{\overline{G}}_{m1}(\overline{R},\overline{R'}) = \sum_{l,m}\frac{2-\delta_m}{2\pi}\Big[\sum_{\lambda}\frac{\kappa_p}{(\kappa_p^2-k^2)I_{\lambda p}}\overline{M}_{e\,m\lambda}(\kappa_p)\overline{N'}_{e\,m\lambda}(\kappa_p) + \sum_{\mu}\frac{\kappa_q}{(\kappa_q^2-k^2)I_{\mu q}}\overline{N}_{e\,m\mu}(\kappa_q)\overline{M'}_{e\,m\mu}(\kappa_q)\Big] \tag{B.41}$$

In order to avoid a possible confusion of field type and source type of various kinds of dyadic Green's functions, another representation form of them is

$$\overline{\overline{G}}_{e1} = \overline{\overline{G}}_{EJ} \tag{B.42}$$

$$\overline{\overline{G}}_{m1} = \overline{\overline{G}}_{EM} \tag{B.42}$$

$$\overline{\overline{G}}_{e2} = \overline{\overline{G}}_{HM} \tag{B.43}$$

and

$$\overline{\overline{G}}_{m2} = \overline{\overline{G}}_{HJ}, \tag{B.44}$$

where $\overline{\overline{G}}_{EJ}(\overline{R},\overline{R}')$ denotes the electric dyadic Green's function produced by electric current density. $\overline{\overline{G}}_{EM}(\overline{R},\overline{R}')$ is the electric dyadic Green's function produced by magnetic current sheet. $\overline{\overline{G}}_{HM}(\overline{R},\overline{R}')$ is the magnetic dyadic Green's function produced by a magnetic current sheet. $\overline{\overline{G}}_{HJ}(\overline{R},\overline{R}')$ represents the magnetic dyadic Green's function produced by electric current density. Therefore, these nomenclatures are used in chapter 3.

References

[B-1]C.T.Tai, *Dyadic Green Functions in Electromagnetic Theory.* IEEE Press, New York, 1993.

[B-2]J.R.Descardeci, "A note on using dyadic Green's functions on spheres and cones," *IEEE Antennas and Propagation Magazine,* vol.38, no.1, p.59, Feb. 1996.

[B-3]C.Phongcharoenpanich, M.Krairiksh and J.Takada, "Dyadic Green's functions of the concentric conducting spherical cavity," *Proceeding of the 1997 Asia-Pacific Microwave Conference*, Hong Kong, vol. 2, pp. 757-760, Dec. 1997.

List of Publications

1. C.Phongcharoenpanich, M.Krairiksh and J.Takada, "Investigations of Radiation Characteristics of a Circularly Polarized Conical Beam Spherical Slot Array Antenna," *IEICE Trans. Electronics*, vol. E82-C, no.7, pp.1242-1247, July 1999.
2. M.Krairiksh, C.Phongcharoenpanich, K.Meksamoot and J.Takada, "A Circularly Polarized Conical Beam Spherical Slot Array Antenna," *International Journal of Electronics*, vol.86, no.7, pp.815-823, July 1999.
3. C.Phongcharoenpanich, M.Krairiksh and J.Takada, "A Concentric Conducting Spherical Cavity-Backed Slot Array Antenna Radiating Circularly Polarized Conical Beam," *Proceeding of the 1999 Progress in Electromagnetics Research Symposium*, Taipei, vol.2, p.708, Mar. 1999.
4. C.Phongcharoenpanich, M.Krairiksh and J.Takada, "Dyadic Green's Functions of the Concentric Conducting Spherical Cavity," *Proceeding of the 1997 Asia-Pacific Microwave Conference*, Hong Kong, vol. 2, pp. 757-760, Dec. 1997.
5. C.Phongcharoenpanich, M.Krairiksh, K.Meksamoot and J.Takada, "Radiation Characteristics of a Circularly Polarized Conical Beam Spherical Slot Array Antenna," *Proceeding of the 1998 Asia-Pacific Microwave Conference*, Yokohama, vol. 3, pp. 1229-1232, Dec. 1998.
6. C.Phongcharoenpanich, M.Krairiksh and J.Takada, "Impedance Characteristics of a Circularly Polarized Conical Beam Spherical Slot Array Antenna," *Proceedings of the AP2000 Millennium Conference on Antennas and Propagation*, Davos, vol.1, p.203, Apr. 2000.
7. C.Phongcharoenpanich, M.Krairiksh and J.Takada, "MoM Analysis of a Circularly Polarized Conical Beam Spherical Slot Array Antenna,"

Proceedings of the 2000 International Symposium on Antennas and Propagation, Fukuoka, vol.4, pp.1625-1628, Aug. 2000.

8. C.Phongcharoenpanich, M.Krairiksh and J.Takada, "Polarization Characteristics of a Circularly Polarized Conical Beam Spherical Slot Array Antenna," *Proceedings of the 5th International Symposium on Antennas, Propagation and Electromagnetic Theory*, Beijing, pp. 638-641, Aug. 2000.
9. C.Phongcharoenpanich, M.Krairiksh and J.Takada, "Characteristics of a Circularly Polarized Conical Beam Spherical Slot Array Antenna," *Proceedings of the 2000 Asia-Pacific Microwave Conference*, Sydney, pp.38-41, Dec. 2000.
10. C.Phongcharoenpanich, M.Krairiksh and J.Takada, "Performance of a Circularly Polarized Conical Beam Spherical Slot Array Antenna," *Proceedings of the 2000 Asia-Pacific Symposium on Broadcasting and Communications*, Bangkok, pp.145-150, Dec.2000.
11. C.Phongcharoenpanich, M.Maruekin, M.Krairiksh and J.Takada, "A Circularly Polarized Conical Beam Spherical Slot Array Antenna for Land Mobile Satellite Communication," *Proceedings of the 39th Kasetsart University Annual Conference*, Bangkok, pp.217-226, April 2001.
12. C.Phongcharoenpanich, M. Krairiksh, and J.Takada, "Theory and Experiment of a Circularly Polarized Conical Beam Spherical Slot Array Antenna," *Proceedings of the 2001 IEEE International Symposium on Antennas and Propagation and USNC/URSI National Radio Science Meeting*, Boston, vol.3, pp.380-383, July 2001.

Curriculum Vitae

Author: Chuwong Phongcharoenpanich

Date of Birth: September 11, 1974

Bachelor Degree: B.Eng.(Hons.) in Telecommunication Engineering

Institution: Faculty of Engineering,
King Mongkut's Institute of Technology Ladkrabang

Year of Graduation: 1996

Master Degree: M.Eng. in Electrical Engineering

Institution: Faculty of Engineering,
King Mongkut's Institute of Technology Ladkrabang

Year of Graduation: 1998

Master Thesis: Electromagnetic Field Analysis of the Conducting Spherical Cavity and Segment

Undergraduate Research:

1. The Design of the Planar Slotted-Waveguide Array Antenna (1995)
2. The Design of Variable Phase Shifter (1994)
3. The Design of Phase Shifter from Partially-Filled Rectangular Waveguide (1994)

Awards: Outstanding paper contribution in 5th International Symposium on Antennas, Propagation and Electromagnetic Theory at Beijing, China on August 15-18, 2000

Scholarship: Local graduate Scholarship from the National Science and Technology Development Agency: NSTDA (1996-1997)

Experiences: - Graduate Research Assistant in Steerable Spherical Slot Array Antenna Project under the career development award of the National Science and Technology Development Agency: NSTDA (1997-1999)

- Lecturer of Department of Telecommunication Engineering, Faculty of Engineering, King Mongkut's Institute of Technology Ladkrabang (since 1999)